КРИСТАЛЛОГРАФИЯ

SOVIET PHYSICS

Crystallography

VOLUME 2 NUMBER 5

A Translation

of the journal

Crystallography

of the

Academy of Sciences of the USSR

(RUSSIAN ORIGINAL VOL. 2, NO. 5)

Published by the

AMERICAN INSTITUTE OF PHYSICS

INCORPORATED

SOVIET PHYSICS

Crystallography

A translation of the journal "Crystallography" of the Academy of Sciences of the USSR

A publication of the
AMERICAN INSTITUTE OF PHYSICS

Governing Board

FREDERICK SEITZ, *Chairman*

Members

WALTER S. BAIRD
JESSE W. BEAMS
RAYMOND T. BIRGE
R. H. BOLT
J. W. BUCHTA
J. H. DILLON
VERNET E. EATON
HERBERT A. ERF
IRVINE C. GARDNER
S. A. GOUDSMIT
C. KITTEL
WINSTON E. KOCK
R. BRUCE LINDSAY
WALTER C. MICHELS
G. E. PAKE
R. RONALD PALMER
JOSEPH B. PLATT
RALPH A. SAWYER
H. D. SMYTH
JOHN STRONG
GEORGE E. UHLENBECK

Officers and Staff

ELMER HUTCHISSON
Director
HENRY A. BARTON
Associate Director
WALLACE WATERFALL
Secretary and Treasurer
EDWARD P. TOBER
Mgr., Production and Distribution
THEODORE VORBURGER
Advertising Manager
RUTH F. BRYANS
Publication Manager
KATHRYN SETZE
Assistant Treasurer
ALICE MASTROPIETRO
Circulation Manager
EUGENE H. KONE
Director of Public Relations
WILLIAM C. KELLY
Director of Education Projects

American Institute of Physics Advisory Board on Russian Translations

ROBERT T. BEYER, *Chairman*

FREEMAN DYSON, DWIGHT GRAY, MORTON HAMERMESH, DAVID HARKER, VLADIMIR ROJANSKY, HARROLD F. WEAVER

Advisory Editor, Soviet Physics – Crystallography: DAVID HARKER, Protein Structure Project, Polytechnic Institute of Brooklyn, Brooklyn 2, New York.

"Soviet Physics – Crystallography" is published by the American Institute of Physics, with the cooperation of the American Crystallographic Association, for the purpose of making available in English reports of current Soviet research in crystallography as contained in the journal "Crystallography" of the Academy of Sciences of the USSR. The translation begins with the 1957 issues.

Transliteration of the names of Russian authors follows the system employed by the Library of Congress.

This translating and publishing project was undertaken by the Institute in the conviction that dissemination of the results of research everywhere in the world is invaluable to the advancement of science. The National Science Foundation of the United States encouraged the project initially and is supporting it in large part by a grant. Translation and printing are being handled by Consultants Bureau, Inc.

The American Institute of Physics and its translators propose to translate faithfully all of the scientific material in the "Crystallographic Journal of the Academy of Sciences of the USSR" appearing after January 1, 1957. The views expressed in the translated material, therefore, are intended to be those expressed by the original authors, and not those of the translators nor of the American Institute of Physics.

One volume is published annually. The volume numbering coincides with that of the original Russian journal.

Subscription Prices:

Per year (6 issues), starting with Vol. 2, No. 1

General: United States and Canada	$25.00
Elsewhere	27.00
Libraries of non-profit academic institutions:	
United States and Canada	10.00
Elsewhere	12.00
Back numbers, all issues	5.00

Subscriptions should be addressed to the American Institute of Physics, 335 East 45th Street, New York 17, New York.

Copyright American Institute of Physics Incorporated, 1959

SOVIET PHYSICS

Crystallography

VOLUME 2, NUMBER 5 SEPTEMBER-OCTOBER 1957

THE DEVELOPMENT OF CRYSTALLOGRAPHY IN THE USSR IN THE LAST FORTY YEARS

Russian pre-revolutionary science left a rich heritage to Soviet crystallography. One needs only to mention such names as: N. I. Koksharov, A. V. Gadolin, E. S. Fedorov and G. V. Wulff to realize that they were outstanding, not only in Russian science, but in world science as well.

N. I. Koksharov's works on the goniometric crystal measurement of numerous Russian minerals are mentioned in all Russian and foreign handbooks as unsurpassed in accuracy.

A. V. Gadolin (1828-1892) derived the 32 groups of macrosymmetry of crystals and devised a method of representing them on a sphere, still widely applied.

E. S. Fedorov's (1853-1919) scientific merits are very great. It is to him and to A. Schoenflies who worked simultaneously and in rather close collaboration with him that the development of the 230 space group symmetries — the laws of the distribution of particles in crystals — can be attributed. Fedorov's groups are the mathematical bases of x-ray crystal structure analysis, which originated 20 years after the publication of his works and confirmed brilliantly his theoretical conclusions. His graphs for the 230 groups were included, with minor alterations, in "International Tables for X-ray Crystal Structure Analysis." By establishing the law of crystallographic limits and by developing a correct system of mounting crystals, Fedorov built a thorough theoretical base under the then existing method of studying only the external shapes of crystals. The two-circle (theodolite) goniometer invented by him made it possible to rationalize and simplify radically the technique of crystal measurement. He also simplified just as radically the methods of studying the optical properties of crystals in sections, by inventing a universal optical stage, which bears his name and is used by mineralogists and petrographers the world over.

G. V. Wulff (1863-1925) accomplished a great deal for the development of physical crystallography. Classical works on the growth and physical properties of crystals are due to him. He expanded to crystal growth the Gibbs-Curie principle of the equilibrium of a crystal with its environment. Today many theoretical works on crystal growth, native as well as foreign, proceed from Wulff's theorem. He shares with W. L. Bragg the glory of deriving the formula which is the basis of x-ray crystal structure analysis and connects the wavelength of x-ray radiation with the glancing angle and interplanar distance. Wulff's stereographic net has found wide application in crystallographic calculations. The reduction of all symmetry operations to systematically applied mirror reflections is now at the basis of all studies of symmetry.

Prior to x-ray structural analysis, crystallography had a very weak bond with physics and even a weaker one with technology. This area of knowledge was not yet considered as an independent science, but as a division of mineralogy. Following the discovery of x-rays (1912)* the situation changed sharply. The lattice-like structure of crystals, i. e., of almost all solid bodies, became a generally recognized fact. The development of structural analysis took pre-eminence over morphological studies of crystals. After 1912 the study of crystals became gradually one of the main problems of physics and chemistry. The just discovered method of direct atomic crystal structure determination transformed natural science.

Noting the considerable accomplishments of the old Russian crystallography, one must not forget that this science, prior to the revolution, was not connected with practice. The number of scientists devoted to crystallography was very small.

The October Socialist Revolution opened great possibilities for the development of science. The accomplishments of Soviet physics, chemistry, mathematics and other sciences and their part in the technical progress of our country are generally known. During the years of Soviet power, crystallography became an independent science, closely related to other sciences and to modern technology.

The development of Soviet crystallography can be divided into two stages, each of which occupies approximately 20 years. In the first stage, i. e., before the Academy of Sciences was moved to Moscow, crystallography was developing very slowly. But with the Academy transferred to the capital, the number of crystallographic studies began to increase rapidly. At present we are witnessing the flowering of crystallography in our country.

Following the death of E. S. Fedorov and G. V. Wulff, the small nucleus of crystallographers was concentrated mainly in Leningrad in the crystallography department of the Mining Institute and in the geology department of the University, and also (from 1925) in A. V. Shubnikov's laboratory at the Mineralogical Museum of the Academy of Sciences of the USSR.

The crystallographers of the Mining Institute (V. V. Dolivo-Dobrovolsky, I. I. Shafranovskii and others) headed by A. K. Boldyrev were developing E. S. Fedorov's geometric inheritance. Methods of crystallographic determination of a substance, and classification and nomenclature in the study of symmetry were being perfected, also goniometric and x-ray diffraction studies of crystals were carried out. The most important result of these works was the creation of a fundamental "Determinative Table for Crystals" and "X-ray Diffraction Determinative Table for Minerals." Fedorov's Institute was organized at the Mining Institute. Annual sessions, which are very popular, are held here in Fedorov's memory, on crystallography, mineralogy and petrography. The manufacture of crystallographic and crystal structural models was set up at the Mining Institute. A. K. Boldyrev (1883-1946) was the initiator of these undertakings.

At the University of Leningrad, E. S. Fedorov's student, O. M. Ansheles (1885-1957) was improving upon the computational and graphic methods of crystallography, and carrying on work on the immersion method and on crystal genesis (together with V. B. Tatarskii and later with V. A. Frank-Kamenetskii).

G. V. Wulff's closest student, A. V. Shubnikov, with his group of co-workers, directed the studies on piezoelectric quartz, which laid the foundation of the piezoelectric quartz industry in the USSR, and related crystallography with technology for the first time. A. V. Shubnikov was foremost in setting up a special laboratory for growing single crystals, so essential for physics and technology, devoting much time to the study of the mechanism of crystal growth and to original experimental and theoretical works on the symmetry of physical phenomena.

In Moscow the development of crystallography was less marked. D. K. Motsok (1802-1944), the representative of mathematical crystallography, worked on the symmetry of multidimensional space (Institute of Nonferrous Metals and Gold). E. E. Flint and A. N. Liamina (1894-1947) made x-ray diffraction and optical goniometric studies at the Institute of Mineral Raw Materials. It was also there that V. V. Arshinov (1879-1955), N. E. Vedeneeva (1882-1955), S. V. Grum-Grzhimailo and N. M. Melankholin were developing the original apparatus and method of crystallo-optical researches.

In Baku Ia. Z. Vezir-Zade directed the optical goniometric and x-ray diffraction work.

In 1930, on A. E. Fersman's initiative, the Lomonosov Institute of Geochemistry, Mineralogy and Crystallography of the Academy of Sciences of the USSR emerged in Leningrad. A. V. Shubnikov became head of the crystallographic section of this Institute. There, works on piezoelectric quartz, and on the treatment and growth of crystals were carried out, bringing crystallography closer and closer to technology, physics and chemistry.

* As in original – Publisher's note.

In the Leningrad Physicotechnical Institute, A. V. Shubnikov organized the growing of large single crystals of potassium sodium tartrate. The study of these crystals led I. V. Kurchatov to the establishment of ferroelectricity. A. F. Ioffe discovered the effect, now well known, of the strengthening of rock salt by dissolving its surface. M. V. Klassen-Nekliudova detected the periodicity accompanying the plastic deformation of rock salt. The development of research on piezoelectric quartz necessitated a deep "historical" study of quartz morphology and of other crystals (G. G. Lemmlein).

Questions of crystal energy aroused the interest of the geochemists. A. F. Kapustinskii derived a formula for calculating the lattice energy, which received wide recognition from crystallographers and chemists. A. E. Fersman developed the application to geochemistry of what had been learned concerning lattice energy.

With the transfer of the Academy of Sciences to Moscow (1934) the interest in crystallographic research in our country increased considerably.

The Crystallographic Section of Lomonosov Institute of the Academy of Sciences of the USSR became the center for all crystallographers of the country. However, the work of the section did not get adequate scope at the Geological Institute; therefore, in 1937, the section was reorganized into an independent Crystallographic Laboratory of the Academy of Sciences of the USSR, which was to make a firmer bond between physics, chemistry and technology. The first branch crystallographic laboratory was organized simultaneously in Trust No. 13 of the Ministry of Electrical Industry, which made for a considerable expansion of applied research. The crystallographic laboratory was converted into the Institute of Crystallography of the Academy of Sciences of the USSR in the Division of Physicomathematical Sciences (1944).

The most important property of crystals is their symmetry. For a long time after E. S. Fedorov the opinion persisted that the study of crystal symmetry had been brought to its logical conclusion by the derivation of the 230 groups. Shubnikov gave a new impetus to the study of symmetry by introducing the concept of antiequal figures, and correspondingly of antisymmetry. Antisymmetry found application in the study of crystal structure. Lately, N. V. Belov showed the possibility and the logic of the further development of Shubnikov's ideas by introducing the "multicolored" groups of symmetry. Shubnikov's students, I. S. Zheludev and V. A. Koptsik, began to develop ideas of symmetry in the new direction of crystal physics. A. V. Shubnikov's books "Symmetry" and "Symmetry and Antisymmetry of Finite Figures" were devoted to the popularization of the study of symmetry.

To the theory of symmetry is connected the study of simple crystal forms, apparently already fully developed in the old classical crystallography. A. V. Shubnikov introduced the concept of the material figure. This idea was further developed by G. B. Bokii who gave the derivation of all the physically different simple forms. I. I. Shafranovskii's work was the logical continuation of these studies; he derived all the structural variations of the simple forms (1403 forms). By comparing these with simple forms, I. I. Shafranovskii and V. I. Mikheev introduced the concept of the simple edge forms.

Also concerning the theory of symmetry is V. I. Mikheev's work on the homology of crystals, in which one of Fedorov's ideas is developed.

Research on the physical properties of crystals was greatly developed at the Institute of Crystallography. Studies made under the direction of M. V. Klassen-Nekliudova (V. R. Regel', M. A. Chernysheva, G. E. Tomilovskii, V. L. Indenbom) on the mechanical strength, plasticity, twinning and also on the dislocations in crystals should be noted, as well as numerous studies on the artificial twinning and untwinning of quartz crystals (E. V. Tsinzerling), studies concerning the electrical properties of crystals (especially ferroelectric crystals) under Shubnikov's direction (I. S. Zheludev, V. P. Konstantinova), studies on light absorption in crystals (S. V. Grum-Grzhimailo, N. M. Melankholin, L. G. Chentsova) and of others.

Until 1935 there was almost no research in the USSR on the determination of the fine structure of crystals. X-ray diffraction studies were limited mainly to work on the identification of crystalline substances by the Debye pattern method and also to the study of stresses in metallic alloys (S. T. Konobeevskii, V. I. Iveronova, M. I. Zakharova).

From 1935 on, ranks of crystal structure specialists began to form: N. V. Belov, B. K. Brunovskii, G. S. Zhdanov, A. I. Kitaigorodskii, G. B. Bokii, M. A. Porai-Koshits. N. V. Belov's monograph, "The Structure of Ionic Crystals and Metallic Phases" generalized the results of preceding works on structure analysis and gave a new impetus to the development of the principle of close packing of structural units. For the first time important

methods of harmonic analysis for the study of crystal structure were made familiar and put into daily practice at the x-ray laboratory of the Institute of Crystallography. N. V. Belov's and V. P. Butuzov's set of "strips" together with the manual for their application were adopted in all the crystallographic laboratories of the USSR. For the first time the so-called direct methods of crystal structure interpretation were introduced. I. M. Rumanova suggested an original modification of this method, and her method has already been applied to interpret the structures of several crystals (E. G. Fesenko, Kh. S. Mamedov). The laboratory issues annually "Outlines of Structural Mineralogy," of which 37 have appeared.

Owing to Belov's work, structural crystallochemical concepts penetrated into inorganic and organic chemistry, mineralogy and geochemistry. He made a great contribution to the study of the structure of silicates. A large number of crystalline structures had been interpreted, and new types of silicon-oxygen radicals discovered: two-storied rings and chains, more complex than those in pyroxenes or in amphiboles. In addition to Belov's laboratory, a series of large Soviet x-ray structural laboratories were set up: G. S. Zhdanov's (one of the first specialists in structural analysis in the USSR) Karpov's at the Physicochemical Institute, G. B. Bokii's at the Institute of General and Inorganic Chemistry, M. A. Porai-Koshits' in the Medical Department of the Moscow State University, and A. I. Kitaigorodskii's at the Institute of Organic Chemistry. Lengthy monographs appeared dealing with x-ray structural analysis and crystal chemistry (G. S. Zhdanov, Ia. S. Umanskii, N. V. Belov, G. B. Bokii, M. A. Porai-Koshits, A. I. Kitaigorodskii).

Electron diffraction developed rapidly in the USSR. Under the direction of Z. G. Pinsker (who constructed an electron diffraction apparatus with great resolving power), and with B. K. Vainshtein's cooperation, electron diffraction was applied for the first time to the complete determination of a series of structures. Z. G. Pinsker's monograph "Electron Diffraction" translated into English, contributes to the publicizing of the methods worked out in the USSR for electron diffraction structural analysis. B. K. Vainshtein's great achievement was the practical determination of the location of hydrogen atoms in organic crystals. When atoms of heavy metals are present, the location of hydrogen atoms is determined by the electron diffraction method much more simply than it would be by x-ray diffraction.

Dozens of candidates' and series of doctors' dissertations defended during the last 20 years prove that we have caught up with foreign countries in the realm of crystal structure research.

Experimental and theoretical work on the growth of crystals is being developed. In this field Shubnikov's pioneer studies must be noted: on the determination of the equilibrium shape of crystals, artificial formation of twins, crystallization pressure, formation of spherulites, the nature of vicinal faces and other studies, generalized in the monographs "How Crystals Grow" (1935) and "Formation of Crystals" (1949).

These studies were continued and broadened by A. V. Shubnikov's and especially by G. G. Lemmlein's students. Lemmlein carried through a series of refined analyses on the morphology of quartz and traced experimentally the formation of vicinal faces on soluble crystals. He was one of the first to establish the spiral structure of vicinal faces and to reproduce experimentally a series of spiral growth processes for crystals. In cooperation with N. V. Gliki he showed the connection between the polytype phenomena and the processes of crystal growth, using silicon carbide crystals as examples. He developed the "dew method," which makes it possible to detect the details of the spiral structures on the surfaces of crystals, including growth steps 10 A high. Lemmlein studied and cinematographed "the life" of the tiniest inclusions of mother liquor in crystals at variable temperatures, and showed that these inclusions move along the crystal, become transformed, united and finally take an equilibrium shape. It was made clear that these processes are of great significance in nature and in technology.

G. G. Lemmlein's remarkable book "The Zone Structure of Crystals" (1948) teaches crystallographers and mineralogists to approach each crystal as though it were an individual with its own history of formation and development recorded in its morphological peculiarities, especially in its numerous tiniest inclusions, scattered throughout its body. The correct use of crystals in physics and technology is impossible without taking into account all these peculiarities.

A. V. Shubnikov's work on the growth of single crystals was continued at the Institute of Crystallography by: N. N. Sheftal (single crystals of saccharose, Seignette's salt and quartz, and single-crystal films of germanium and silicon), S. K. Popov (apparatus for the synthesis of single crystals by Verneuil's method) of rod- and block-like ruby, application of rods to prepare thread guides in the fiber industry), V. P. Butuzov (the synthesis of quartz

and the apparatus for this purpose and for carrying out phase transformations at superhigh pressures), B. V. Vitovskii (thermostat-chambers, crystals of Seignette's salt), L. M. Beliaev with B. V. Vitovskii and G. F. Dobrzhanskii (luminescent crystals for scintillation counters). A considerable part of these researches has been incorporated into manufacturing and has become the basis for the industrial growing of crystals.

Among research works done outside of the Institute, A. V. Stepanov's studies of the industrial synthesis of optical crystals of alkali halides and of fluorite must be noted; also, a series of studies by young specialists on the growth of piezoelectric crystals: O. M. Ansheles and A. A. Shternberg's work on "dynamic" growing of crystals (Seignette's salt and piezoelectric quartz crystals), P. G. Pozdniakov's and A. A. Shternberg's (crystals of ammonium hydrogen phosphate and of other water-soluble crystals).

As a result of all these studies the Soviet Union had at its disposal, during the Second World War, facilities for the industrial manufacture of Seignette's salt crystals, precious corundum and optical single crystals, and, at present, also of a series of water-soluble, piezoelectric and optical crystals, fluorite, luminescent crystals and of piezoelectric quartz.

The work on the growing of single crystals is combined with the theoretical and experimental study of the growth mechanism, the morphology and the face sculpture of crystals (G. G. Lemmlein and his group — on the growth of organic crystals, N. N. Sheftal — on saccharose, quartz, real crystal formation, V. P. Butuzov, N. Iu. Ikornikova — on quartz).

A varied application in technology has been found for synthetic single crystals. Let us indicate A. S. Shein's piezocrystalline elements of crystalline potassium sodium tartrate which are used for preparing piezoelectric microphones, telephones, adapters, loud-speakers, hydroacoustic transformers, and so forth, and also piezoelectric apparatus of the central scientific laboratory of piezotechnology.

Research on obtaining and studying piezoelectric textures started by A. V. Shubnikov with A. S. Shein was carried out parallel with the work on single crystals. Optical textures of the polaroid type were also widely developed (G. I. Distler). Polaroids for different regions of the spectrum were worked out, especially thermostatic ones for visible light.

Studies made by Soviet crystallographers on the construction of quartz astronomical light filters and bent crystalline films for x-ray spectrographs should also be noted (A. B. Gilvarg).

The State Optical Institute accomplished a great deal in furthering the application of single crystals.

New chairs of crystallography have been created in recent years: at Gorkii University (N. V. Belov), in the chemistry and geology departments of Moscow University (G. B. Bokii), in the department of physics of Moscow University (A. V. Shubnikov). Microcrystallography was given the first place in the teaching of geometric crystallography. The new chairs became the centers of scientific research on the theory of symmetry (thus, at Gorkii University, the complete number (1651) of Shubnikov's symmetry groups was established), structural analysis, crystal growth, the study and application of the physical properties of crystals. The tensor description of the physical properties of crystals occupied an important place in physical crystallography.

At present, in our country, crystallography is emerging on a new and a broader path of development. Side by side with the Institute of Crystallography arise new centers devoted to the growing and study of crystals.

An important number of institutes was set up in connection with the development of semiconductors. The study of the growth of crystals is being expanded in metallurgical, silicate, physics of metals, geophysical and chemical institutes.

The journal "Kristallografiia" began to appear in 1956. Contacts with international crystallographers are widening. At conferences held in the USSR on crystal chemistry and the growth of crystals, scientists of the following countries were present: Bulgaria, Czechoslovakia, Poland, German Democratic Republic, China. In the current year, a large group of Soviet scientists was dispatched to Czechoslovakia to attend the conference on single crystals.

Soviet scientists also take part in congresses organized by the International Union of Crystallographers. At the recent general assembly of this union N. V. Belov was unanimously elected its vice president.

Thus, crystallography in the Soviet Union is acquiring the status of a great science with a ramified net of institutes closely connected with life. In this lies its future progress.

ON THE INITIAL FORMS OF SPHERULITES

A. V. Shubnikov

The article describes various forms of spherulites in the initial period of their formation from many nuclei concentrated at one "point," or from one single-crystal (acicular or tabular) nucleus by its splitting up. The conditions are described under which one or the other initial form of the spherulite appears.

It is known that a spherulite can appear in a supercooled viscous liquid either from many crystal nuclei concentrated at one "point," or from a single-crystal nucleus by its splitting up.

In the first case the formation of the spherulite is governed by a purely geometric factor: the fact that each crystal nucleus can grow in only one direction – along the radius from the given "point" [1]. Under these conditions there is a kind of "struggle for existence" among the growing crystals, as a result of which the only "survivors" are those which by the law of geometric selection [2, 3, 4] are oriented with the directions of greatest radial growth velocity along the radius of the spherulite. As a whole, such a spherulite will be a radially textured crystal aggregate with an isotropic (nontextured) nucleus.

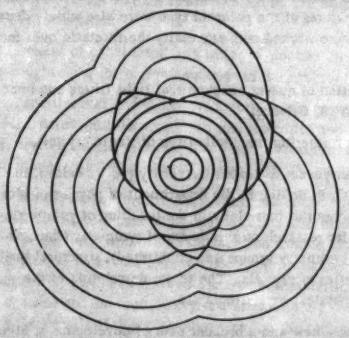

Fig. 1. A trefoil formed by the appearance at three random points on the surface of a growing spherulite of three new spherulites (another crystallographic modification of the same substance) which are growing with greater speed.

The possibility is not excluded of the appearance at one or at several points on the surface of a growing spherulite of new spherulites, which belong to a different polymorphic modification of the crystallizing substance. If the rate of growth of the new spherulites is greater than that of the initial one, the latter will be covered by the new spherulites and will acquire a form which is in section like one, two or several leaflets formed by intersecting logarithmic spirals (Fig. 1) [5, 6].

When the spherulite has been formed from one microcrystal by its branching, the initial spherulite must be of different form depending on whether the microcrystal was of an acicular or a tabular habit. We shall consider each of these cases separately.

If the spherulite is formed from an acicular or prismatic crystal, and if this event is observed under a microscope in the thin layer of melt between the objective and the cover glass, under such conditions that the crystal is forced because of its length to be oriented in the plane of the preparation, the splitting up of the crystal is accompanied by the formation of a two-leafed form. The latter can consist either of extended leaves, or of round eyes ([8], p. 29), or, as was observed by us, of two spiral curls [9].

We shall determine the conditions under which each of these two-leafed forms is produced.

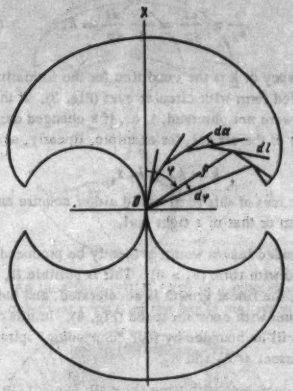

Fig. 2. A drawing illustrating the law of the formation of a two-leafed form with circular "eyes."

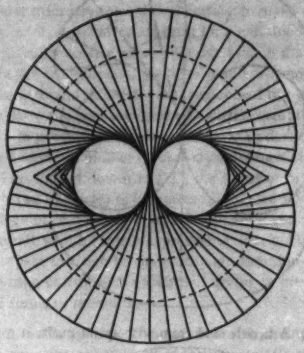

Fig. 3. A two-leafed form with circular "eyes."

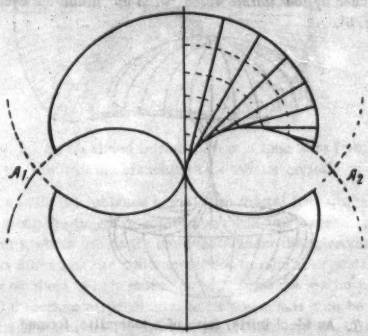

Fig. 4. A two-leafed form with extended leaves.

We assume that we have an acicular crystal of length dl, situated at O and parallel to the X axis (Fig. 2). We assume that as the crystal continues to grow it splits up at both ends into a mass of branches which form a continuous crest.

If the two-leafed form has circular eyes with a diameter a, then the curve of this form can be represented by the equation

$$\rho = a \sin \varphi,$$

which is the equation in polar coordinates of a pair of circles, if the coordinate origin is at O and the initial line along the X axis. It is important to note the following property of the circles. If we divide the circles up into equal elements dl, then all the angles $d\alpha$ formed between each pair of adjacent elements will be the same, and will be twice the corresponding angles $d\varphi$:

$$d\alpha = 2d\varphi.$$

Let the length l of the crystal and of all its branches increase with constant velocity

$$v_1 = \frac{dl}{dt},$$

then the branching occurs simultaneously with an angular velocity which can evidently be expressed as

$$v_2 = \frac{d\alpha}{dt} = 2\frac{d\varphi}{dt}.$$

In the case considered it can be seen that the ratio of these velocities remains constant during the formation of a spherulite:

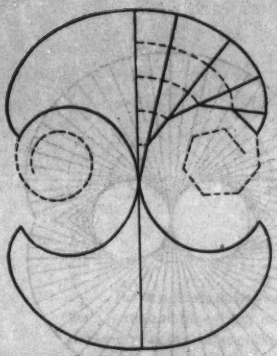

Fig. 5. A two-leafed form with spiral curls.

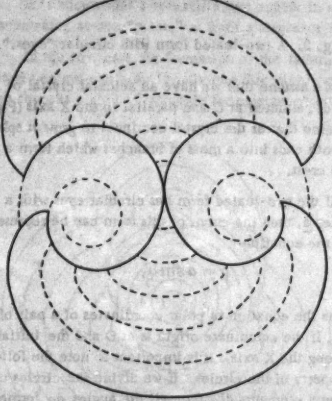

Fig. 6. A two-leafed form in which each eye is made up of half of a spiral curl and half of a circle.

$$\frac{v_1}{v_2} = \frac{dl}{da} = \frac{1}{2}\frac{dl}{d\varphi} = k. \qquad (1)$$

The constancy of k is the condition for the formation of a two-leafed form with circular eyes (Fig. 3). If this condition were not observed, i. e., if k changed during the growth of the crystal, for example, linearly, as

$$k = k_0 + k_1 t,$$

then the leaves of this form would either acquire an extended form or that of a tight curl.

Extended leaves would evidently be produced if k increased with time ($k_1 > 0$). This is possible if, in particular, the linear growth is accelerated, and the branching continues with constant speed (Fig. 4). In this case the form will be bounded by four "unwinding" spirals which intersect at A_1 and A_2.

If k decreases with time ($k_1 < 0$), i. e., if, in particular, the linear growth continues with constant speed, while the branching is accelerated, the form will be bounded by four spirals which "wind up" inside the eyes (Fig. 5).

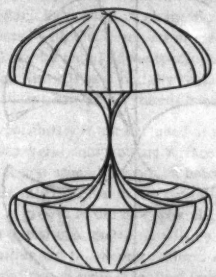

Fig. 7. An ideal initial form of a spherulite, formed from an acicular microcrystal with the same branching in all directions perpendicular to its length.

Actually, the formation of a spherulite never follows the above laws exactly. It is therefore not impossible that one of the branches of the leaf of this form should be extended or round, while the other is curled up inside the eye (Fig. 6), and this is often observed experimentally.

The described shapes of these two-leafed forms are, of course, only plane sections of those three-dimensional figures, the form of which a spherulite must take in the initial stages of its development, when it is formed from a prismatic or an acicular crystal, provided that it is given equal opportunity to grow in all spatial directions. If we assume that a prismatic crystallite has the same opportunity to branch in any direction perpendicular to its length, and that each of its branches has the same property, then the spatial form of the nucleus of a spherulite must be given by a figure of revolution of the two-leafed form about an axis along the length of the crystal nucleus (and not perpendicular to this direction, as was assumed by Matschinski [10]). In practice it is probable that this assumption is not strictly true, and as a result we must also include in the possible forms of the nucleus of a spherulite those in which the corresponding symmetry of the single crystal (Fig. 8) is reflected. The production and investigation of such forms is a matter for future work.

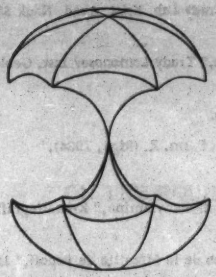

Fig. 8. An idealized initial form of a spherulite formed from a columnar crystal of the hexagonal system.

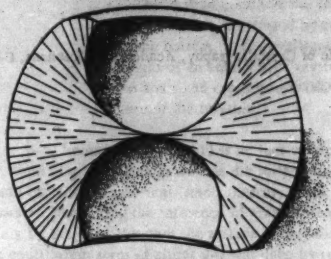

Fig. 9. An idealized initial form of a spherulite formed as the result of the branching of a tabular crystal.

As regards spherulites formed by the splitting up of tabular microcrystals, it is necessary to make the following point. First of all, it must be ascertained whether such spherulites really exist. We can assume that they include the spherulites of graphite which are known to metallurgists and mineralogists, spherulites of pyrophyllite, chlite, and possibly those of azurite, campilite and others. In general, it seems probable to us that the well-known distorted forms of tabular crystals, such as saddle-shaped crystals of dolomite [11], the forms of twisted crystals (an iron rose) of hematite , etc., are initial forms of undeveloped spherulites and that under given conditions any crystal with a clearly expressed tabular habit (a large repeat distance in one particular direction) and with a high plasticity is capable of giving in growth the initial forms of spherulites.

It is also important to point out that the direct observation of the splitting up of tabular crystals of easily melted substances under the microscope in a thin layer of melt between the objective and the cover glass is hindered by the fact that under these conditions the crystal plates are always oriented parallel to the plane of the preparation. Therefore, the initial forms of the spherulites described below must be regarded as being hypothetical to a certain extent.

It can be theoretically predicted that the branching of a tabular crystal must produce initial forms of spherulites which have definite similarities with and points of difference from those which were described above as being due to the branching of an acicular crystal. The main resemblance is that both spatial forms, when a section is made along the major axis of the crystal (this is along the length of acicular crystals and perpendicular to the plane of the tabular ones), must give two-leafed forms, which are easily observable under the microscope in the branched acicular crystals, and which are not observable under the same conditions in tabular crystals. Two-leafed forms of approximately the same shape must be obtained in both cases. In both cases the spatial forms for a more or less uniform branching of the crystal in all directions perpendicular to its major axis must be a body of revolution of the two-leafed form about the major axis of the crystal. However, for tabular crystals, this axis is not the perpendicular to the length of the two-leafed form, drawn through its center, as for the acicular crystals, but is the long axis itself (that which Matschinski mistakenly took as the axis of revolution of an initial form of a spherulite produced from an acicular crystal (Fig. 9).

When for some reason or other the symmetry of the tabular crystal has a greater influence on the initial form of the spherulite being formed from it, the form may differ considerably from a surface of revolution. The distorted forms of crystals of dolomite and campilite which are described in the literature can evidently serve as examples of such initial forms of spherulites ([8], pp. 37, 40).

LITERATURE CITED

[1] A. V. Shubnikov and G. G. Lemmlein, "On the orthotropism of crystal growth," Doklady Akad. Nauk SSSR 61 (1927); Z. Krist. 65, 297 (1927).

[2] R. Gross and H. Möller, "Ueber das Kristallwachstum in röhrenförmigen Hohlräumen," Z. Physik 19, 375 (1923); Neues Jahrb. Mineral. 53, 117 (1925).

[3] H. Möller, Die Gesetze des Keim- und Kristallwachstums mit besonderer Berücksichtigung der Keimauslese und des orientierten Kristallwachstums (Dissertation) (Greifswald, 1924).

[4] A. V. Shubnikov, "On the Gross-Möller selection principle," Trudy Lab. Krist. Akad. Nauk SSSR 2, 119 (1940).

[5] A. V. Shubnikov, "The equation of B. Popov's two-leafed form," Trudy Lomonosov Inst. Geokhim. Krist. i Mineral. 8, 5 (1936).

[6] A. V. Shubnikov, The Formation of Crystals [in Russian] (1947).

[7] B. Popov, "Sphärolithenbau und Strahlungskristallisation," Latv. Farm. Z. (Riga, 1934).

[8] F. Bernauer, 'Gedrillte' Kristalle (Berlin, 1929).

[9] A. B. Shubnikov, "On the peculiarities of the crystallization of diphenylamine," Kristallografiia 1, 3, 374 (1956).

[10] M. Matschinski, "Deux hypothèses sur les causes de la formation de la bifeuille de Popoff," Lincei-Rend. Sci. fis. mat. et nat. 19, 64 (1955).

[11] A. G. Betekhtin, Mineralogiia (1950), pp. 131, 806 (pyrophyllite), 204 (graphite), 365 (hematite), 512 (dolomite), 641 (chlite).

Received May 3, 1957

Institute of Crystallography, Academy of Sciences, USSR

ON THE EQUILIBRIUM FORM OF CRYSTALS IN A GRAVITATIONAL FIELD

A. V. Beliustin

This article considers the influence of gravity on the equilibrium form of a crystal which is bounded by cubic or rhombohedral faces and which is situated at the bottom of a crystallization dish. A formula is obtained which relates the height of an equilibrium crystal with its cross section. The changes in form of free and fixed crystals of $NaNO_3$ are investigated for variations in the temperature of the solution.

As is known, when a liquid is subject only to the forces of surface tension it takes up a spherical form. If the force of gravity acts as well as the surface tension, the equilibrium form is different, although in certain cases it can be close to spherical (small mercury drops on glass). To a certain extent an analogous situation exists for crystals. Neglecting the influence of gravity we may experimentally find an equilibrium form which is determined solely by the condition that the surface energy should be a minimum. Thus, for example, in the determination of the equilibrium form of alums this was done by rotating the crystal [1].

If the crystal is simply lying at the bottom of a crystallization dish, then the thermodynamic condition for equilibrium is that the free energy should be a minimum; this free energy consisting of the surface energy and the potential energy in a gravitational field.

We consider the particular case in which the cube faces alone are possible (the others do not appear because they have a considerably greater surface energy). Let the crystal rest on a cube face and have the form of a square platelet, with height h and side a. Let the crystal density be ρ_1 and that of the solution be ρ_2, and the acceleration due to gravity be g; we obtain for the potential energy of the platelet

$$V = \frac{1}{2} g (\rho_1 - \rho_2) a^2 h^2. \tag{1}$$

We shall express the surface energy differently, depending on whether the crystal has grown onto the bottom or is just resting on it. First we shall consider the case when the crystal rests on the bottom only at a few points and over most of its lower surface is separated from the bottom by a thin layer of the surrounding medium (i. e., the solution). Thus, assuming that the crystal is completely surrounded by the solution, we find for the surface energy:

$$W = (2a^2 + 4ah)\sigma_{12}. \tag{2}$$

Here σ_{12} is the surface energy per cm^2 at the crystal-solution interface. Replacing h in the expression for the free energy $F = V + W$ by $\frac{v}{a^2}$, where v is the volume of the platelet, we have:

$$F = \frac{1}{2} g (\rho_1 - \rho_2) \frac{v^2}{a^3} + 2\sigma_{12} (a^2 + 2\frac{v}{a}). \tag{3}$$

For a given volume the condition for a minimum of the free energy is

$$\frac{dF}{da} = -g(\rho_1 - \rho_2)\frac{v^2}{a^3} + 4\sigma_{12}\left(a - \frac{v}{a^2}\right) = 0. \tag{4}$$

After multiplying by a^3 and substituting $a^3 = \frac{V}{h}$ we have the following equation:

$$\frac{h}{a} = \frac{a}{a + \alpha v}, \tag{5}$$

Here $\alpha = \frac{g(\rho_1 - \rho_2)}{4\sigma_{12}}$.

Hence, the ratio between the height and the breadth of the equilibrium crystal increases as the difference in densities between the crystal and the solution decreases, as the surface energy per unit area increases, and also as the volume of the crystal decreases.

When the crystal has grown onto the bottom of the dish, we have instead of (2):

$$W = (a^2 + 4ah)\sigma_{12} + a^2\sigma_{13} + (s - a^2)\sigma_{23}. \tag{6}$$

Here σ_{13} and σ_{23} are the surface energies per cm^2 for the interfaces crystal-bottom and solution-bottom, respectively, and s is the area of the bottom. As before, by using the condition $dF/da = 0$ and carrying out the corresponding algebra, we find instead of (5):

$$\frac{h}{a} = \frac{\beta a}{a + \alpha v}. \tag{7}$$

Here α is defined as before and $\beta = \frac{1}{2} + \frac{\sigma_{13} - \sigma_{23}}{2\sigma_{12}}$. The conclusions drawn from (5) are evidently still valid.

If the crystal is rhombohedral (correspondingly the platelet takes the form of an inclined prism), then instead of (5) we have

$$\frac{h}{a} = \frac{a}{ka + \alpha v}, \tag{8}$$

where $k = \frac{1}{\cos\delta}$ and δ is the angle between the sloping face of the rhombohedron and the vertical.

Finally, when a rhombohedral crystal sticks to the bottom we have

$$\frac{h}{a} = \frac{\beta a}{ka + \alpha v}. \tag{9}$$

The formulas obtained, especially (5) and (8), are of considerable interest because of the possibility of their use in the determination of the values of the free surface energy σ_{12} at the crystal-solution (melt) interface. This can of course be done under conditions which approximate closely enough to the equilibrium form, provided the crystals are measured with sufficient relative accuracy. In connection with this, experiments were carried out with the aim of finding methods of producing reasonable-sized crystals which were as close as possible to equilibrium. At the same time some of the conclusions which follow from the above formulas were tested.

Rhombohedral crystals of sodium nitrate ($NaNO_3$) were used in the investigations. Just as in [1] temperature oscillations were used, but for a crystal resting on the bottom of the dish these led to an increase in area as a consequence of reduction in height, and this is explained by the action of concentration currents [2]. In the final stage of the process the crystals often reached a diameter of 2-3 mm. In other respects the conditions given in [3] for obtaining the equilibrium form more quickly and more reliably were observed. Cylindrical cavities of diameter

2.5 and 4.5 mm, depth 1.5 to 2.5 mm in sheets of plexiglas were used as crystallization dishes. At the bottom of each of these was placed a small crystallite of $NaNO_3$. Then a small amount of an unsaturated aqueous solution of the same substance was introduced. The depth of the layer of solution was 1-1.5 mm. The dish was closed by a cover glass and the gap between this and the top of the crystallization dish was filled with vaseline, so that the solution was sealed off. After preparation in this way the chamber was placed alternately in contact with water at temperatures of $20°C + \Delta t$ and $20°C - \Delta t$. In different experiments $\Delta t = 1, 3, 5°C$. The dish was maintained at the given temperature for 5 min. Every 60 min (sometimes 30 or 120 min) the horizontal dimensions of the crystal were determined under the microscope, and in some cases the length of the projection of the inclined faces was also measured, in order that the height of the crystal could be estimated.

At first, experiments were made on crystals which were lying freely on the bottom. It was established that the process of expansion of the crystal consists of two stages. In the first, an increase in the horizontal dimensions is accompanied by a decrease in the height of the platelet, then the process of reduction in height slows down and gradually stops altogether. At the same time the distortions of the faces which are at first observed disappear. In the second stage the expansion proceeds fairly smoothly and is not accompanied by a decrease in height. This is possible because of the appearance of a cavity on the lower side of the crystal, which in its turn is explained by the precipitation of material around the edge of the lower side of the crystal and the raising of the crystal which accompanies this. As the crystal expands, its pressure per unit area on the bottom decreases and the deposition of material on the lower surface is made easier. Simultaneously the concentration currents, which bring about quicker dissolution from the top surface, become weaker. Thus we arrive at an explanation of the fact that the reduction in height of the crystal gradually ceases.

A crystal with a cavity must not of course be considered to be in equilibrium. With the aim of eliminating these cavities, experiments were made in which the crystallization dish, together with the crystal, was periodically turned over. As a result of this the lower face of the crystal became the upper and became smooth as the processes of growth and dissolution were reversed. In this case, as distinct from the previous one, the expansion of the crystal eventually ceased altogether, and it acquired a certain limiting form. However, the horizontal dimensions of the platelet which was obtained were dependent on the amplitude of the temperature oscillations: the greater the amplitude, the broader the resultant crystal. Consequently, the limiting form is not yet in general the equilibrium one. However, we may conclude from general thermodynamic considerations that the form is nearer to equilibrium, the slower the temperature changes, i. e., the smaller the amplitude of its oscillations for a given period. Since the platelets obtained for amplitudes of 5 and 1°C differed in size by less than 10%, the application of temperature oscillations to a crystal subject to gravity may be considered a useful method for obtaining forms which are very close to equilibrium.

Further experiments were made with platelets which were fixed to the bottom of the crystallization dish. Since $NaNO_3$ crystals do not adhere to the bottom, they were glued at the center of the base with glue BF-2. It was established that when the crystal was in a solution whose temperature was varied as above, its expansion eventually ceased altogether: as in the previous case the crystal takes up a limiting form. This latter again depends on the amplitude of the temperature oscillations: the larger the oscillations the flatter the crystal becomes. The crystal comes closer and closer to its equilibrium form, in the last stage at least, as the processes of dissolution and growth are carried out more and more slowly.

The results of the measurements on the almost-equilibrium crystals of $NaNO_3$ which we obtained confirmed the deduction from (8) and (9) that the ratio h/a decreases as the crystal volume increases. Also the height of equilibrium fixed crystals was considerably less than that of free crystals of the same horizontal dimensions, which confirms the role of the coefficient β in (9). It seems that β differs little from $1/3$.

Sufficiently accurate quantitative data can not yet be given because of the inaccuracy of the measurements of the height h (this was estimated from the size of the projection of the inclined face of the rhombohedron). It is possible that sufficient accuracy in the measurement of h will only be obtained by using larger crystals, but this leads to a considerable increase in the time needed to reach the equilibrium form (in our experiments this time varied from a few hours to several tens of hours).

SUMMARY

1. From the condition that the sum of the surface and the potential energy of a crystal at the bottom of a crystallization dish should be a minimum, we derived formulas which relate the height and breadth of free or fixed cubic (rhombohedral) crystals which are in equilibrium.

2. The formulas obtained may be used to determine the surface energy of crystal-solution (melt) interfaces.

3. The processes of the change in form of a free crystal, situated at the bottom of a crystallization dish and subjected to the action of temperature oscillations, eventually ceases altogether if the upper and lower faces of the crystal are made to change places periodically. The limiting form which is obtained depends on the amplitude of the temperature oscillations.

4. A crystal which is fixed to the bottom and subject to oscillations of temperature also acquires a certain limiting form which depends on the amplitude of the oscillations.

5. Small amplitudes of temperature oscillation give a form close to equilibrium for both free and fixed crystals.

The author thanks A. V. Shubnikov for his examination of the article and for discussion of the points which were raised.

LITERATURE CITED

[1] A. V. Shubnikov, Crystal Growth [in Russian] (1935), p. 203.

[2] A. V. Shubnikov, The Formation of Crystals [in Russian] (1947), p. 54.

[3] G. G. Lemmlein, "On the problem of the experimental conditions necessary for obtaining crystals of equilibrium form," Doklady Akad. Nauk SSSR 98, 6, 973 (1953).

Received January 30, 1957

Institute for Research in Technical Physics, Gor'kii University

THE MACROSCOPIC THEORY OF THE FORMATION OF DISLOCATIONS IN CRYSTAL GROWTH

V. L. Indenbom

The formation of dislocations in the process of crystal growth is treated not as a chance process, connected with errors in growth, but as a necessary consequence of the nonuniform temperature distribution in the growing crystal: it is only because of the formation of dislocations that the incompatible temperature deformations do not lead to thermoelastic strains. The macroscopic dislocation density due to a temperature distribution $T = T(x)$ is characterized by the tensor

$$\hat{\beta} = -\text{grad}\, T \times \hat{\alpha},$$

where $\hat{\alpha}$ is the tensor representing the thermal expansion coefficients of the crystal. In the simple cubic lattice the diagonal terms of $\hat{\beta}$ correspond to the density of screw dislocations, while the off-diagonal terms correspond to the densities of edge dislocations.

The theory which is developed is applicable not only to crystal growth, but also to zone melting, case-hardening, and even to the process of cooling a crystal after tempering. In the last two cases the dislocations are not formed as a result of displacement of growing atomic planes, but as the result of the incompatibility of the plastic deformations.

INTRODUCTION

Up to the present, the basic problems of the formation of screw dislocations in growing crystals have been studied in detail by many workers. The recent papers of Lemmlein and Dukova [1, 2] consider the detailed mechanism of the formation of screw dislocations in the growth of the branches of a dendritic crystal, and they point out a series of interesting effects which are connected with the interaction of dislocations. We must suppose that the Lemmlein-Dukova mechanism can explain the formation of edge as well as screw dislocations. In the former case, the dislocation does not become a center of spiral growth, but can be discovered by other methods, for example, from the strain field [3].

The usual approach to the formation of dislocations as a chance act connected with certain "growth errors" does not enable us to establish a relation between the dislocation density and the conditions of crystal growth. This question does not play an important role in the theory of growth, since the rate of crystal growth does not depend on the number of screw dislocations. The dislocation density is however of decisive significance in the study of the real structure of crystals and of their structure sensitive parameters (for example, hardness, plasticity, conductivity, etc.) [4].

Recently, Billig [5], starting from a qualitative analogy with plastic deformation, showed that the dislocation density N, brought about by growing a crystal by the Kyropoulos method, is described by the formula

$$N = \frac{\alpha}{b} \frac{\partial T}{\partial r}, \qquad (1)$$

where $\underline{b}$ is the magnitude of the Burgers vector, α the linear thermal expansion coefficient, and $\frac{\partial T}{\partial r}$ the radial temperature gradient in the crystal. The author stipulated neither the direction of the dislocation lines nor the direction of the Burgers vector.

The present paper attempts to refine Billig's qualitative considerations and to establish an accurate relation between the distributions of dislocations and of temperature in a growing crystal.

The Macroscopic Dislocation Density Tensor

Following Bilby [6, 7] and Kröner [8, 9] we shall consider the dislocation density macroscopically, averaging it over an area which intersects a large number of individual dislocations. In this case the dislocation density may be represented by a tensor of the second rank $\hat{\beta}$, the components of the $\underline{i}$th row of which are numerically equal to the components of the total Burgers vector of all the dislocations which intersect unit area perpendicular to the $\underline{i}$ axis. For an area of arbitrary orientation with unit vector $\mathbf{n}$ normal to it the total Burgers vector is evidently equal to the product of the vector $\mathbf{n}$ and the tensor $\hat{\beta}$:

$$\mathbf{b} = \mathbf{n}\hat{\beta} \tag{2}$$

or in expanded form

$$b_k = n_i \beta_{ik}. \tag{2'}$$

As is known (see, for example, [4]) the Burgers vector of any dislocation must be a translation vector of the lattice and can be represented as an algebraic sum of $\mathbf{t}$-vectors — translation vectors which are of minimum length and which are independent in the sense that none of them can be represented as either the sum or the difference of other $\mathbf{t}$-vectors. A unit dislocation has a Burgers vector which, neglecting sign, coincides with one of the $\mathbf{t}$-vectors. If we separate all the possible types of unit dislocation for a given crystal, the tensor $\hat{\beta}$ can be split up into a sum of multiplicative tensors, each of which corresponds to the density of unit dislocations of a given type, i. e.,

$$\hat{\beta} = \mathbf{N}^{(j)} \cdot \mathbf{b}^{(j)}. \tag{3}$$

Here $\mathbf{N}^{(j)}$ is the flux density of dislocations with Burgers vectors $\mathbf{b}^{(j)}$, while $\mathbf{b}^{(j)}$ covers all possible $\mathbf{t}$-vectors. The period in Eq. (3) denotes dyadic vector multiplication [10], so that the expanded form of (3) is

$$\beta_{ik} = N_i^{(j)} \cdot b_k^{(j)}. \tag{3'}$$

Even though there is no difficulty in calculating the tensor $\hat{\beta}$ from the known densities of dislocations of each type, a unique solution of the inverted problem without introducing additional considerations is possible only for the case of three noncoplanar $\mathbf{t}$-vectors. The problem has much in common with that of obtaining dislocation models for grain boundaries with a given disorientation [4]. Proceeding by analogy, we first construct the reciprocal triad $\tilde{\mathbf{b}}^{(j)}$ to the noncoplanar vectors $\mathbf{b}^{(j)}$ such that

$$\mathbf{b}^{(i)}\tilde{\mathbf{b}}^{(j)} = \delta_{ij}. \tag{4}$$

To do this it is sufficient to put

$$\tilde{\mathbf{d}}^{(1)} = \frac{\mathbf{b}^{(2)} \times \mathbf{b}^{(3)}}{\mathbf{b}^{(1)}\mathbf{b}^{(2)}\mathbf{b}^{(3)}}. \tag{5}$$

$\tilde{\mathbf{b}}^{(2)}$ and $\tilde{\mathbf{b}}^{(3)}$ are found by cyclic permutation of suffices. By multiplying both sides of (3) on the right by $\tilde{\mathbf{b}}^{(j)}$ and taking into account Relation (4), we obtain an equation for the flux density of dislocations of the $\underline{j}$th type

$$\mathbf{N}^{(j)} = \hat{\beta}\tilde{\mathbf{b}}^{(j)} \tag{6}$$

or in expanded form

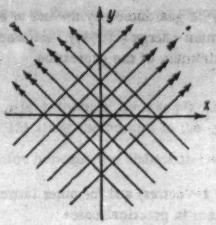

Fig. 1. A square dislocation network, described by the density tensor (9).

$$N_i^{(j)} = \beta_{ik}\tilde{b}_k^{(j)}. \tag{6'}$$

Using (6), we may write the tensor $\hat{\beta}$ as the sum of three multiplicative tensors

$$\hat{\beta} = \beta\tilde{b}^{(j)} \cdot b^{(j)}. \tag{7}$$

$\hat{\beta}$ may be split up most simply for the simple cubic lattice, where

$$\tilde{b}^{(i)} = \frac{b^{(i)}}{b^2}.$$

Here the β_{ik} give directly the density of dislocations which lie along the i axis and which have a Burgers vector along the k axis. The diagonal terms of $\hat{\beta}$ correspond to screw dislocations and the off-diagonal terms correspond to edge dislocations.

It should be emphasized that such a simple interpretation of the physical meaning of the components of the tensor $\hat{\beta}$ cannot be transferred, as was done by Kröner, to a more general case. Figure 1, for example, shows a plane square network of screw dislocations which bisect the angles between the X and Y axes. The Burgers vectors are shown by feathered arrows and the dislocation directions are shown by double arrows. The corresponding dislocation density distribution has the form

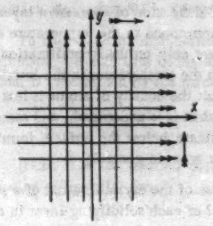

Fig. 2. A square network of edge dislocations equivalent to that shown in Fig. 1.

$$\hat{\beta} = \begin{Vmatrix} 0 & Nb & 0 \\ Nb & 0 & 0 \\ 0 & 0 & 0 \end{Vmatrix}, \tag{9}$$

where N is the density of each group of dislocations; this tensor may be compared with a square network of edge dislocations parallel to the coordinate axes (Fig. 2). Thus, the simplest interpretation of the tensor $\hat{\beta}$ is valid only in the system of coordinates whose axes coincide with those of the simple cubic lattice.*

Even in the body-centered cubic lattice, where the complete system of t-vectors consists of four vectors of the type $^1/_2$ <111>, the splitting up of $\hat{\beta}$ into a sum of multiplicative tensors and the construction of the corresponding dislocation model cannot be carried out uniquely. In fact, Eq. (3) relates the possible changes $\delta N^{(i)}$ in the dislocation density for the ith sort by the condition

$$\delta N^{(i)} \cdot b^{(i)} = 0, \tag{10}$$

i. e., the dislocation model has three extra degrees of freedom which correspond to an arbitrary choice of the vector of the density of dislocations of one of the four types, for example, $N^{(4)}$.

We now construct from (5) the vectors $\tilde{b}^{(j)}$ which form the reciprocal triad to the first three Burgers vectors ($j = 1, 2, 3$). By multiplying both sides of the equation (10) on the right by $\tilde{b}^{(j)}$ we can express the possible changes in the density of dislocations of the jth type in terms of the change in density of those dislocations which have Burgers vector $b^{(4)}$:

$$\delta N^{(j)} = -(b^{(4)}\tilde{b}^{(j)})\,\delta N^{(4)}. \tag{11}$$

Using the solution of (6) as an initial model, we finally obtain

$$N^{(j)} = (\hat{\beta} - N^{(4)} \cdot b^{(4)}) \cdot \tilde{b}^{(j)}. \tag{12}$$

* The first invariant (the trace) of the tensor $\hat{\beta}$ is of course independent of the choice of coordinates, and it may be interpreted as an "average density of screw dislocations."

It is clear that the single-valuedness of the factorization of the tensor $\hat{\beta}$ can only be guaranteed by the use of some additional condition, for example, that the dislocation model should have minimum energy (cf. [4]). Estimating this energy from the total length of dislocation lines, we then have to find the minimum of the expression

$$W(N^{(i)}) = N^{(i)} + \sum_{j=1}^{3} |(\hat{\beta} - N^{(i)} \cdot \mathbf{b}^{(i)})\tilde{b}^{(j)}| \qquad (13)$$

for an arbitrary value of the vector $N^{(i)}$.

The problem is still more complex for the face-centered cubic lattice (six t-vectors) and for other lattices. However, we may expect that considerations of symmetry will simplify the problem in practical cases.

The Appearance of Dislocations in Crystal Growth

Analogously to the way in which this was done in the calculation of the residual deformations and strains produced in the solidification of glass [11], we now consider the process of the solidification of successive layers of a crystal. In the layer which is being formed the interatomic distances must correspond to the temperature of crystallization, while the interatomic distances in the layers underneath depend not only on the cyrstallization temperature, but also on the temperature in the interior of the crystal. As a result the density of atoms is less in the layer being formed than it is underneath, and some atomic planes will terminate below the surface, forming dislocations (of the edge type, in general).

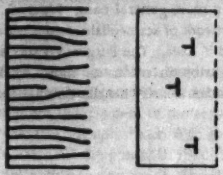

Fig. 3. The formation of edge dislocations in the motion of a plane crystallization front. Some of the atomic planes finish within the solidified part of the crystal, because the average distance between atomic planes corresponds to the temperature of the relevant part of the crystal. The general distribution of the dislocations is shown on the right.

In the simplest case of the crystallization of a film (Fig. 3) the dimensions l of each solidifying layer in a direction parallel to the face are determined by the average number ν of atomic planes in this layer, the temperature of expansion αT and the elastic deformation of the layer ϵ^{el}:

$$l = \nu(1 + \alpha T)(1 + \epsilon^{el}). \qquad (14)$$

From the conditions of compatibility of the total deformations it follows that for a film l = const (cf. [11]).

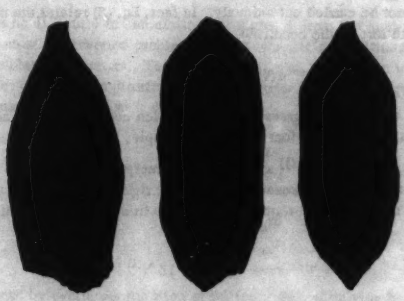

Fig. 4. Examples of isotherms in germanium crystals grown by the Kyropoulos method (Billig [5]). To show up the isotherms a specially chosen impurity was added to the melt during the growth of the crystal.

Hence, in the absence of elastic strains (in the general case we need to take into account the conditions for their equilibrium) we have

$$\nu(1+\alpha T)=\text{const}, \tag{15}$$

i. e., the number of atomic planes in any layer must change with the temperature of that layer. By differentiating Eq. (15) along the normal to the crystallization front and neglecting in comparison with unity we obtain a simple relation between the dislocation density $N=\frac{1}{b\nu}\frac{\partial\nu}{\partial n}$ and the temperature gradient:

$$N=-\frac{\alpha}{b}\frac{\partial T}{\partial n}. \tag{16}$$

The agreement between (1) and (16) is only apparent, since for Billig the crystallization front was not perpendicular to the radius of the crystal (see Fig. 4). Thus even the simple consideration of the problem in one dimension shows that Billig's formula needs to be modified.

To calculate the dislocation density distribution in an anisotropic crystal in an inhomogeneous temperature distribution, we note that in the absence of internal macroscopic strains the opening of the ends of the Burgers contour is determined by the circulation of the thermal expansion tensor:

$$\mathbf{b}=\oint d\mathbf{r}\,\hat{\alpha}T. \tag{17}$$

(Here $\hat{\alpha}$ is the thermal expansion tensor.) Using the dislocation density tensor, (17) can be written in the following differential form

$$\hat{\beta}=-Rot(\hat{\alpha}T) \tag{18}$$

or

$$\beta_{ik}=-\epsilon_{ijl}\frac{\partial}{\partial x_j}(\alpha_{ik}T). \tag{18'}$$

Here ϵ_{ijl} is an antisymmetric third-order tensor for which $\epsilon_{ijl}=1$, if i, j, l are an even cyclic permutation of the integers 1, 2, 3.

If the coefficients of the thermal expansion are constants over the temperature interval considered the differentiation in the two equations above applies only to the function $T=T(\mathbf{r})$ and we have

$$\hat{\beta}=-\text{grad}T\times\hat{\alpha} \tag{19}$$

or

$$\beta_{ik}=-\epsilon_{ijl}\frac{\partial T}{\partial x_j}\alpha_{ik} \tag{19'}$$

In a coordinate system with one axis (the Z axis, for example) along the temperature gradient, the tensor $\hat{\beta}$ becomes

$$\hat{\beta}=\begin{Vmatrix} \alpha_{yx} & \alpha_{yy} & \alpha_{yz} \\ -\alpha_{xx} & -\alpha_{xy} & -\alpha_{xz} \\ 0 & 0 & 0 \end{Vmatrix}\frac{\partial T}{\partial z}. \tag{20}$$

(20) simplifies still further if we choose the X and Y axes along those of the ellipse produced by the section of the ellipsoid of the expansion coefficients by the XY plane. In this case $\alpha_{yx}=\alpha_{xy}=0$ and

$$\hat{\beta}=\begin{Vmatrix} 0 & \alpha_{yy} & \alpha_{yz} \\ -\alpha_{xx} & 0 & -\alpha_{xz} \\ 0 & 0 & 0 \end{Vmatrix}\frac{\partial T}{\partial z}, \tag{20'}$$

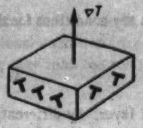

Fig. 5

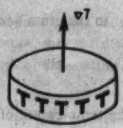

Fig. 6

Fig. 5. The simplest dislocation model for the general case of a temperature field. The directions of the dislocation lines are parallel to the axes of the section of the ellipsoid of the expansion coefficients by a plane which is tangent to the isothermal surface. The slope of the extra half-planes is determined by the anisotropy of the thermal expansion of the crystal.

Fig. 6. The simplest dislocation model for a crystal with isotropic thermal expansion. If the temperature gradient is replaced by the factor γ, the same model is valid for the antisymmetric part of the dislocation density tensor in the anisotropic case.

which corresponds to the model in Fig. 5, which consists of a rectangular network of edge dislocations situated parallel to the X and Y axes. The extra planes of these dislocations are inclined to the Z axis at angles whose tangents are α_{yz}/α_{yy} and α_{xz}/α_{xx}, respectively.

For a crystal with isotropic thermal expansion

$$\hat{\alpha} = \alpha I \tag{21}$$

(I is the unit tensor) and the dislocation density is described by the antisymmetric tensor

$$\beta = -\alpha \operatorname{grad} T \times I. \tag{22}$$

Here the simplest dislocation model can be constructed from a square network of edge dislocations whose extra planes are parallel to the temperature gradient and finish on the isothermal surfaces (see Fig. 6).*

In the general case the tensor $\hat{\beta}$ may be divided into a symmetric part $\hat{\beta}^s$ and an antisymmetric part $\hat{\beta}^a$. The tensor $\hat{\beta}^s$ is evidently determined by the anisotropy of the thermal expansion of the crystal and, like every symmetrical tensor, may be reduced to diagonal form, which corresponds to a model made up entirely of screw dislocations.

The antisymmetric tensor $\hat{\beta}^a$ is equivalent to a vector γ where

$$\gamma_i = -\frac{1}{2}\,\epsilon_{ijk}\,\beta^a_{jk} = -\frac{1}{2}\,\epsilon_{ijk}\,\beta_{jk}. \tag{23}$$

The inverse relation is

$$\beta^a_{ij} = \epsilon_{ijk}\,\gamma_k \tag{23'}$$

or

$$\beta^a = -\gamma \times I. \tag{23''}$$

Using the identity $\epsilon_{ijk}\epsilon_{jlm} = \delta_{im} - \delta_{kl} - \delta_{il}\,\delta_{km}$, we obtain from (19") and (23) the relations

$$2\gamma_i = -\epsilon_{ijk}\epsilon_{jlm}\frac{\partial T}{\partial x_l}\alpha_{mk} = -\frac{\partial T}{\partial x_k}\alpha_{ik} + \frac{\partial T}{\partial x_i}\alpha_{kk}, \tag{24}$$

i. e.,

$$\gamma = \frac{1}{2}\left(I\,Sp\hat{\alpha} - \hat{\alpha}\right)\operatorname{grad} T. \tag{24'}$$

The components of the vector γ with respect to the axes X_1, X_2, X_3 of the ellipsoid of the coefficients of thermal expansion are

$$\gamma_1 = \beta_{23} = \frac{\alpha_2 + \alpha_3}{2}\frac{\partial T}{\partial x_1}; \tag{24"}$$

* It should not of course be forgotten that Figs. 5 and 6 do not refer to any real crystal structure. In fact, to find a dislocation model from the $\hat{\beta}$-tensor it is necessary, as has already been emphasized in the previous section, to split up the $\hat{\beta}$-tensor into multiplicative tensors which correspond to the system of t-vectors in the crystal.

γ_2 and γ_3 are obtained by cyclic permutation of suffices.

We obtain a simple expression for the components of the tensor $\hat{\beta}^a$ if we take one of the coordinate axes along the vector γ. In this case (23') shows that the two nondiagonal components of $\hat{\beta}^a$ perpendicular to γ are the only nonzero terms. In magnitude these components are equal to $|\gamma|$ but they have the opposite sign. The corresponding dislocation model can be thought of as a square network of edge dislocations, analogous to the model shown in Fig. 6, but with the difference that here the role of the temperature gradient is played by the vector γ. In the isotropic case the temperature gradient and the vector differ only by a numerical factor α:

$$\gamma = \alpha \operatorname{grad} T, \tag{25}$$

The Dislocation Density and the Rate of Cooling

Equation (19) establishes a linear relation between the dislocation density formed in the growth of a crystal and the temperature gradient. Since, other things being equal, the latter is proportional to the rate of cooling of the crystal, the rate of cooling must be proportional to the dislocation density. This dependence was noted by Suzuki and Imura [12].

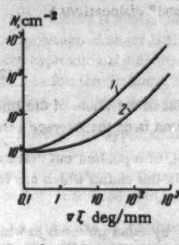

Fig. 7. The dislocation density as a function of the temperature gradient for crystals with the parameters of 1) aluminum and 2) silicon. It is assumed that the dislocation density due to thermal fluctuations is constant and equal to 10^4 lines/cm^2.

A recent paper by Ovsienko and Sosnina [13] investigated the increase in the degree of mosaicness of aluminum single crystals when the rate of growth was increased. The authors used as specimens thin two-millimeter sheets, the temperature distribution in which was almost completely determined by the heat loss from the large faces. It is therefore not surprising that when the rate of drawing-out the crystals was varied between 0.1 and 6 mm/min, the total angle of misorientation increased by only a factor of two (from 24' to 50'). The authors do not give data which could be used in the calculation of the total dislocation density, but we can however estimate the total temperature drop δT from the angle of misorientation if we assume that

$$\alpha \delta T \sim \theta. \tag{26}$$

For $\alpha = 28 \cdot 10^{-6}$ [14] this gives a reasonable order of magnitude for δT (from 240 to 520°).

For aluminum b = 2.856 A, and therefore the dislocation density formed in a temperature gradient of 100 deg/mm must be approximately 10^6, and for a gradient of 10 deg/mm it must be about 10^5 lines/cm^2, etc. According to Forty [15], the dislocation density in aluminum crystals which have been grown slowly from the melt and well annealed is usually about 10^6/cm^2.

For germanium $\alpha = 4.2 \cdot 10^{-6}$ and b = 3.5 A, and therefore a temperature gradient of 100 deg/mm corresponds to a dislocation density of $1.2 \cdot 10^5$, and a gradient of 10 deg/min to $1.2 \cdot 10^4$ lines per cm^2. Experimentally Billig [5], using the density of etch pits on crystals grown in a temperature gradient of the order of tens of degrees per mm, obtained estimates of the dislocation density from $4 \cdot 10^3$ to 10^5/cm^2. Here a more detailed comparison of theory and experiment is unfortunately impossible, as Billig did not measure the axial temperature gradient.

It is evident that we must not expect that dislocations will not be formed at all as the temperature gradient tends to zero. Because of thermal fluctuations there will always be a certain number of randomly oriented dislocations, the average Burgers vector of which will be zero for any macroscopic area. This "background" of dislocations does not however, affect the conclusions of the theory developed above, which deals with quantities averaged over macroscopic areas, since the background dislocations disappear in this averaging process.

It is difficult to estimate the background dislocation density from the existing data. If we assume that in the carefully annealed crystals (10^4 dislocations/cm^2) the majority of the dislocations are of the background type, then the temperature distribution will alter the original "natural" background dislocation density only for gradients of the order of several deg/mm, while for gradients of the order of several tens of deg/mm this original dislocation density is already negligible.

Figure 7 shows the qualitative dependence of the dislocation density on the temperature gradient for crystals with the parameters of aluminum and germanium,* constructed on the assumption that the background dislocation density is independent of the temperature gradient and is approximately 10^4 lines/cm^2.

The Density of Dislocations Which Intersect an Area of Given Orientation

In the comparison with experiment of the calculated dislocation density we used figures which referred to the density of etch pits, which correspond to the emergence of a dislocation on some face of the specimen. Using the macroscopic dislocation density tensor (18) and Relation (2) we can calculate the average Burgers vector for dislocations which intersect an area with normal n

$$\mathbf{b} = \mathbf{n}\hat{\beta} = (\operatorname{grad} T \times \mathbf{n})\hat{\alpha}. \tag{27}$$

In particular, for isothermal surfaces

$$\operatorname{grad} T \times \mathbf{n} = 0,$$

and the average Burgers vector of dislocations which intersect any macroscopic sector of the isothermal surface must be zero. (We again emphasize that this result is independent of the "background" dislocations.)

For a crystal with isotropic thermal expansion

$$\mathbf{b} = \alpha \operatorname{grad} T \times \mathbf{n}, \tag{28}$$

i. e., the average Burgers vector is perpendicular to the temperature gradient and lies in the plane of the small area, such that the screw component of the dislocations which intersect any small area is on the average zero.

It is interesting to compare this deduction with the observations of Dukova [2], who pointed out that in the formation of branches in growing dendrites of paratoluidine, the screw dislocations in the chains which are formed are as a rule alternately positive and negative.

For crystals grown by the methods of Kyropoulos, Verneuil, and Chokhral'skii or by other methods in which the crystal is in an axially symmetrical temperature field, it is important to distinguish between the effects due to the axial and radial temperature gradients. The radial temperature gradient is always zero in the central regions of the crystal and increases gradually towards the exterior, while the axial temperature gradient is practically constant (strictly constant for plane isotherms) over the crystal section. For normal rates of growing crystals the axial temperature gradient is considerably greater than the radial, and thus the majority of the dislocations are caused not by the radial temperature gradient (as was assumed by Billig [5]), but by the axial gradient.

Judging by the form of the isotherms (see Fig. 4) in Billig's experiments, it is only at the surface of the crystal that the radial and axial temperature gradients were approximately equal in a few cases (the first photo). Usually the ratio of the gradients is much less than unity, as can be found from the inclination of the normal to the isotherms to the axis of the crystal. It therefore follows that the distribution of etch pits over the cross section of the specimen corresponds mainly to the distribution of the axial and not the radial temperature gradient.

In fact Billig did not as a rule observe a large difference between the etch pit densities in the central and peripheral regions of a section through the central portion of the bar. Analogous conclusions about the almost identical dislocation densities in the central and peripheral regions of crystals grown by the Verneuil method may be made on the basis of the experiments described by Klassen-Neklliudova and Tomilovskii [16, 17] on the etching of crystals of synthetic corundum.

If we write the dislocation density tensor due to an axially symmetric temperature distribution in cylindrical coordinates r, θ, z, then for a crystal with isotropic expansion it follows from (24) that

$$\hat{\beta} = \alpha \begin{Vmatrix} 0 & \frac{\partial}{\partial z} & 0 \\ -\frac{\partial}{\partial z} & 0 & \frac{\partial}{\partial r} \\ 0 & -\frac{\partial}{\partial r} & 0 \end{Vmatrix} T(r,z), \tag{29}$$

* As in original; the figure caption refers to aluminum and silicon — Publisher.

i. e., the components of the tensor $\hat{\beta}$ are, respectively,

$$\left.\begin{aligned} \beta_{rr} = \beta_{\theta\theta} = \beta_{zz} = 0 \\ \beta_{r\theta} = -\beta_{\theta r} = \alpha \frac{\partial T}{\partial z} \\ \beta_{\theta z} = -\beta_{z\theta} = \alpha \frac{\partial T}{\partial r} \end{aligned}\right\} \qquad (30)$$

By comparing (30) and with (1) we see that Billig [5] gave correctly only two components of the tensor $\hat{\beta}$, and moreover those which make only a small contribution to the total number of dislocations.

CONCLUSION

The formation of dislocations in the solidification of a crystal because of inequalities in the temperature distribution takes place not only in the growth of a crystal, but also in zone melting, tempering, and even during the cooling of a crystal after annealing. In the two latter cases the dislocations are of course formed not by the displacement of growing atomic planes but by incompatible plastic deformations.

The theory is applicable without any modifications to the instances calculated if the temperature gradient in the specimen changes little in the time the crystal takes to solidify. Otherwise the dislocation distribution can be only approximately estimated from the temperature distribution at the moment of reaching a certain effective "solidification temperature," while a rigorous solution of the problem demands an account of the consequent redistribution of dislocations in the process of cooling the crystal.

None of the applications of the theory can be considered fully discussed, since the tensor $\hat{\beta}$ has not been split up into the densities of dislocations of various types. With the aim of simplifying this and of facilitating a rigorous comparison of theory and experiment, the study of cubic crystals with slip directions along the cube edges, and of body-centered cubic crystals with slip directions along the diagonals of the cube, is of great interest.

A wider use of the theoretical results must in each case give a complete picture of the dislocation distribution and will enable us to relate the real structure of a crystal to the conditions of its growth.

LITERATURE CITED

[1] G. G. Lemmlein and E. D. Dukova, "The formation of screw dislocations in the process of crystal growth," Kristallografiia 1, 351-355 (1956).

[2] E. D. Dukova, Dissertation, Inst. Krist. Akad. Nauk SSSR (1956).

[3] V. L. Indenbom and T. E. Tomilovskii, "Macroscopic edge dislocations in a corundum crystal," Kristallografiia 2, 1, 190-192 (1957). *

[4] V. T. Read, Dislocations in Crystals [Russian translation] (1953).

[5] E. Billig, "Some defects in crystals grown from the melt," Proc Roy. Soc. A 235, 37-55 (1956).

[6] B. A. Bilby, "Types of dislocation source," Report of the Conference on Defects in Crystalline Solids 124-133 (1955).

[7] B. A. Bilby, R. Bullough, and E. Smith, "Continuous distributions of dislocations," Proc. Roy. Soc. A 231, 263-273 (1955).

[8] E. Kröner, "Der fundamentale Zusammenhang zwischen Versetzungdichte und Spannungfunktionen," Z. Physik 142, 463-475 (1955).

[9] E. Kröner and G. Rieder, "Kontinuumstheorie der Versetzungen," Z. Physik 145, 424-429 (1956).

[10] A. I. Lur'e, Spatial Problems of the Theory of Elasticity [in Russian] (1955)

* [Soviet Physics – Crystallography, pp. 183-87.]

[11] V. L. Indenbom, "Towards a theory of the tempering of steel," J. Tech. Phys. 24, 925-928 (1954).

[12] T. Suzuki and T. Imura, "Substructures and networks of dislocations in face-centered cubic metals," Report of the Conference on Defects in Crystalline Solids 347-358 (1955).

[13] D. E. Ovsienko and E. I. Sosnina, "The influence of the rate of growth of single crystals of aluminum on their mosaic structure," Fiz. Metallov i Metallovedenie 3, 374-382 (1956).

[14] B. G. Lifshits, The Physical Properties of Metals and Alloys [in Russian] (1956), p. 281.

[15] A. J. Forty, The Direct Observation of Dislocations in Crystals [Russian translation] (1956).

[16] M. V. Klassen-Neklioudova and G. E. Tomilovskii, "The durability of corundum crystals as a function of their orientation," Trudy Inst. Krist. Akad. Nauk SSSR 8, 215-224 (1953).

[17] M. V. Klassen-Neklioudova, "The mechanical properties of corundum crystals," J. Tech. Phys. 12, 529-551 (1942).

Received February 7, 1957

Institute of Crystallography of the Academy of Sciences, USSR

AN INSTRUMENT FOR THE MECHANICAL DETERMINATION OF THE SEPARATION BETWEEN LATTICE PLANES

Dr. Frantishek Kgol'

This article describes an instrument which enables the distances d_n to be found mechanically without long and time-consuming calculations. This instrument enables one to interpret x-ray photos taken by any of the methods which are usually used in the structural analysis of polycrystalline materials. It can be operated even by a laboratory assistant who has no higher education.

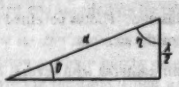

Fig. 1. A geometrical representation of the Bragg-Wulff equation.

The construction of the instrument is based on two theorems in geometry and their resemblance to the basic equations of x-ray structure analysis.

a) We consider the Bragg-Wulff equation, which can be written in two ways:

$$\sin\vartheta = \frac{\lambda/2}{d} \quad \text{or} \quad \cos\eta = \frac{\lambda/2}{d}, \text{ where } \eta = 90^\circ - \vartheta. \qquad (1)$$

These relations can be simply expressed by the sides of a right-angled triangle (see Fig. 1).

b) For the back-reflection methods we must define the angle η, while the x-ray photos give us the angle 2η

$$2\eta = \frac{r}{D},$$

where r is the radius of the interference circle and D is the distance from the specimen to the film (see Fig. 2).

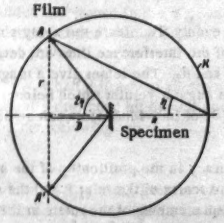

Fig. 2. A geometrical determination of the angle of reflection from the reflected beam.

If we describe a circle K with radius $R = \sqrt{r^2 + D^2}$, the inscribed angle η can be used to determine d.

Description and Construction of the Apparatus

The instrument consists of a flat plate to which two axes are fixed perpendicularly (O_1 and O_2, Fig. 3). A ruler P with two scales and a movable decimal vernier is rotatable about the axis O_1. The levers R_1 and R_2, which always subtend the same angle at the axis, and the simple lever R rotate about the axis O_2. The ends of these levers trace out the circle K which passes through the axis O_1. Two systems of straight lines are ruled on the baseboard; these, S_1 and S_2, are parallel to the zero position of the ruler P at distances which are proportional to the wavelengths of the characteristic radiation K_{α_1,α_2} and K_β of various anodes (for instance, Mo, Cu, Co, Fe, Cr). In the system S_1 the straight lines which correspond to the wavelengths K_{α_1} and K_{α_2} are not separated, but they are in the system S_2. The scales S_1 and S_2 bear the same ratio to the wavelengths as does the scale on the measuring ruler P.

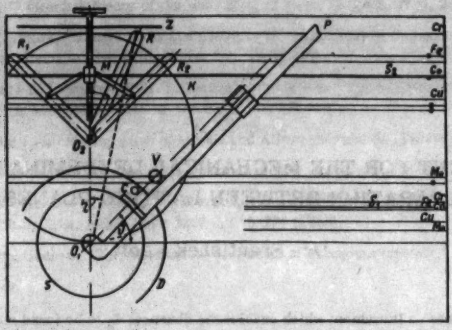

Fig. 3. A schematic representation of the instrument for the mechanical determination of the distances between lattice planes.

Under the base there are holders D and Z for the x-ray photos to be measured. Photos obtained in a cylindrical camera are fixed in the cylindrical holder D, whose radius equals that of the camera.

The instrument has several cylindrical holders which enables photos from cameras with several different diameters to be interpreted.

The holder Z is designed for back-reflection photos; it can be moved towards the axis O_2 or it can be fixed in a plane parallel to the axis O_2. The holder Z is always of the same shape as the camera in which the photo was taken (for example, a cone).

To make the interpretation easier, two small electric lamps which evenly illuminate the x-ray photos through light blue mat glass are fixed to the axes O_1 and O_2. The positions of the interference lines are determined with the help of lenses which are fixed to the movable levers P, R, R_1, and R_2. The lenses give a magnification of 2-5 times. There is an angular scale S around the axis O_1, and the angular vernier which belongs to it is fixed on the ruler P so that angular displacements of P and the positions (ϑ) of individual spots can be determined.

The instrument must be carefully made in order that the necessary accuracy in the positioning of the axes O_1 and O_2 should be obtained in the interpretation. It is also necessary that the scales of the ruler P and the sets of lines S_1 and S_2 should be identical. S_1 and S_2 must also be parallel. All displacements of the rulers in the measurement of interference lines must be made carefully using screws and the rulers may be locked into position.

1. The Use of the Instrument in the Interpretation of X-ray Diffraction Photos

The determination of the separations between lattice planes from x-ray diffraction photos obtained by the power method and from a polycrystalline substance.

In the Straumanis-Ewing method the film is placed asymmetrically in the camera (see Fig. 4), and as a result of this identical interference cones, situated symmetrically about the hole in the film for the incident beam, are obtained for both large and small angles (AA', BB').

The angle ϑ is found from the relation

$$\text{arc } 2\vartheta = \frac{r}{R}, \quad \text{or} \quad \text{arc } \vartheta = \frac{r}{2R}; \tag{2}$$

this means that if the photo is placed on a circle of radius 2R, r will then equal the angle ϑ.

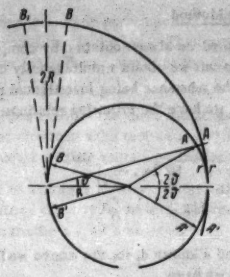

Fig. 4. The method for the interpretation of diffraction photographs obtained by the Straumanis-Ewing method.

The diffraction photo obtained is therefore placed in the holder D, which has a radius twice that of the camera in which the photo was taken. Using the symmetrical reflections AA' and BB' we adjust the photo so that the center of AA' coincides with the horizontal line (the zero of ϑ) and so that the center of BB' coincides with the vertical line ($\vartheta = 90°$).

After the ruler P has been rotated until the cross wires coincide with a reflection, the ruler is clamped and the vernier N is moved so as to find the point of intersection with the line of S_1 or S_2 which corresponds to the wavelength λ of the x-radiation which produces the reflection being measured on the diffraction photo. The quantity measured on the ruler P is the desired length $\underline{d}$ (cf. Fig. 1). When the diffraction photograph has been obtained using unfiltered radiation, the interference lines which are due to the characteristic radiation β can easily be found. To do this we rotate the ruler P so that its point of intersection with the K_α line (this point fixes d_k) lies on the K_β line. We then find in the lens the corresponding reflection from K_β, if it is visible, and mark it with the cutter C. The determination of individual reflections is simplified and speeded up by this method.

By turning the ruler P to the other reflections we find the corresponding lattice separations d, without any calculation and by a purely mechanical method. By using this instrument a whole diffraction photograph can be interpreted in the time which was previously taken to measure individual reflections.

Large separations $\underline{d}$, which correspond to small angles ϑ, are found from the scale S_1, on which the distances between the straight lines which are proportional to λ are five times smaller than those on the scale S_2. In normal measurements we choose the scale 1 A = 1 dm;* but for greater accuracy we choose 1 A = 1 mm. For this the lines which correspond to the K_{α_1} and K_{α_2} lines are 2 mm apart; this a necessary condition for the interpretation of lattice periods when photos are taken by the back-reflection method. $\underline{d}$ can be measured with an accuracy of $\pm 1 \cdot 10^{-4}$ A.

When diffraction photos of metal wires or powders are being taken, the positions of the reflections will be slightly displaced by the absorption of radiation in the specimen, so that the actual position ϑ_{cor} is determined by the following relation:

$$\vartheta_{cor} = \vartheta_{meas} - \rho \cos^2 \vartheta_{meas},$$

where ϑ_{meas} is the position of the reflection as measured and ρ is the radius of the specimen under investigation. This correction is significant for small ϑ, i. e., for large interplanar distances. According to the Bragg-Wulff equation

$$d = \frac{\lambda}{2 \sin \vartheta_{cor}},$$

and here $\vartheta_{cor} < \vartheta_{meas}$. Hence, we obtain the same value of $\underline{d}$ for ϑ_{meas} if we replace λ by λ_{cor}, which depends on the radius of the specimen ρ. In this case

$$d = \frac{\lambda}{2 \sin \vartheta_{cor}} = \frac{\lambda_{cor}}{2 \sin \vartheta_{meas}}.$$

From this relation we can first determine λ_{cor} for the quantities ϑ_{cor} and ρ, and thus we obtain a system of straight lines S_1 and S_2, which, however, will not be parallel to the lines $\vartheta = 0°$. Their angle of inclination will be proportional to the radius of the specimen, and therefore can be ruled on the instrument for a given specimen. The determination of the interplanar distances $\underline{d}$ remains simple and speedy, but accurate work demands the introduction of the above correction for the thickness of the specimen.

* As in original – Publisher's note.

2. The Interpretation of Photographs Taken by the Back-Reflection Method

In the interpretation of diffraction photographs obtained by this method we always obtain $\underline{d}$ by comparing it with the known d_r for an etalon (of pure Au or Ag, for example). To do this we obtain simultaneously on the diffraction photo reflections from the substance being investigated $\underline{r}$ and from the etalon r_r (see Fig. 5), and we have the following relations:

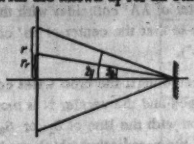

Fig. 5. The method of interpreting back-reflection photographs.

$$\cos\eta_r = \frac{\lambda}{2d_r}, \quad \operatorname{tg} 2\eta_r = \frac{r_r}{D}; \qquad \cos\eta = \frac{\lambda}{2d}, \quad \operatorname{tg} 2\eta_r = \frac{r}{D}. \tag{3}$$

For a known wavelength λ and a known d_r for the etalon we find η_r, and then by eliminating D from (3) we have

$$\operatorname{tg} 2\eta = \frac{r}{r_r} \operatorname{tg} 2\eta_r .$$

By measuring $\underline{r}$ and r_r we find η and then we have

$$d = \frac{\lambda}{2\cos\eta}.$$

This takes up much time and labor for the measurement of a large number of diffraction photos.

Fig. 6. A photograph of one of the instruments.

To use the instrument described above for the determination of the distances $\underline{d}$ we proceed as follows.

The known distance d_r is set on the ruler P using the vernier N, and then the ruler is rotated until the vernier intersects the line on the scale S_2 which corresponds to the wavelength of the K_α radiation used. After the ruler P has been clamped, we move the vernier to its intersection with the circle K. Then we open out the levers R_1 and R_2 with the help of the nut M until they coincide with the point of intersection of the circle K and the ruler P. Thus the angle $2 \times 2\eta_r$ will be found, and for the same etalon this will be a constant over a whole series of photographs.

Then the x-ray photo is placed in the holder Z, which is moved towards O_2 until the corresponding reflections r_r coincide with the cross wires in the lenses on R_1 and R_2. Possible eccentricity is eliminated by moving

the holder in a plane perpendicular to the direction O_2M. Then we move the lever R until the reflection $\underline{r}$ appears at the cross wires of the lens. Then we move the ruler P to the point of intersection of the lever R with the circle K and we move the vernier N to the K_{α_1} line on the scale S_2 and measure off the distance $\underline{d}$ from the scale of the ruler P (cf. Fig. 1).

When used for the mechanical determination of interplanar distances in polycrystalline materials, this instrument eliminates the tedious and difficult work of interpreting x-ray photographs. The instrument can be used for all characteristic radiations and for various types of x-ray photographs.

The accuracy achieved is the same as that for the calculation methods, since in both methods the distances d_r are found directly from the positions of the reflections. On the other hand, the accidental errors which occur in these methods are eliminated.

Received February 5, 1957

The Prague Scientific Research Institute for Materials and Technology

THE STRUCTURE OF CRYSTALS OF COBALTOUS HEXAFLUOGERMANATE HEXAHYDRATE $[Co(H_2O)_6][GeF_6]$

T. S. Khodashova

Compounds of the form $[Me^{II}(H_2O)_6][Me^{IV}X_6]$ belong as a rule to the structural type $[Ni(H_2O)_6][SnCl_6]$ [1], where the complex ions are packed as in the CsCl type and the structure is slightly deformed with respect to L_3. In particular, the corresponding hexafluosilicates have such a structure. There are only isolated instances of compounds of this type with packing of complex ions as in the NaCl type [2, 3].

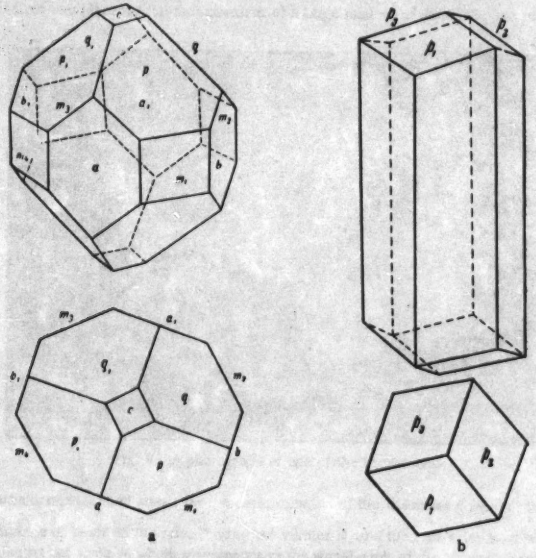

Fig. 1. Crystals of $[Co(H_2O)_6][GeF_6]$.

Goniometric measurement of a series of hexafluogermanates showed that $[Co(H_2O)_6][GeF_6]$ forms hexagonal crystals (Fig. 1, b), as well as crystals sharply different from these in habit (Fig. 1, a). The structural analysis of this compound sought to ascertain: 1) whether the Co salt has two modifications or one and 2) if one, then to which of the two above-named structural types it belongs.

The x-ray structural analysis (the Laue, powder, oscillation methods) showed that the crystals of both forms are completely identical and belong to the prismatic form of symmetry of the monoclinic crystal class, being at the same time pseudohexagonal. In addition, the principal pseudoaxis passes through the vertex app_1. The faces a, p, p_1 (Fig. 1, a) correspond to faces of the obtuse rhombohedron type p_1, p_2, p_3 in Fig. 1, b, the faces m_1, m_4, c form a second rhombohedron (not shown in Fig. 1, b) and the six remaining faces are the faces of a pseudohexagonal prism. Moreover, the crystals are pseudocubic: 6 faces (m_1, m_2, m_3, m_4, c_1, c_2) form a pseudocube, the remaining 12 faces, a pseudorhombododecahedron (Fig 1, a). The crystals form polysynthetic twins.

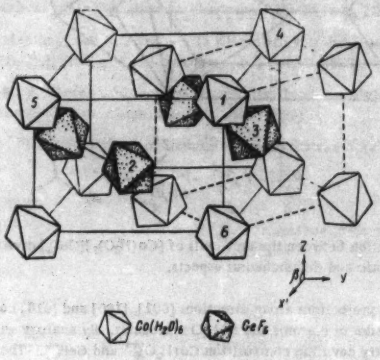

Fig. 2. Structure of $[Co(H_2O)_6][GeF_6]$.

The density of the crystals is d = 2.21 g/cm³. The parameters of the cell are a = 17.30 ± 0.05 kX, b = = 19.48 ± 0.05 kX, c = 13.30 ± 0.05 kX, β = 100°10′. a : b : c = 0.888 : 1 : 0.683. According to goniometric data a : b : c = 0.889 : 1 : 0.682 [4].

With such an arrangement the cell is face-centered, the number of formula units being N = 16. However, on the strength of the very clearly expressed pseudoperiodicity in all three directions, we can in a first approximation consider a primitive cell 8 times smaller with the parameters

$$a' = \frac{a}{2} = 8.65\,kX, \quad b' = \frac{b}{2} = 9.74\,kX, \quad c' = \frac{c}{2} = 6.66\,kX,$$
$$\beta' = \beta = 100°10', \quad N' = 2.$$

In conformity with the extinctions, the space group of such a pseudocell is $C_{2h}^5 - P\,2_1/a$.

In the rhombohedral aspect the cell of $[Co(H_2O)_6][GeF_6]$ crystals has the parameters a = 11.7 kX, α = = 113°, N = 4. The space group of this pseudorhombohedral cell probably is $D_{3d}^5 - R\bar{3}m$.

The x-ray structural analysis, having been carried out with Mo-radiation using data from the zero and first layer lines taken by rotation around the three crystallographic axes, permitted a determination of the general features of the structure – the character of the packing of the complex ions and their orientation. A more detailed analysis (precise determination of the F and H_2O coordinates) is difficult.

A description of the structure will be given for the pseudoprimitive monoclinic cell (Fig. 2).

The arrangement of the Co and Ge atoms, both similar in scattering power, is immediately determined by the pseudoextinctions which correspond to the face-centered rule (h′k′l′ for intense reflections either all even or all odd), i. e., the heavy atoms occupy twofold positions (a) and (d).

Hence, it follows that the complex ions are packed in a structure of the CsCl type.

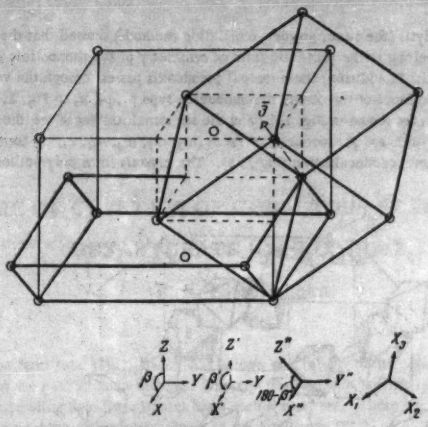

Fig. 3. Relation between the unit cells of $[Co(H_2O)_6][GeF_6]$ crystals in the monoclinic and rhombohedral aspects.

Analysis of the Patterson projections along directions [001], [100] and [010] confirmed that the Co and Ge atoms are surrounded by octahedra of F atoms and of H_2O molecules. By analogy with other compounds of this type the complex ions apparently have the composition $Co(H_2O)_6^{++}$ and GeF_6^{--}. The distance Me–X equals 1.8–1.9 A, which agrees with the data available in the literature, Ge–F = 1.74 A [4], Co–H_2O = 1.93 A [5].

The octahedra are turned in such a way that their third-order axes coincide approximately with the direction of the diagonal x'z', which is the pseudotriad axis of the cell in the rhombohedral aspect (Figs. 2 and 3). The mutual orientation of the complex Co and Ge ions is determined by the following circumstance: the pseudoprimitive cell is base-centered on the face x'y' with respect to the Co and Ge atoms, i. e., the intensities of the reflections h'k'0 with h' + k' = 2n – 1 are determined only by the coordinates of the light atoms. The existing relation – among the reflections h' + k' = 2n – 1 (on the x-ray pattern, taken along [001]) there are relatively intense reflections with k' = 2n – indicates pseudoperiodicity in the projection along axis y', conditioned by special arrangement of the light atoms. This can occur only in the case of an approximately identical orientation of the octahedra 1 and 2. Octahedra 1 and 3, which are on the pseudotriad axis, are oriented nonidentically (2 and 3 are connected by the glide plane). It is precisely owing to this that the symmetry of the structure becomes monoclinic, but approaching the rhombohedral (the symmetry of group $R\bar{3}m$, to which the $[Co(H_2O)_6][GeF_6]$ crystals should have belonged, certainly requires identical orientation of the octahedra, which occur one under the other in the direction of axis $\bar{3}$).

The doubling of the periods a', b', c' is in all probability caused by a slight turning of octahedra 4, 5 and 6 with respect to octahedron 1.

Thus, the face-centered cell is 8 times larger than the real cell or – in the assumed arrangement – the base-centered cell is 2 times larger with the parameters: a" = 17.3 kX, b" = 19.48 kX, c" = 9.70 kX, β" = 139°, N" = 8. The symmetry of such a cell is C_{2h}^3 – C2/m. The eight Co (or Ge) atoms occupy positions 2(a), 2(c) and 4(e), the 8 atoms of Ge, positions 4(h) with y = 0.25 and 4(i) with x = 0.25 and z = 0.5.

In Fig. 3 is shown the connection between the monoclinic cells (the solid line designates the face-centered cell, the double line the base-centered and the broken line the primitive pseudocell) and the pseudorhombohedral cell. A dashed line designates the pseudotriad axis.

The structure of $[Co(H_2O)_6][GeF_6]$ is very close to the structure of the $[Ni(H_2O)_6][SnCl_6]$ type. The difference consists in the increased dimensions of the cell and a different mutual orientation of the complex ions $Me^{II}(H_2O)_6$ and $Me^{IV}X_6$. In Fig. 2 the broken line forms the pseudocell, analogous to the real rhombohedral cell in the structure of $[Ni(H_2O)_6][SnCl_6]$.

The author expresses thanks to K. A. Avduevska for submitting the crystals of cobaltous hexafluogermanate for the structural analysis.

LITERATURE CITED

[1] L. Pauling, "On the crystal structure of nickel chlorostannate hexahydrate," Z. Krist. 72, 482 (1930).

[2] T. Watanabé, M. Atoji, and C. Okazaki, "The crystal structure of hexammine-cobaltic hexachlorothalliate $Co(NH_3)_6TlCl_6$ and hexammine-cobaltic hexabromthalliate $Co(NH_3)_6TlBr_6$," Acta Cryst. 3, 6, 405 (1950).

[3] M. Linhard, W. Manthey, and K. Plieth, "Die Kristallstruktur des Diaquotetrammin-cobalt (III)—hexachloro-thallats $[Co(NH_3)_4(H_2O)_2][TlCl_4]$," Z. Elektrochem. 57, 9, 862 (1953).

[4] J. L. Hoard and W. B. Vincent, "Structures of complex fluorides. Potassium hexafluogermanate and ammonium hexafluogermanate," J. Am. Chem. Soc. 61, 2849 (1939).

[5] B. K. Vainshtein, "Electron diffraction determination of the structure of $CoCl_2 \cdot 2H_2O$," Doklady Akad. Nauk SSSR 68, 301 (1949).

Received January 17, 1957

N. S. Kurnakov Institute of General and Inorganic Chemistry

A METHOD FOR DETERMINING THE AMPLITUDES OF THE THERMAL VIBRATIONS OF THE VARIOUS KINDS OF ATOMS IN SOLID SOLUTION

A. P. Zviagina and V. I. Iveronova

Contrasting the measured relative intensities of x-ray interferences with those calculated using the theoretical values of the atomic scattering factors, and assuming no static distortions in the lattice, it is possible to determine the temperature index B, without the need of x-ray patterns at different temperatures. In fact, the slope of the straight line

$$\ln J_t/J_e = k + 2B\frac{\sin^2\Phi}{\lambda^2} \tag{1}$$

yields the index of dynamic distortion B, and consequently, the square of the atomic displacements due to thermal vibration averaged over time. Debye has worked out the relationship between the index B and the characteristic temperature θ for monatomic cubic crystals:

$$B = \frac{6h^2}{mk\theta}\left[\frac{\Phi_{(x)}}{x} + \frac{1}{4}\right], \text{ where } x = \frac{\theta}{T}. \tag{2}$$

But the analogous relationship for solid solutions is unknown. However, it has been shown that, for a series of cubic ionic compounds, the characteristic temperature calculated from Eq. (2) corresponds well with the one determined experimentally.

Thus the basis has been established for transferring Relationship (2) to solid solutions and using it for calculating the characteristic temperature.

It is possible to consider a well-ordered solid solution as a compound in which no obvious static displacements are to be expected.

A knowledge of the dynamic displacement B makes it possible not only to calculate the characteristic temperature θ for a well-ordered solid solution, but also to evaluate the amplitude of the thermal vibrations for each kind of atom separately. The amplitude of the thermal vibrations of each atom * must depend on the strengths of its bonds with its neighbors, i. e., on the atoms surrounding it. Atoms of each kind are identical among themselves, as structurally they occupy equivalent positions and are surrounded by similar atomic configurations. Therefore, all atoms of one kind have similar bonds in the lattice, and consequently, similar amplitudes of thermal vibration. The atomic scattering function for the fundamental reflections can be written then as

$$f = (1-c)f_1 e^{-B_1\frac{\sin^2\Phi}{\lambda^2}} + cf_2 e^{-B_2\frac{\sin^2\Phi}{\lambda^2}}, \tag{3}$$

where c is the concentration of the second component, f_1 and f_2 are the atomic scattering functions of the two components, and B_1 and B_2 are the indices of thermal vibration for the two kinds of atoms.

* Proportional to the mean square displacement $\sqrt{3\overline{D}_s^2} = \sqrt{\overline{U}^2}$.

Two unknowns, B_1 and B_2, characterizing the bond strengths of the atoms in the solution, enter into the right side of Eq. (3). Any pair of experimental intensities $I = I(n)$, where $n = \sin^2\vartheta/\lambda^2$ with two different values for n, gives a system of two equations of the type (3).

Eliminating one of the unknowns from the system (B_1 or B_2), the following equation is obtained:

$$f'' = (1-c)f''_1 e^{-B_1 n''} + cf''_2 \left[\frac{f' - (1-c)f'_1 e^{-B_1 n'}}{cf'_2}\right]^{n''/n'} \quad * \qquad (4)$$

which can be solved graphically. The right side of Eq. (4), which is a function of the variable B_1 — $\varphi(B_1)$ represents a curve with a minimum (Fig. 1). The experimental value of f'' appears in absolute units** on the left side of the equation. The intersection of the straight line $f'' = \text{const}$ with the graph $\varphi(B_1)$ gives the value of B_1 sought. The horizontal straight line f'' must in general intersect the curve $\varphi(B_1)$ twice at two different values for B_1 (Fig. 1). The choice of one of the two roots B_1 is determined by agreement of the solution for various pairs of reflections. This method of determining B_1 is effective only if the experiment is fairly accurate. Actually, an error in B_1 results not only in an inaccurate measurement of the quantity f'', but also in the slope and "breadth" of curve $\varphi(B_1)$.*** The slope of the curve increases with the distance between the first and second experimental points (i. e., with an increase of $n'' - n'$). But if there is a great difference $n'' - n'$ in the second term of (4) the error in f' is raised to the power n''/n', which increases greatly the "breadth" of the curve $\varphi(B_1)$.

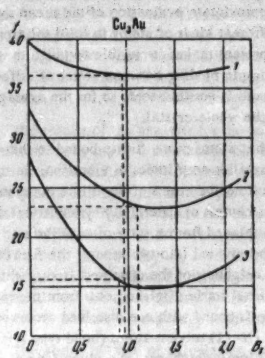

Fig. 1. Solid curves represent the right side of Eq. (4) for various pairs n' and n" for the alloy Cu_3Au. The first curve corresponds to $\frac{\sin\vartheta}{\lambda}$ equal to 0.6 and 0.7; the second to 0.4 and 0.9; the third curve to 0.1 and 1.0. The dotted horizontal straight lines give the corresponding values of f'', $B_1 = 2B_{Au}$.

Examining Eq. (4) we find that the slope of the curve depends exponentially on the ratio $k = \frac{cf_1}{(1-c)f_2}$; therefore, for some alloys (Ni_3Fe), where this ratio is very small ($k \approx 1/2$), the slope is so insignificant that the changes in $\varphi(B_1)$ from $\varphi(0)$ to $\varphi_{min}(B_1)$ lie almost within the experimental error of measuring f'', and to speak of any accurate value of B_1 is without meaning; the curve is fairly steep for alloy Cu_3Au ($k \approx 1$) and for the corresponding pair of f' and f''.

The alloy Cu_3Au was not ordered completely; therefore, the static distortions ($\alpha_{st} = 0.66$) were isolated by taking exposures at two different temperatures, and the remaining effect attributed to thermal vibrations ($B = 0.60$). The above-mentioned method was used to determine the thermal indices for the different kinds of atoms B_{Au} and B_{Cu}. Average statistical atomic displacements from a state of equilibrium correspond well with the data of the work [2] where $\sqrt{\overline{u^2}}$ are determined by comparing the superstructural and fundamental reflections. It is obvious from the table of results of the calculation for the alloy Cu_3Au, that the amplitude of atomic vibration is smaller for gold than for copper.

Similar considerations may be applied to dilute solid solutions as well, in which the dissolved atoms are so far removed from one another that the distorted regions created by them do not overlap.

---

* f' and f'' are the measured values of the atomic scattering factor for reflections n' and n"; correspondingly, f'_1 and f''_1 are the tabular ones.

** To obtain f in absolute units so as to solve Eq. (4) it is not necessary to take absolute intensity measurements. It is sufficient to use the value of B determined experimentally from Eq. (1) and to approximate the experimental f by an exponential $f = f_0 e^{-Bn}$.

*** By "breadth" of the curve $\varphi(B_1)$ we understand the region of variation of this function when f' is changed within limits of experimental error.

Alloy	Components	From measurements at 2 temperatures θ	T_k	θ_{av}	T_{av}	θ_{calc}	$\left(\sqrt{\overline{u^2_{dyn}}}\right)_A$	$\left(\sqrt{\overline{u^2_{dyn}}}\right)_{A}$ according to [1]
Cu_3Au	Cu	0.60	240	0.60	0.06	0.85	0.18	0.16
	Au					0.40	0.12	
Fe—W	Fe	0.34	425	0.33	0.01	0.34	0.11	0.12
	W					0.05	0.05	

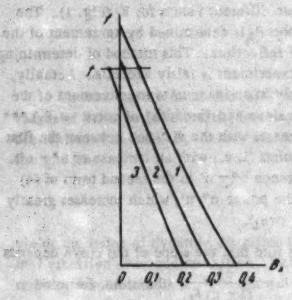

Fig. 2a. Parametric family of curves typical of Eq. (5) when $\frac{\sin\vartheta}{\lambda} = 0.8$ for various values of α. The first curve $\alpha = 0$, the second curve $\alpha = 0.025$, the third curve $\alpha = 0.05$. The points of intersection of the experimental values with the curves give the function $\alpha(B_x)$.

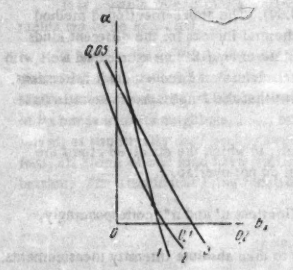

Fig. 2b. Curves of the functions $\alpha(B_x)$ obtained from curves of the type in Fig. 2a for various $\frac{\sin\vartheta}{\lambda}$. The 1st, 2nd and 3rd curves correspond to $\frac{\sin\vartheta}{\lambda}$ equal to 0.4, 0.8, 1.0.

Even if the approximate evaluation of the mean square displacements of different kinds of atoms in solid solution with thermal vibrations present makes it possible to judge the magnitude of the interatomic binding between atoms of different kinds, it does not make it possible to do so for the average binding throughout the whole crystal.

It is obvious that atoms more firmly bound to their nearest neighbors have smaller amplitudes of vibration. In the case of a dilute solid solution, the atoms of the dilute component can be considered as centers of spherically symmetrical deformation and not as displaced from a state of equilibrium. The solvent atoms may be divided into two groups: the first is the group of the closest neighbors of the dissolved atoms, which experience the maximal static displacements from the lattice points (α). Each one is bound with one dissolved atom (bond type A—B) and with (N — 1) solvent atoms (bond type A—A), (N is the number of closest neighbors for a given type of structure). If all N bonds of type A—B were concentrated on one of the closest neighbors of the dissolved atom, and normal solvent bonds were attributed to the remaining (N — 1) neighbors, then the mean square of the thermal vibrations around the whole coordinate sphere ($\overline{u^2} \sim B$) (if considered as independent) would not change.

This makes it possible to distinguish atoms in the solvent with wholly normal bonds from atoms characterized by bond type A—B, i. e., those with similar dynamic displacements as the dissolved atoms (B_x). (The vibration amplitudes in the first approximation do not depend on mass, as was shown in [1, 3].)

The remaining atoms of the solvent (the second group) are surrounded by atoms of the same kind, and therefore have the same vibration amplitudes as in the pure solvent (B_1). The index of static displacement for these atoms, which, according to the law $1/r^2$, decreases from the center of deformation, is approximately $k \approx 0.1$ of the maximal distance between the nearest neighbors ($\alpha^1 = k\alpha$). k depends on the type of lattice and on the concentration. The atomic scattering function of a dilute solid solution with concentration c can be written as follows:

$$f = cf_2 e^{-B_x n} + cf_1 e^{-2\alpha} \cdot e^{-B_x n} + c(N-1) f_1 e^{-\alpha} e^{-B_1 n} + [1 - c(N+1)] f_1 e^{-2\alpha} \cdot e^{-B_1 n}. \quad (5)$$

The left side represents an experimentally measured quantity in absolute units, and the right side is dependent on the two unknowns B_x and α. The right side can be represented as a parametric family of curves $f(B_x) = ae^{-B_x n} + bc$ with the parameter α (Fig. 2a). From the points of intersection of each of these curves with the straight line f, we find the function $\alpha(B_x)$ (Fig. 2b).

Having repeated this operation for several values of f, we find B_x and α at the intersection point of the curves $\alpha(B_x)$. The accuracy of the results obtained, except that of f, is also determined by the slopes of the curves $f = ae^{-B_x n} + b$ which increase as $a \sim f_2$ increases and decrease as $b \sim f_1$ decreases. Consequently, it is for relatively light metals alloyed with heavy ones that the most accurate results can be obtained. Thus, it is possible to evaluate from the experimentally determined f-curve for dilute solid solutions at room temperature, not only the magnitude of the static atomic displacements (α) but also the thermal vibration amplitude of the dilute atom (B_x), i. e., the bond strengths in solid solution between atoms of various kinds.

The results of the analysis for the solid solution Fe–W (1.9 atomic% W) are shown in the table. The thermal vibrations of the W atoms turned out to be very weak ($\sqrt{\overline{u}^2} = 0.05$). This results in a decrease of static atomic displacements for the Fe atoms in comparison with those expected. It is possible to find the over-all indices of static and dynamic distortions for the solid solution as a whole (α_{av} and B_{av}) by averaging after α and B_x have been determined. Since the concentration of W is small, in spite of the considerable diminution of the vibration amplitude of W, the average characteristic temperature of the solvent, within the limits of error, does not differ from the quantity θ, determined by comparing intensities at two temperatures. For the same reason the average value of the static distortion α_{av} is small and hardly perceptible on the slope of the f-curve. It can be assumed that the small distortions (static as well as dynamic) near the W atoms, depend on the strengthening of the Fe–W bonds in comparison with the Fe–Fe bonds.

The above method of calculation for some completely ordered dilute solid solutions can be applied to determine from the room temperature x-ray diffraction patterns, the static and dynamic displacements, not only of the solvent as a whole, but also of every kind of atom separately.

SUMMARY

This paper discusses an x-ray diffraction method of determining the thermal factors B_1 and B_2 (and correspondingly the mean square thermal displacements) separately for the different atoms in binary solid solution.

The method is applicable to ordered and very dilute solutions. It was tested on alloys Cu_3Au (ordered) and Fe–W (1.9% W).

The mean square thermal displacements of copper and gold atoms were found to be equal to 0.18 and 0.12 A, respectively; those of tungsten and iron atoms to 0.05 A and 0.11 A.

LITERATURE CITED

[1] J. Waller and R. W. James, "On the temperature factors of x-ray reflection for sodium and chlorine in the rock-salt crystal," Proc. Roy. Soc. 117, 776, 214 (1927).

[2] D. R. Chimpan, "X-ray study of the local atomic arrangement in partially ordered Cu_3Au," J. Appl. Phys. 27, 7, 739 (1956).

[3] K. Lonsdale, "Vibration amplitudes of atoms in cubic crystals," Acta Cryst. 1, 142 (1948).

Received February 22, 1957

M. V. Lomonosov Moscow State University

ELECTRON DIFFRACTION ANALYSIS OF THE PROCESSES OF DECOMPOSITION OF SUPERSATURATED SOLID SOLUTIONS IN SYSTEMS Al–Cu AND Ag–Cu

Z. G. Pinsker and N. A. Skobel'tsyna

When films of Al–Cu were studied, one observed the effects of quenching and the subsequent decomposition of the solid solution on annealing in the temperature range 130-180°C. The θ-phase separates at once in polycrystalline samples, but in monocrystals – the decomposition of the solid solution is accompanied by the separation of a cubic phase with a = 8.38 A.

When the system Ag–Cu was studied, the effect of quenching was observed. Annealing at 250°C leads to the separation from the α-phase of a tetragonal structure: a = 4.15, c = 11.67 A. When the films are treated to 350°, this phase dissolves in the solid solution.

I. The System Al–Cu

The practical significance of the processes which accompany the variations of mechanical properties of some supersaturated solid solutions have long been of interest to researchers. However, many fundamental phenomena, as well as the metastable structures which are formed during decomposition, have not been thoroughly studied as yet. This is true even of the classical system, Al–Cu, to which most of the work has been devoted [1]. The widespread conception of the nature of the decomposition processes in the supersaturated solution of Cu in Al is the following: low-temperature ageing is related to the formation of planar accumulations of copper atoms in the solid solution, and parallel to them a series of lamellae of aluminum atoms with distorted interplanar distances. These planar groups are parallel to lattice planes of the type (100) of the solid solution. In the literature they are known as Guinier-Preston I zones (GPZ-I). Artificial ageing takes place on annealing, accompanied by the formation of superstructures in solid solution (zones GPZ-II), of the transition phase of the compound, related to $CuAl_2$ (θ'-phase), and finally by the formation of the normal structure $CuAl_2$ (θ-phase) (obviously, together with the basic Al structure). There are several divergences of opinion in connection with this scheme: Are GPZ-I formed on artificial ageing, and is there a genetic connection between GPZ-I and GPZ-II? Is one or are several layers of Cu incorporated into GPZ-I, and what is the lattice structure of the solid solution adjacent to the layers of Cu? Are the above-mentioned structures formed through displacement or from nuclei? Have the structures GPZ-II and the θ'-phase definite inherent periods, or can they be represented by different unit cells? What are the spatial and dimensional relationships between these structures and the lattice of the solid solution? Many other questions exist. The extremely important problems of the correlation between structural changes and the course of hardening, the influence of stress, the role of diffusion, etc., are not mentioned here.

So far the x-ray diffraction method has been the only one used for studying the processes under consideration. Along with the well-known work of Guinier, Preston and other authors, which led to the discovery of the above-mentioned scheme, A. M. Elistratov's paper [2] concerning the diffraction effects observed on the patterns of ageing alloys is of considerable significance. As this author has shown, no account was taken in the above-mentioned researches of the influence of block formation and microcracks, the role of which is, in some respects, equivalent to the GP zones.

Electron diffraction studies of ageing processes in thin layers of the alloys Al–Cu and Al–Ag [3] have been published recently together with x-ray researches. The conclusion reached is that the decomposition processes of supersaturated solutions in thin layers or crystallites are very rapid. Thus, when analyzing films of the alloy Al–Cu containing less than 5% copper, the authors did not observe at any time any diffraction from intermediate phases. Moreover, they did not succeed in following the quenching process. Only the film obtained from alloy evaporation and condensation on the substrate showed the solid solution structure. Annealing above the solution temperature and then quenching below 0°C never yielded any pattern of a single-phase solid solution, nor any intermediate phases, but invariably gave a mixed electron diffraction pattern of Al and the normal structure $CuAl_2$–θ, although the time between the quench and the beginning of diffraction observation was ~ 20 min. Analogous results were obtained when films of the alloy Al–Ag were studied. Quenching the alloy did not lead to fixation of the solid solution; decomposition during formation was observed in all the experiments, together with the aluminum structure in the hexagonal γ-phase. An attempt was also made to follow through the decomposition process in thicker films of Al–Cu, but no definite result was obtained and no metastable phases were observed.

In our study, films of the alloy Al–Cu were obtained by two methods: by volatilization of an alloy with a copper content ~ 20% and by evaporation of Al and Cu from two sources. During the alloy volatilization onto rock salt or celluloid at room temperature, a quenched solid solution was formed. Vapor condensation from two sources was performed on the cleavage surface of sodium chloride crystals heated to 300°C and higher. The quenching of these films was effected in the following manner. They were heated in a vacuum at a temperature higher than the copper solution temperature (450–500°), then thrown by a special device off the surface of the furnace onto a glass lamina at room temperature. Then the small salt crystals with quenched films were split further into 2–3 pieces for structure control in the quenched and tempered states. The annealing was performed in a vacuum in a range of temperature up to 250°C for different intervals of time (up to 6 hrs).

The analysis of the electron patterns obtained led us to the following conclusions. For the polycrystal films it was established that the patterns of quenched samples correspond to the Al lattice. The subsequent annealing of the films at 50–60°C led only to the appearance of one line with d = 4.28 A on the electron patterns, which corresponded to the most intense reflection from $CuAl_2$ – (110). Prolonging the annealing even to 36 hrs at the above temperature did not change the picture. Increasing the temperature of annealing to 80–100° produced a different effect – other lines of the θ-phase appeared. Annealing for an hour in the temperature range of 130–150°C the lines of the θ-phase reached the maximum intensity; moreover, a partial orientation of crystallites of $CuAl_2$ in relation to Al is observed in certain instances (see electron patterns, Figs. 1 and 2).

It should be pointed out that a reflection with d = 3.53 A with average intensity is observed on electron pattern No. 159 of this series; this reflection is in the form of an arc, similar to the arcs from Al on the same pattern, and evidently corresponds to the superstructure or θ'-phase lattice.

Referring to electron pattern No. 170 (Fig. 1) of the same series, we observe, along with the polycrystalline part, thickenings on the series of rings, which indicate the presence of a definite preferred orientation of some crystallites. For the Al crystallites, as in the majority of the other patterns, an orientation of the following type appears:

$$(111)_{Al} \parallel (100)_{NaCl}$$

and besides, $[110]_{Al} \parallel [100]_{NaCl}$ or $[110]_{NaCl}$. The azimuthal orientation increases as the length of heating is increased or during repeated thermal treatment.

The same photograph, No. 170, discloses an accurate orientation of a part of the small crystallites of $CuAl_2$

$$(110)_{CuAl_2} \parallel (111)_{Al} \quad \text{and} \quad [110]_{CuAl_2} \parallel [110]_{Al}$$

The characteristic feature of electron pattern No. 170 is the strong intensity of the lines from $CuAl_2$.

A different picture is observed when films, containing a monocrystal component along with the polycrystalline part are treated. Here we shall give the results of annealing of quenched films at temperatures of 130–180°C for three hours. In neither case was the formation of θ-phase observed. Electron patterns of type No. 225 (Fig. 3) obtained from films annealed for 3 hrs at 180°C are of the greatest interest. Although the temperature and the

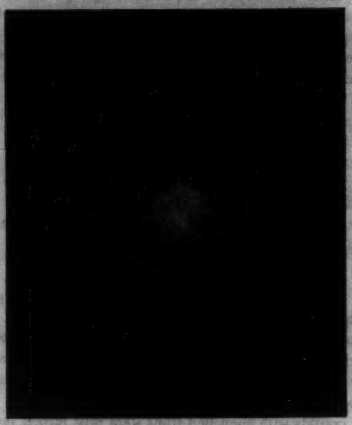

Fig. 1. The electron pattern from the annealed solid solution Cu in Al. Reflections from Al and from θ-phase ($CuAl_2$) are present, partially oriented in relation to Al.

Fig. 2. The same as in Fig. 1. The orientation is not present. Along with Al the film contains a cubic phase with the period a = 8.38 A.

Fig. 3. The electron pattern from the annealed sample of the solid solution Cu in Al. Besides Al, the film contains the transition tetragonal phase: a = = 4.15 A; and c = 11.67 A; the crystallites of this phase are oriented with the base plane parallel to the substrate.

Fig. 4. The electron pattern from an annealed sample of the solid slution Cu in Ag.

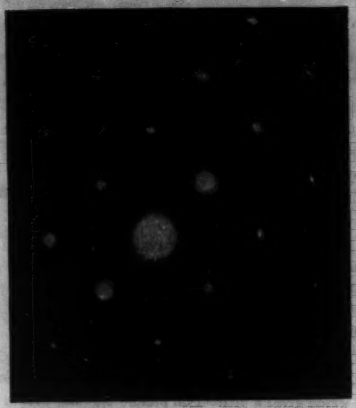

Fig. 5. The same as Fig. 4. The crystallites of the tetragonal phase form a twin with planes ac – (100) parallel to the substrate.

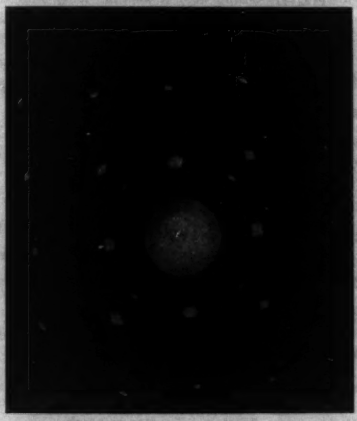

Fig. 6. The same as Fig. 4. The tetragonal phase is represented by the diffraction from the polycrystal.

duration of annealing of these films is greater than that used for the polycrystalline ones, the electron patterns are distinguished by a stronger general background and diffuseness of lines and spots. This, apparently, is connected with the considerable thickness of the samples and the slower course of the decomposition processes and subsequent transformations. From this study we conclude that this electron pattern presents diffraction from two phases: Al and a cubic phase (call it α') with a period a = 8.38 A. The Al crystallites are oriented with their cube planes parallel to the cube plane of NaCl with the cube edge directions coinciding. The crystallites of the second phase occur (along with the polycrystalline part) in two orientations

1) $(100)_{\alpha'} \parallel (100)_{Al}$ and $[100]_{\alpha'} \parallel [100]_{Al}$,
2) $(110)_{\alpha'} \parallel (100)_{Al}$ and $[100]_{\alpha'} \parallel [110]_{Al}$.

A square net of reflections: 220, 400, 440, . . ., is observed on the photographs in agreement with these conditions; and on the rings, 311, 331, . . . corresponding to the second type of orientation of the pair of thickenings. A series of reflections from the α'-phase was also observed on other electron patterns of this group.

Nothing can be said as yet concerning the composition of this phase. Apparently, it is analogous to one of the phases which is formed during artificial ageing. The proximity should be noted of the magnitude $8.38/\sqrt{2} = 5.92$ to the periods 5.71 and 5.80 of the θ'-phases according to Preston.

The first of the above-mentioned types of orientation of the α'-phase in relation to Al is analogous to Preston's observations. A considerable intensity for reflections of the type hk0 with $\Sigma h = 4n + 2$ is observed analogous to the θ-phase and to our α'-phase. However, further structure analysis of this phase should be postponed until new experimental data are obtained.

Thus, the electron diffraction study of the ageing processes of the Al–Cu alloys led to two basic results. In polycrystalline films, when the size of the crystallites is $1\text{-}3 \cdot 10^{-5}$ cm, annealing at 80-130°C for an hour leads to the formation of the stable phase $CuAl_2$ (θ-phase) without any intermediate structures. Moreover, unlike the results of preceding electron diffraction researches, the quenching of the solid solution appears to be fully feasible. Another important result of our work is the observation of the intermediate cubic phase with the period a = 8.38 A during the annealing of monocrystalline films of $5 \cdot 10^{-6}$ cm thickness and over. The essential condition for the formation of transition phases in microsamples is the development of stresses in the contact planes of phases and in the lattice of the solid solution. Of general interest are the observations concerning the very small crystallites and especially the possible existence of solid solution crystals of minimum size in which the decomposition process is accompanied by the formation of transition phases. Obviously, further systematic study is necessary in this case.

II. The System Ag–Cu

As is known, during the annealing of Ag–Cu alloys, which contain no more than 14% copper and are first quenched from the solution temperature (800°C for 14% Cu) decomposition takes place and β-phase is separated, i. e., crystallites of silver solution in copper.

The alloy films in our experiments were prepared by gradual and separate sublimation of silver and copper onto small rock salt crystals, which were first annealed. Following the sublimation they were annealed at 500°C for 30 min, and then the crystals were thrown off onto a cold surface. In our experiments with the Ag–Cu alloy we observed quenching with the formation of single-phase solid solution only in some instances (if the metal film was in direct contact with the cold surface). In other cases the film structure appeared identical to that of the samples that had been annealed.

The electron patterns of the quenched films correspond to a mosaic monocrystal, and that was to be expected, as it is well known that Ag films on rock salt reveal a high degree of orientation under slight annealing. A characteristic distribution of reflections along the straight lines drawn through the lattice of hk0 spots is also observed on the electron pattern. This picture is connected with the deformation of the silver films at the time of their removal from the rock salt and transfer to the celluloid.

The annealing of the quenched films was performed in the temperature range 100–350°C. At 100° (annealing for 1 hr) the separation of a new phase already takes place, which gives a diffraction picture together with the diffraction from the Ag lattice (see Figs. 4, 5,6). The separation of this phase is observed up to 250°. Annealing at 350° leads to the dissolving of the precipitated phase, and, at this temperature, by quenching the film, it is possible to re-establish the initial structure of the single-phase solid solution. The analysis of electron patterns of the above-mentioned phase leads to a tetragonal unit cell with periods a = 4.15 and c = 11.67 A. It was possible to reproduce on various photographs the diffraction from the polycrystalline film, as well as that from the monocrystalline twin, in which the mutually perpendicular components are oriented with ac planes parallel to the substrate.

It is worthy of attention that the interplanar distance d_{110} of silver, equal to 2.88 A, is between the values d_{110} = 2.93 and d_{103} = 2.835 of the new phase. Evidently, this phase can be considered as a superstructure on the framework of the silver lattice, which was formed as a result of copper atom segregation.

Thus, electron diffraction research showed that the processes which accompany the decomposition of the supersaturated copper solid solution in silver require further structural study.

LITERATURE CITED

[1] See, for example, the most recent works of: J. M. Silcock, T. I. Heal, and H. K. Hardy, "Structural ageing characteristics of binary aluminum–copper alloys," J. Inst. Metals 82, 239-248 (1953); V. Gerold, "Über die Struktur der bei Aushärtung einer Aluminum–Kupfer–Legierung auftretenden Zustände," Z. Metallk. 45, 599, 607.

[2] A. M. Elistratov, "The x-ray method of analysis of the initial stages of ageing," Izv. AN SSSR, Ser. Fiz. 15, 60-66 (1951); A. M. Elistratov, S. D. Finkel'shtein, and T. Iu. Gol'dshtein, "X-ray diffraction analysis of the initial stages of ageing of beryllium copper," Doklady Akad. Nauk SSSR 58, 669-672 (1953).

[3] A. Winkelmann, "Elektroneninterferenzuntersuchungen an ausscheidungfähigen Legierungen in Dünnen Schichten," Z. Metallk. 47, 621-63 (1956). In it is also cited literature on electron diffraction research.

Received May 18, 1957

Lobachevskii Gor'kii State University, Inst. Krist., Akad. Nauk SSSR

ELECTRON-DIFFRACTION INVESTIGATION OF POLYMERS

IV. A STUDY OF THE STRUCTURAL CHANGES IN POLYCHLOROTRIFLUOROETHYLENE IN THE CRYSTALLINE MELTING POINT RANGE

A. V. Ermolina, G. S. Markova, and V. A. Kargin

Polymeric substances are formed from groups of atoms regularly arranged in the chain molecule. The elements of order arising in consequence of this are in the first instance connected with the existence of these large chain molecules. It is quite obvious that even amorphous polymers ought to be more ordered systems than are low molecular liquids.

During the crystallization of polymers there arises a high regularity of mutual distribution of molecular chains, which introduces additional elements of order into the system. The study of the phenomena which occur during the crystallization of polymeric substances should not be limited to examination of the order in a crystalline polymer. A comparison should also be made of the order existing in the crystalline polymer with the order in a polymer known to be in the amorphous state. Otherwise the order existing in the chain molecule may be confused with the order arising in a system of molecules in the process of crystallization.

A comparison of the order existing in the same polymer occurring in the crystalline and the amorphous states is the point of the present investigation.

EXPERIMENTAL

We have investigated samples of polychlorotrifluoroethylene [1] which were prepared in the form of thin films on hot glycerol (160°C) by evaporation of the solvent from a solution of the polymer in mesitylene.

The work was carried out on the electron diffraction camera EM-4 [2]. Sodium chloride, deposited on a collodion backing, served as the standard during determination of the interplanar spacings.

The thin films of polymer prepared from solution, of not more than 0.02-0.03 μ in thickness, were always found to be crystalline.

For obtaining the polymer in the amorphous state (in the form of a melt), an electric oven was constructed and placed directly in the electron diffraction camera. The annealing temperature was controlled by a thermocouple placed in the housing of the oven in close proximity to the sample under study. The thermocouple was calibrated with respect to the melting point of thallic nitrate and metals (Sn, Bi, Cd) in the chamber of the electron diffraction camera.

Thin films of the metals and the salt were prepared by depositing on a collodion backing in a vacuum deposition apparatus VUP-2 [3]. The metallic films and the films of polychlorotrifluoroethylene were coated with a thin layer of quartz for protecting them from destruction in the course of annealing.

The electron diffraction patterns from the crystalline films of polychlorotrifluoroethylene contain about 20 rings of uniform intensity around the circumference (Fig. 1). All the rings can be explained on the basis of a hexagonal cell with periods $a = 6.34$ A, $c = 35$ A.

In Table 1 are given the interplanar spacings of crystalline polychlorotrifluoroethylene. Estimation of the intensity of the reflections was made visually according to a scale with five steps.

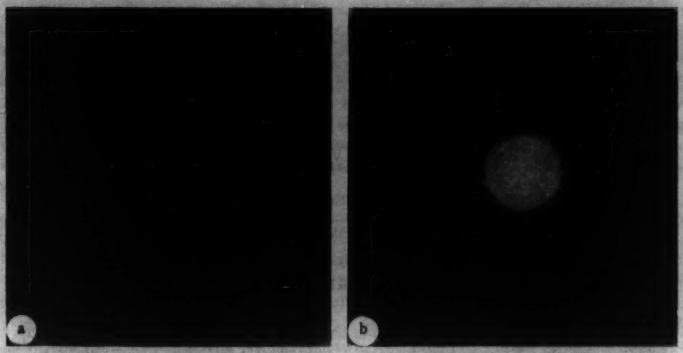

Fig. 1. Electron diffraction patterns from films of polychlorotrifluoroethylene: a) crystalline, b) amorphous (liquid).

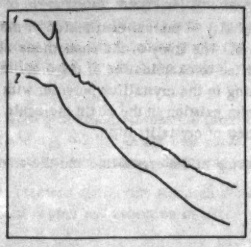

Fig. 2. Microphotometer traces of electron diffraction patterns of polychlorotrifluoroethylene: 1) crystalline, 2) amorphous.

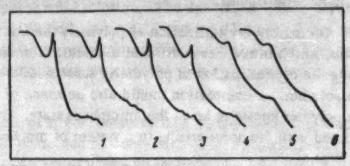

Fig. 3. Microphotometer traces of electron diffraction patterns of polychlorotrifluoroethylene, obtained at different temperatures: 1) at 20°C, 2) at 80°C, 3) at 150°C, 4) at 210°C, 5) at 240°C, 6) at 280°C.

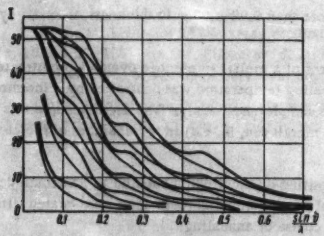

Fig. 4. Microphotometer traces.

The photometry of the electron diffraction patterns was carried out on the recording microphotometer MF-4. In Fig. 2 are presented the microphotometer traces from electron diffraction patterns of the crystalline and amorphous polymer. In Fig. 3 is given a series of microphotometer traces of electron diffraction patterns obtained with cyrstalline and melted films of the polymer, at different temperatures.

To show the order existing in an amorphous polymer, the radial distribution method was used. Until recently this method has been used chiefly in the study of the structure of liquid and amorphous bodies [4], and in a number of papers it is used in the study of polymers [5].

The radial distribution function has been calculated for the case of a polyatomic molecule, the atoms of which are different [6]. The treatment of electron diffraction patterns for obtaining an experimental intensity curve was carried out in the same way as in [7, 8]. In Fig. 4 are given the microphotometer traces for amorphous polychlorotrifluoroethylene. In this case the microphotometer traces of quartz with corresponding exposure times served as background, since the polychlorotrifluoroethylene melt had been obtained on a quartz backing.

TABLE 1

Interplanar Spacings of Polychlorotrifluoroethylene

No.	d A	Intensity	No.	d A	Intensity
1	5.48	very very strong	10	3.04	very weak
2	5.35	very strong	11	2.70	average
3	5.14	strong	12	2.67	average
4	4.48	average	13	2.58	weak
5	3.18	average	14	2.09	weak
6	3.17	weak	15	2.01	weak
7	3.12	very weak	16	1.84	weak
8	3.10	very weak	17	1.76	very weak
9	3.05	very weak	18	1.58	very very weak
			19	1.33	very very weak

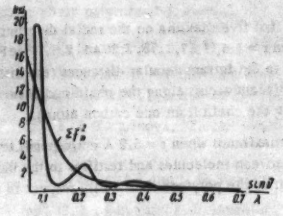

Fig. 5. Experimental curve of intensity, and Σf_n^2, the curve of the atomic factor.

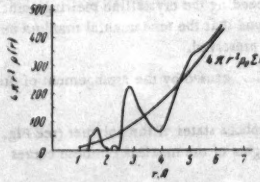

Fig. 6. Radial distribution curve.

After density curves were plotted and the intensity at different values of $\frac{\sin\vartheta}{\lambda}$ determined, an experimental intensity curve of the amorphous polymer was obtained (Fig. 5). Normalization of the intensity curve was carried out with respect to the atomic factor curve, calculated for the repeated atomic grouping of the polymer. In the calculation of the atomic factor curve, correction for incoherent scattering is taken into account. Using the formula proposed by B. K. Vainshtein, function i_s was calculated

$$i_s = \frac{I_s - \Sigma f_n^2}{\Sigma f_e^2}.$$

Here I_s is the experimental intensity for the given value of $\frac{\sin\vartheta}{\lambda}$; Σf_n^2 is the atomic factor with correction for incoherent scattering; Σf_e^2 is the atomic factor of the atom selected as the unit of measure of the scattering power.

The radial distribution function was calculated from the formula

$$4\pi r^2\rho(r) = 4\pi r^2\rho_0 \sum_n K_n^2 + \frac{2r}{\pi}\int si_{(s)} \sin sr\, ds.$$

Here $\sum_n K_n^2$ takes into account the difference in the scattering power of the atoms and is equal to the sum of the squares of the relative scattering powers of the atoms in the molecule. The scattering power of carbon, the lightest atom of the molecule, is taken as the unit of measure of scattering power.

In Fig. 6 is given the radial distribution curve for amorphous polychlorotrifluoroethylene. Maxima in the curve occur for r equal to 1.40, 1.57, 1.75, 2.25, 2.8 and 5.2 A.

For comparison of the order existing in crystalline and amorphous samples, we have calculated the experimental intensity curve for crystalline polychlorotrifluoroethylene. In Fig. 7 the experimental intensity curves for the crystalline and the amorphous polymer are presented for comparison.

DISCUSSION OF RESULTS

For an analysis of the data obtained, we turn to the structure of the repeated atomic grouping of the polychlorotrifluoroethylene molecule:

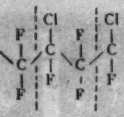

It is known [9, 10] that in the polychlorotrifluoroethylene molecule the following distances are likely:

C–F = 1.36 A
C–C = 1.54 A
C–Cl = 1.75 A
F–F (from one C) = 2.16 A
F–F (from adjacent C's) = 2.7 A
C–C (in zigzag) = 2.8 A

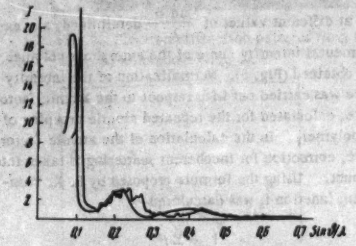

Fig. 7. Experimental intensity curves of crystalline and amorphous polychlorotrifluoroethylene.

The first five maxima on the radial distribution curve, when r = 1.4, 1.57, 1.75, 2.25 and 2.8 A (see Fig. 6), correspond to the intramolecular distances (the distances between adjacent atoms along the chain and between atoms along the chain from one carbon atom).

The maximum when r = 5.2 A corresponds to the distances between molecules and testifies to the ordered arrangement of the polymer chains with respect to one another.

In a comparison of a number of microphotometer traces from a series of electron diffraction patterns obtained in the process of annealing the sample down to a temperature exceeding the crystalline melting point (Fig. 3), it is found that the fundamental maxima on these traces are preserved.

This indicates the existence in the polymer melt of elements of order, caused by the arrangement of the same polymer chains.

In a comparison of the intensity curves for the crystalline and amorphous states of the polymer (see Fig. 7), a marked similarity between them is observed. The difference in the heights of the maxima on these curves amounts to 13% in all.

This circumstance is evidence of the rather high degree of order existing in polychlorotrifluoroethylene in the amorphous state and not of a significant imperfection in the polymer crystals, as might have been supposed on the basis of other experimental data.

Thus, polychlorotrifluoroethylene even in the amorphous state is a highly ordered system. The degree of order of the polymer in the crystalline state is very close to the order in the amorphous state, differing by the presence of additional elements of order. Evidently during crystallization of polychlorotrifluoroethylene there occurs the formation of supplementary spatial bonds, whereby the order in the arrangement of the chains is preserved to about the same degree as it was in the amorphous state.

SUMMARY

1. Electron diffraction patterns of films of crystalline and melted polychlorotrifluoroethylene were obtained at different temperatures down to the melting point of the crystals.

2. A radial distribution curve was calculated, on which were shown maxima corresponding to the intramolecular interatomic distances, and a maximum corresponding to the intermolecular distance.

3. It is established that polychlorotrifluoroethylene in the amorphous state is a well- ordered liquid. During crystallization of this polymer there occurs an improvement of the order already existing in the amorphous state.

LITERATURE CITED

[1] H. S. Kaufman, "X-ray examination of polychlorotrifluoroethylene," J. Am. Chem. Soc. 75, 1477 (1953).

[2] G. O. Bagdyk'iants, "Industrial model of the electron diffraction camera EM-4," Izv. AN SSSR, Ser. Fiz. 17, 225 (1953).

[3] A. N. Frimer and A. K. Nefedov, "Apparatus for electron-microscopic preparation (VUP-1)," Izv. AN SSSR, Ser. Fiz. 15, 336 (1951).

[4] R. James, Optical Principles of X-ray Diffraction [Russian translation] (Moscow, 1950), pp. 421-434.

[5] A. Bjornhaug, O. Ellesen, and B. A. Tönnesen, "An approach to the solution of the structure problem in organic chain polymers," J. Polymer Sci. 12, 621 (1954).

[6] B. K. Vainshtein, "Toward the theory of the radial distribution method," Kristallografiia 1 (1957).*

[7] I. I. Iamzin, "Atomic scattering of electrons (proof of the laws of atomic scattering of electrons by means of intensities of electron diffraction patterns)," Trudy Inst. Krist. 5, 69-112 (1949).

[8] L. I. Tatarinova, "Electron-diffraction investigation of amorphous antimony," Trudy Inst. Krist. 11, 104-114 (1955).

[9] L. S. Bartell and L. O. Brockway, "Structure of CH_3F and CH_3Cl," J. Chem. Phys. 23, 1860 (1955).

[10] C. W. Bunn and E. R. Howells, "Structure of molecules and crystals of fluorocarbons," Nature 174, 549 (1954).

Received February 22, 1957

L. Ia. Karpov Institute of Physical Chemistry

* [See Soviet Physics – Crystallography.]

ELECTRON-DIFFRACTION STUDY OF THE OXIDATION OF ALUMINUM ALLOYS

Iu. D. Chistiakov and M. V. Mal'tsev

The protection of metals and alloys from oxidation under present production and operating conditions is of paramount importance.

With poor protection, fuel losses are increased, contamination of the metal by oxide impurities is increased, the heat resistance of products of this metal decreases, the surface quality deteriorates, the corrosion resistance decreases, etc.

Protection of the metal from oxidation in the solid and particularly in the molten state, as is well known, is accomplished by a thin surface film, on the nature and properties of which its protective qualities in many respects depend.

Study of the structure and properties of the surface films which form on molten and solid metals and the investigation of ways for improving them are most important for increasing the quality of industrial alloys and decreasing their production losses.

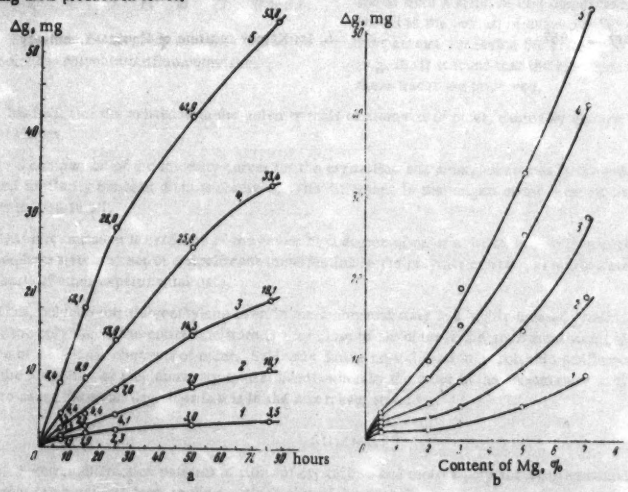

Fig. 1. Oxidizability of Al–Mg alloys at 500°C; a) as a function of oxidation time, b) as a function of Mg content in alloy.

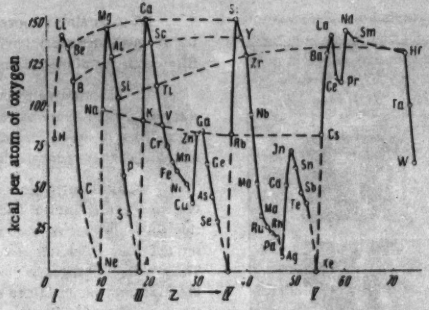

Fig. 2. Periodicity of heats of formation of oxides of different metals.

All these problems acquire a special significance in the production of aluminum alloys, since the base of these alloys, aluminum, is an extremely active metal.

In our earlier publications [1-3] the oxidation processes both of pure aluminum and of the most important industrial aluminum alloys were investigated, and the structure and properties of the surface phases which form in the process of oxidation both in the solid and in the molten state were studied.

It was shown that the structure and properties of oxide films on these alloys depend basically on the alloy itself – specifically on the content of metals chemically more active than aluminum (for example, magnesium).

As a result of electron-diffraction investigation of the structure of oxide films on molten and solid metals it was established that all the industrial aluminum alloys can be divided into four basic groups (depending on their Mg content):

I) Not containing Mg (pure Al, AMts,* etc.), having on the surface of the molten metal an oxide film consisting of pure aluminum oxide (γ Al_2O_3).

II) Containing from 0.01 to 0.05% Mg, having on the surface an oxide film consisting of a mixture of γ Al_2O_3 and $MgO \cdot Al_2O_3$.

III) Containing from 0.05 to 1.5% Mg (the majority of industrial alloys), having a surface film consisting of a mixture of MgO and $MgO \cdot Al_2O_3$.

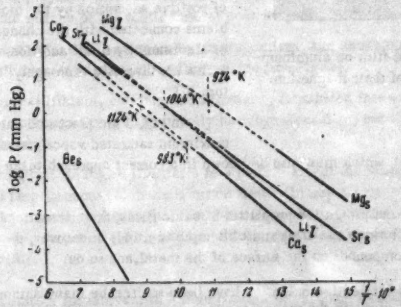

Fig. 3. Temperature dependence of maximum saturated vapor pressure of different metals.

* Transliteration of Russian – Publisher's note.

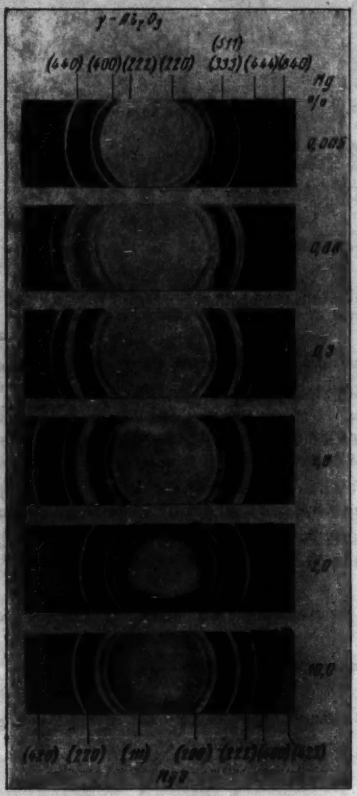

Fig. 4. Structure change in oxide film on aluminum-magnesium alloys as a function of their magnesium content.

IV) Containing above 1.5% Mg (some duraluminis, magnaliums, etc.), having on the surface an oxide film consisting of magnesium oxide (MgO).

The quantitative aspect of the oxidation process was also studied in our papers. In Fig. 1 is shown the dependence of the oxidizability of the alloys on time (a) and the quantity of magnesium in the alloy (b).

Further investigations showed that besides magnesium a whole series of "active" metals have a considerable influence on the structure and properties of the surface films which form on aluminum and its alloys. These radical changes in the structure and properties of the films may be explained by a tendency toward selective oxidation of additions of "active" metals, specially introduced, or present in the alloy as impurities of the basic components.

It was established [4, 5] that the activity of the different metals is determined first of all by the decrease in free energy of formation of the compound (oxide, nitride, etc.) by surface activity, i. e., by the tendency toward positive adsorption of the introduced metal by the molten surface, by the rate of diffusion of this metal into the alloybase , by the saturated vapor pressure and by other factors.

The choice of additions of "active" metals, to a first approximation, may be guided by data on the heats of formation of oxides and nitrides [5]. The graph presented in Fig. 2 may serve as an example, where the periodicity of the heats of formation of the oxides of different metals is shown in kilocalories per g-atom of oxygen.

A greater heat of formation of the oxide is associated with a greater "activity" of the metal.

Additions of various metals which reduce the surface tension of aluminum are surface-active, capable of positive adsorption by the molten surface. The problems connected with the change in the surface tension of aluminum by small additions of surface-active elements are discussed thoroughly in contemporary literature [6].

In Fig. 3 are presented data characterizing the maximum saturated vapor pressure of some elements at different temperatures [7, 8, 9], which must also be known in a correct approach to the choice of "active" additions.

In an accurate appraisal of the protective properties of oxide films, the orientational and dimensional congruence of the resulting film and base of the alloy must be borne in mind; moreover, the oxidation products ought not to yield low-melting compounds on the surface of the metal, and so on.

The problems connected with selective oxidation have been studies by many authors; the most detailed survey of papers bearing on this is given in the monograph [10]. However, very little attention is paid to aluminum alloys, which are of such great importance technologically. Work carried out in this field makes it possible

Fig. 5. Composition of oxide film on aluminum-beryllium alloys.

to recommend to industry special additives, the introduction of which into alloys would afford protection from oxidation, promote purity of the metal and improve a number of technological properties.

On the basis of the premises expressed above, we have selected the following "active" metals: beryllium, lithium, calcium, strontium, barium and magnesium, as additions to aluminum alloys.

The effect of these additions on the structure formation of oxide films which form on molten and solid metals was examined. Investigations of the structure of the surface films were carried out by means of electron-diffraction phase analysis with the electron-diffraction camera EM-4. Simultaneously with these investigations, a study was made of the structure of oxide films with the help of electron shadow microscopy, on the same instrument, with magnifications from 1000 to 5000 times.

As a result of these investigations it was established that all additions of "active" metals take part to a greater or lesser degree in the process of formation of the surface film.

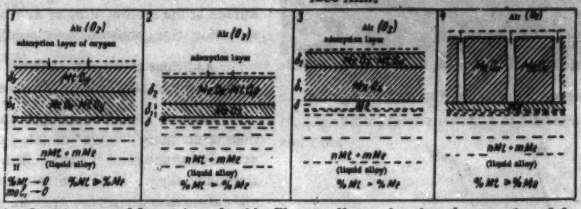

Fig. 6. Diagram of formation of oxide film on alloys related to the quantity of the more "active" metal (Me).

The degree of participation of the metal introduced into the alloy (versus the base) in the formation of the oxide film is determined by its "activity."

Thus, for example, only when the content is above 1.5% will magnesium, introduced into aluminum, yield an oxide film on the surface of the molten metal consisting of pure magnesium oxide (see Fig. 4).

Beryllium is more "active" compared with magnesium, and above 0.05-0.2% Be in binary Al—Be alloys, the surface oxide film consists of pure beryllium oxide (see Fig. 5).

Such additions as lithium, calcium and strontium, introduced into aluminum, act in an analogous manner. They form, at low concentrations, a structurally heterogeneous film, but assume a fundamental role in its formation after a certain point.

The diagram given in Fig. 6 illustrates to a certain extent the kinetics of the formation process of heterogeneous (1-3) and homogeneous (4) oxide films on similar binary alloys,* as related to the quantity of an introduced additive (Me) more active than the alloy base (Mt). With one of the conditions there is the possibility of forming a spinel type compound ($MeO \cdot Al_2O_3$), which forms in the oxide film at low concentrations of the additive (Me) in the alloy.

* Diagram (4) is correct for alloys with a high content of "active" additive, the oxide of which does not yield an unbroken surface film (for example, Al—Mg alloys with > 1.5% Mg).

Fig. 7. Composition of oxide film on Al–Mg–Be alloys.

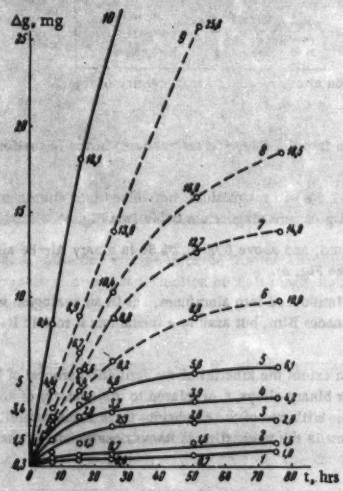

Fig. 8. Effect of Be, Li and Ca on the tendency toward oxidation of Al–Mg alloys at 500°C.

It is essential to note two basic points in the process of selective oxidation of binary alloys:

1. The less noble the more "active" metal is in the alloy, the sooner it is oxidized, forming a sublayer on the surface of the metal, after which the oxide of the alloy base begins to form on this sublayer.

2. The heterogeneity of the oxide film is not that of a finely dispersed mixture, but alternating thin layers are always formed from the oxides which give a characteristic diffraction effect on the electron diffraction patterns. This is also confirmed by the electron microscope investigations of oxide films removed from molten metals.

The circumstances are analogous in the case of more complex (multicomponent) alloys. In such cases as, for example, Al–Mg–Be, the addition to the alloy of the most "active" metal, Be, is the determining factor in the process of formation of the oxide film. Thus, in an alloy of Al + 5.0% Mg + 0.05% Be (see Fig. 7) the structure of the oxide film is heterogeneous and consists of a mixture of the oxides MgO and BeO, but on the surface of the molten alloy of Al + 5.0% Mg + 0.5% Be the oxide film consists of pure beryllium oxide.

Additions of calcium, lithium and strontium when introduced into an Al–Mg alloy give an analogous picture.

However, it should not be supposed that only additions of the more "active" metals determine the composition and structure of the oxide film on the surface of aluminum alloys. Such elements as silicon, iron and manganese also act on the structure of the oxide film on these alloys. However, the kinetics of oxide film formation involving these metals is not completely clear and requires further investigation.

Besides the electron-diffraction examinations, we have investigated the oxidation processes of aluminum alloys by the gravimetric method. Based on the results of the investigation, graphs were constructed showing the oxidizability of Al–Mg alloys with different additions (Be, Li and Ca) at 500°C (Fig. 8). Analysis of these graphs shows (cf. Fig. 1) that the tendency toward oxidation of Al–Mg alloys on introduction of small additions of beryllium is reduced by 50–100 times (depending on the magnesium content in the alloy). Calcium and lithium act in an analogous manner, but the effect upon introduction of these metals is considerably smaller than that with the introduction of Be.

Thus, it is shown that aluminum alloys, depending on the composition and particularly on the presence in them of additions more "active" than aluminum, tend toward selective oxidation.

With proper utilization in industry, all this can be of considerable help in the difficulties experienced with the oxidation of alloys during their production and use.

LITERATURE CITED

[1] M. V. Mal'tsev , Iu. D. Chistiakov, and M. I. Tsypin, Doklady Akad. Nauk SSSR 99, 5 (1954).

[2] M. V. Mal'tsev , Iu. D. Chistiakov, and M. I. Tsypin, Izv. AN SSSR, Ser. Fiz. 20 (1956).

[3] Iu. D. Chistiakov and M. V. Mal'tsev, "Toward the question of the purity of metal and the contamination of molten metal by oxidation and other impurities," Foundary Industry (in press).

[4] Iu. D. Chistiakov, Investigation of Some Physicochemical Properties of Molten Aluminum and Its Alloys (Dissertation) [in Russian], Moscow Institute of Gold and Nonferrous Metals (Moscow, 1956).

[5] G. V. Samsonov and Iu. D. Chistiakov, "Metallothermal methods in chemistry and metallurgy," Uspekhi Khim. 25, 10, 1223-1248 (1956).

[6] A. M. Korol'kov, "Surface tension of aluminum and its alloys," Izv. AN SSSR,OTN 2, 35-42 (1956),

[7] Iu. A. Priselkov and A. N. Nesmeianov, "Determination of the vapor tension of calcium and strontium below the melting point by means of labeled atoms," Doklady Akad. Nauk SSSR 95, 6, 1207-1210 (1954).

[8] M. Moncherat, J. Phys. Radium 7, 10 (1939); 10, 441 (1939).

[9] R. Holden, Speiser, and R. Johnston, "The vapor pressures of inorganic substances," J. Am. Chem. Soc. 70, 3897-3899 (1948).

[10] O. Kubashevskii and V. E. Hopkins, Oxidation of Metals and Alloys (D. V. Ignatov, editor) [Russian translation] (IL, 1956).

Received February 22, 1957

M. I. Kalinin Moscow Institute of Nonferrous Metals and Gold

A DOUBLE CRYSTAL NEUTRON SPECTROMETER

V. N. Bykov, S. I. Vinogradov, V. A. Levdik, and V. S. Golovkin

A double crystal neutron spectrometer is described. It is shown that the instrument can be used to analyze either single crystals or polycrystalline specimens.

Atomic reactors provide the opportunity of having a sufficiently intense, well collimated flux of thermal neutrons for diffraction work on crystals with the object of determining the crystal and magnetic structures, studying the ordering processes, and solving other problems.

We used for these purposes one of the horizontal channels leading from the active zone of a power station reactor and having a neutron flux of $2 \cdot 10^{12}$ neutrons/cm^2 · sec [1].

A considerable length of the channel, made in the form of a steel tube 65 mm in diameter, passing a monitoring reflector and more than 4 m of protective cover, provided a beam of neutrons naturally collimated to 24'. Thus the integrated flux of thermal neutrons in the beam incident on the monochromator was equal to 10^7 neutrons/cm^2 · sec.

The neutrons were made monochromatic by reflecting the beam from the (200) plane of a lead crystal, measuring 135 × 55 × 20 mm. The reflection angle θ was chosen from the following considerations. For a fixed collimation of the beam for a given single crystal the resolving power $\Delta\theta$ is the same for all θ. The integrated reflecting power ρ from the face of a large mosaic crystal for given wavelengths can be estimated in the following way [2]:

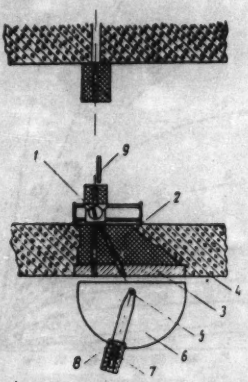

Fig. 1. Plan of the apparatus for studying neutron diffraction.

$$\rho \sim \lambda^3 \frac{1+\cos^2 2\theta}{2\sin 2\theta} \quad \text{or} \quad \rho \sim \frac{1}{v^3}\frac{1+\cos^2 2\theta}{2\sin 2\theta}.$$

The total intensity J of the thermal neutron beam reflected in the velocity interval $\Delta v = v_2 - v_1$ can be written in the form

$$J = \int_{v_1}^{v_2} \rho(v) I(v)\, dv = \rho(v_\xi) I(v_\xi)\, \Delta v,$$

where $I(v) = \frac{4\pi}{v_0^3\sqrt{\pi}} v^3 e^{-\left(\frac{v}{v_0}\right)^2}$ is the specific intensity of the neutron flux and $v_\xi \in (v_2 - v_1)$. It is easy to show that for $\theta \approx 16°$ and less, as in our case, $\rho \sim \frac{1}{v^3}$ and $\Delta v \sim v^3 \Delta\theta$; consequently

$$J = I(v_\xi)\Delta\theta \sim v_\xi' e^{-\left(\frac{v_\xi}{v_0}\right)^2}. \qquad (1)$$

Fig. 2. Monochromator block with monitoring counter.

Thus, the reflected beam of neutrons has the same velocity distribution as has a "white" beam incident on the crystal.

The efficiency of a sufficiently long boron counter with a transparent window is independent of the neutron velocity; therefore, its count is proportional to the neutron flux.

The chosen angle θ corresponds to a maximum in the neutron flux distribution (I) which corresponds to $v_E = 1.225 v_\theta$, where v_θ is the most probable velocity from the Maxwellian distribution. Usually a power station reactor works under conditions where $v_\theta = 3 \cdot 10^5$ cm/sec; thus $\lambda = 3.98 \cdot 10^{-5}$, $1/v_E = 1.08$ A and $\theta = 12°40'$.

Fig. 3. Turning arrangement.

The peak width of the beam reflected from the monochromator is, at its base, 1°20', which demonstrates the deterioration in resolving power due to the considerable mosaic quality of the lead crystal. The peak half-width of 37' corresponds to a wavelength scatter of $\Delta\lambda = 4.9 \cdot 10^{-2}$ A, or to an uncertainty in the neutron energies of about 9%. The reflected beam also contains 2.5% of diffusely scattered neutrons. The total monochromatic flux was 10^4 neutrons/cm^2·sec.

The monochromator (see Fig. 1) block is arranged as a goniometer so that the lead crystal can be moved and turned in all directions. The reflected monochromatic beam passes through the channel in the protective cover of paraffin with boron carbide 2 and lead 3 mounted in an 800 mm thick wall of reinforced concrete. The beam, cut down by cadmium slots, is incident on the specimen under investigation which is fastened in the goniometric head on spindle 5 of the spectrometer.

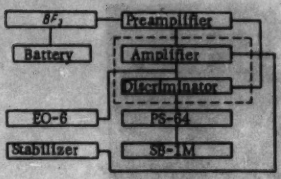

Fig. 4. Block diagram of the neutron-counting arrangement.

The instruments used for measuring the intensity of the monochromatic reflections would be correctly called diffractometers, however, according to already established custom, we shall call them spectrometers.

In the literature three basic types of neutron spectrometers are described: a) instruments for use in powder diffraction methods with applications for large specimens (in view of the negligible intensity of the neutron beam) [3], b) small instruments of the Pepinsky neutron goniometer type [4], c) spectrometers of lighter construction for studying single crystal specimens using small counters [5].

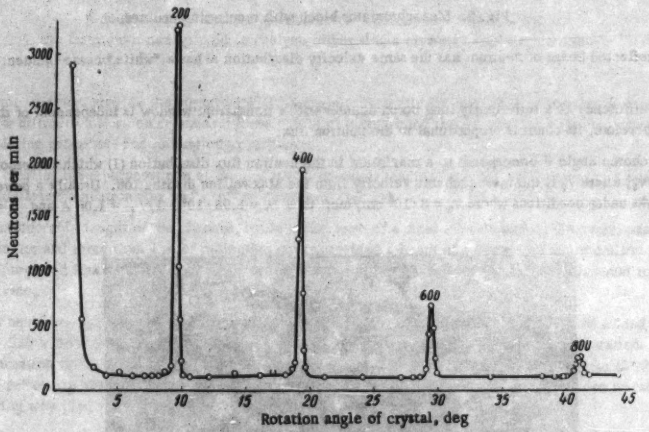

Fig. 5. Diffraction curve for a single KBr crystal.

We took as a basis the last type of spectrometer. The construction of our instrument (Fig. 3) allows the distance from the specimen to the counter to be changed (from 200 to 1000 mm), which gives, as stated above, the required intensity for studying either single crystals or polycrystalline specimens.

The spectrometer table 6 is a steel slab in the form of a 1100 mm diameter circle cut off on one side. Through the center of the table passes spindle 5 (see Fig. 1) revolving on bearings in the column. The goniometer head with specimen is attached on the upper part of the spindle and a rigidly attached graduated circle on the lower. Angles can be measured with the circle to an accuracy of 2'. Readings were taken using optical tubes. Round the spindle column revolves a carriage carrying the counter 7, protected with boron carbide 8. The carriage and spindle are connected together by a system of gears providing a ratio of 2:1 for the angular rotation. The construction also provides for independent motion of the carriage and spindle. The travel of the counter and rotation of the specimen are performed either by hand or by a synchronized motor with a toothed wheel engaging a rack fixed to the upper edge of the table. A block diagram of the neutron-counting arrangement is shown in Fig. 4.

A 20 mm diameter counter with a working length of 270 mm and filled to 700 mm Hg with boron trifluoride enriched 4.7 times with isotope B^{10}, was used as a detector. From the detector the impulse enters the amplifier unit consisting of preamplifier and amplifier which are equipped with television-type pin tubes. The parameters of the amplifier unit are as follows: the admission band is 3 Mcps, the input impulse negative, the output impulse

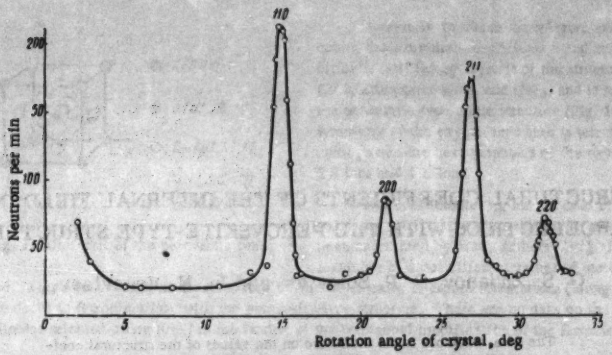

Fig. 6. Diffraction curve for polycrystalline iron.

positive, the maximum amplification factor is 10^4 and the output amplitude 95 v. A discriminator of the Schmidt cell type is mounted on the same chassis as the amplifier. The amplifier unit has a stabilized feed. Impulse registration was carried out by a type PS-64 counting instrument and a mechanical counter. Working in parallel is a monitor channel, the counter 9 and counting arrangement of which are similar to the arrangement of the primary channel.

As an example, we show the neutron diffraction pattern of a single KBr crystal of dimensions 6 x 6 x 8 mm (Fig. 5) and an 8 mm diameter polycrystalline specimen of iron (Fig. 6) which demonstrate the possibility of using comparatively small specimens to obtain sufficiently intense diffraction peaks with good resolution.

The experiments carried out show that the spectrometer described satisfies the requirements, both of intensity and resolving power, demanded of instruments of the same type for carrying out structure investigations.

In conclusion, I express my thanks for help rendered in this work to Doctor of Math. Phys. Sciences A. K. Krasin and to Doctor of Chemical Science V. S. Liashenko and also to L. S. Gudkov for participating in the growing of the single crystal.

LITERATURE CITED

[1] D. I. Blokhintsev and N. A. Nikolaev, Construction and Theory of Reactors (Lectures of the Soviet Delegation to the International Conference on the Peaceful Uses of Atomic Energy), 1955.

[2] R. James, Optical Principles of the Diffraction of X-ray Beams (IL, 1950).

[3] E. O. Wollan and C. G. Shull, "The diffraction of neutrons by crystalline powders," Phys. Rev. 73, 8, 830 (1948).

[4] R. Pepinsky, B. C. Frazer, and M. L. McKeown, "New goniometers for single-crystal neutron diffraction studies," Rev. Sci. Instr. 25, 7, 699 (1954).

[5] G. E. Bacon and R. F. Dyer, "A spectrometer for single-crystal neutron diffraction," J. Sci. Instr. 32, 7, 256 (1955).

Received March 24, 1957

STRUCTURAL COEFFICIENTS OF THE INTERNAL FIELD IN FERROELECTRICS WITH THE PEROVSKITE-TYPE STRUCTURE

G. S. Zhdanov, S. P. Solov'ev, and Iu. N. Venevtsev

The data available in the literature on the values of the structural coefficients of the internal field in crystals with the perovskite-type structure is critically examined.

The relation between the structural coefficients for the case of dipoles oriented in the directions [001], [011], and [111] in a cubic cell of perovskite type is determined.

The structural coefficients for the tetragonal cell of lead titanate at room temperature are calculated, taking into consideration the displacement of the ions.

INTRODUCTION

One of the problems in the theory of ferroelectric properties connected with the perovskite-type structure is the role of the internal electric field which acts on the constituent ions in these compounds. The solution of this problem essentially depends upon the accurate evaluation of the so-called structural coefficients which enter into the field equations.

The field, which acts on the ith ion, is

$$E_i = E + \sum_{k=1}^{m} \left(\frac{4\pi}{3} + C_{ik}\right) p_k , \qquad (1)$$

where m is the number of sublattices into which the initial structure is divided, so that each of them contains only ions of the ith kind; E is the external field strength; p_k is the dipole moment, connected with ions of the kth kind; C_{ik} are the structural coefficients.

The structural coefficients C_{ik} in their own physical sense determine the field strength, in addition to the Lorentz field, produced by sublattices of unit dipoles of the kth kind and which act on ions of the ith kind.

The structural coefficients depend only on the structural geometry. In the case of dipoles aligned in the direction of the Z axis, coincident with the unit cell edge, the structural coefficients are determined by the expression

$$C_{ik} = \sum_{j} \frac{2z'_{jk} - x'_{jk} - y'_{jk}}{\left(x'_{jk} + y'_{jk} + z'_{jk}\right)^{5/2}}. \qquad (2)$$

Here x_{jk}, y_{jk}, z_{jk} are coordinates of the jth dipole of the kth kind with respect to the dipole of the ith kind, and the summation is made over all dipoles of the kth kind, forming an infinite lattice. As dipoles are related to ions of the appropriate kind, then in the limit we shall say "ions" instead of "dipoles."

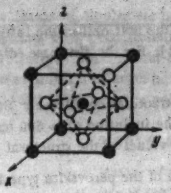

Fig. 1. Unit cell of the perovskite type.

In crystals in which the microscopic symmetry is cubic, the structural coefficients equal zero. This condition is satisfied by crystals of the structure types NaCl, CsCl, ZnS (sphalerite), and CaF_2; and is not satisfied by the perovskite-type cubic structure (Fig. 1). The point symmetry of the oxygen ions here is tetragonal and not cubic, since the next neighbors of the oxygen ions are 2 B ions and 4 A ions.

The coefficients C_{1k} for the case of dipoles oriented along [001] in the perovskite-type structure have been calculated by many authors [1-7]. However, in a number of cases different values of the coefficients were obtained. There are no data in the literature for the other cases of dipole orientations (along [011] and [111]), which occur in ferroelectrics with the perovskite-type structure. There are no data on the structural coefficients for dipoles oriented along [011] in the lattice of the tetragonal modification of the ferroelectric $PbTiO_3$.

The question about the structural coefficients for the different cases of dipole orientations in the cubic cell of the perovskite type and for the case of orientation along [001] in the tetragonal cell of $BaTiO_3$ and $PbTiO_3$ are considered in the present paper.

1. Structural Coefficients for a Cubic Cell of the Perovskite Type

The structural coefficients are expressed by means of a convergent series (2), which one can calculate approximately by summation not over all the infinite lattice, but only over the limited part included in the Lorentz sphere. This method of calculation is called the Lorentz method. More accurate results can be obtained, for example, by the methods of Ewald [8] and Madelung [9]. In these methods rapidly converging series are used by means of which one calculates the potential of the field at any point of the unit cell of the crystal. The structural coefficients are then obtained by differentiating the potential with respect to the coordinates of the point for which the internal field is to be determined.

The values of the structural coefficients in the case of a cubic cell depend upon the orientation of the dipoles in the crystal. In [2] was shown the calculation of the field S(r),* created by a unit dipole, which forms

TABLE 1

Values of the Structural Coefficients, Calculated by Different Methods, for the Case of Dipoles Oriented Along [001] in the Cubic Cell of the Perovskite Type*

Coordinates of points in the unit cell, x, y, z	Data of McKeehan			Data of Jaynes	
	$S_z(x,y,z)$			$4\pi/3+S_z(x,y,z)$	
	general expression	Lorentz method	Ewald method	Ewald method	method of field decomposition
0, 0, 0	0	0	0	4.18879	4.18879
$\frac{1}{2}, \frac{1}{2}, \frac{1}{2}$	0	0	0	4.18879	4.18879
$0, \frac{1}{2}, \frac{1}{2}$	Q	4.39297	4.33387	8.52266	8.52264
$\frac{1}{2}, \frac{1}{2}, 0$	$-2Q$	−8.78595	−8.66773	−4.47894	−4.47895
$0, 0, \frac{1}{2}$	$-2P$	30.95208	30.08205	34.27084	34.2697
$\frac{1}{2}, 0, 0$	P	−15.47604	−15.04102	−10.85223	−10.8519

* The values $S_z(x, y, z)$ and also $4\pi/3 + S_z(x, y, z)$ shown in the table are dimensionless and are given in units of the volume of the unit cell, V.

* We used the designation adopted in [10, 12].

three cubic Bravais lattices and a diamond lattice, at different points $\underline{r}$ inside the unit cell of the lattice. The calculation was performed for the case of dipoles oriented along [001] and [111]. For the first case (dipoles oriented along [001]) this calculation was expanded in [10, 11].

Dipoles oriented along [001]. The value of the field $S(r)$, appearing as structural coefficients [$S(r) \equiv C_{ik}$] in the work of McKeehan [2] was also calculated by the Lorentz method with the inclusion of ~ 580 terms, and also by the Ewald method, which makes it possible to obtain the most accurate values of the structural coefficients.

Slater [12] showed that for the calculation of the internal field in crystals of the perovskite type for the case of dipoles oriented along one of the cube edges (Z axis) it is sufficient to know six of the values of $S(r) = S_z(x, y, z)$ found by McKeehan:

$$S_z(0, 0, 0), \quad S_z\left(\tfrac{1}{2}, \tfrac{1}{2}, \tfrac{1}{2}\right), \quad S_z\left(0, \tfrac{1}{2}, \tfrac{1}{2}\right), \quad S_z\left(\tfrac{1}{2}, \tfrac{1}{2}, 0\right), \quad S_z\left(\tfrac{1}{2}, 0, 0\right), \quad S_z\left(0, 0, \tfrac{1}{2}\right),$$

where x, y, and z are the coordinates of the points of the unit cell in which the field is to be determined.

In Table 1 are given values of the coefficients S_z (or values $4\pi/3 + S_z$), calculated by McKeehan, and also the values calculated some time ago by Jaynes [6] by the method of field decomposition.

The values of the coefficients obtained by Jaynes almost exactly coincide with the coefficients calculated by McKeehan by the Ewald method; therefore by comparison

$$P = -\frac{15.04102}{V} \text{ and } Q = \frac{4.33387}{V}.$$

The aggregate of structural coefficients for the perovskite-type cell may be represented in the form of a fifth-order matrix

$$C_{ik} = \begin{pmatrix} 0 & 0 & -2Q & Q & Q \\ 0 & 0 & -2P & P & P \\ -2Q & -2P & 0 & Q & Q \\ Q & P & Q & 0 & -2Q \\ Q & P & Q & -2Q & 0 \end{pmatrix} \tag{3}$$

or a fourth-order matrix

$$C_{ik} = \begin{pmatrix} 0 & 0 & -2Q & 2Q \\ 0 & 0 & -2P & 2P \\ -2Q & -2P & 0 & 2Q \\ Q & P & Q & -2Q \end{pmatrix} \tag{4}$$

The matrix (3) corresponds to subdividing the structure of perovskite ABO_3 into 5 sublattices: $A + B + O_I + O_{II} + O_{III}$, and the matrix (4) into 4 sublattices: $A + B + O_I + (O_{II} + O_{III})$, where the sublattices of O_{II} and O_{III} ions are combined.

In subsequent work [1, 5] the calculation of the structural coefficients was made anew by the Lorentz method with the inclusion of a smaller number of ions (~ 100-220) than in [2]. Therefore, the values of P and Q were computed less exactly. The calculation of P and Q according to the values of C_{ik}, cited by Skanavi [1], gives $P \approx -\frac{14}{V}$ and $Q \approx \frac{4}{V}$; Kozlovskii [5] obtained $P = -\frac{15.6}{V}$ and $Q = \frac{6.9^*}{V}$, van Santen and de Boer [4] quoted values of $P = -\frac{15.1}{V}$ and $Q = \frac{4.3}{V}$, not indicating detailed calculations.

* In the matrix of the coefficients, followed by Skanavi, the column C_{i4} erroneously occupies the place of the column C_{i1}, and the coefficient C_{44} is calculated incorrectly. The value of Q calculated by Kozlovskii is also incorrect.

Orientation of dipoles along [011] and [111]. In the case of dipoles oriented along [001] there is one nonzero component of the coefficient $S_z(x, y, z)$. In the case of dipoles oriented along [011] and along [111] one has, respectively, two (S_y and S_z) and three (S_x, S_y, S_z) nonzero components of the coefficients. Thus it is possible to establish a relation between the values of the components of the coefficients for the dipoles oriented along [011] and [111] with the value of the components of the coefficients S_z for orientation along [001].

TABLE 2

Values of the Projected Structural Coefficients for Dipoles Oriented Along [001], [011] and [111] in the Ideal Cubic Cell of the Perovskite Type

x, y, z	l	$S_l(x, y, z)$		
		[001]	[011]	[111]
0, 0, 0	1	0	0	0
	2	0	0	0
1/2, 1/2, 1/2	3	0	0	0
	1	0	0	$-2Q/\sqrt{3}$
0, 1/2, 1/2	2	0	$Q/\sqrt{2}$	$Q/\sqrt{3}$
	3	Q	$Q/\sqrt{2}$	$Q/\sqrt{3}$
	1	0	0	$Q/\sqrt{3}$
1/2, 1/2, 0	2	0	$Q/\sqrt{2}$	$Q/\sqrt{3}$
	3	$-2Q$	$-2Q/\sqrt{2}$	$-2Q/\sqrt{3}$
	1	0	0	$P/\sqrt{3}$
0, 0, 1/2	2	0	$P/\sqrt{2}$	$P/\sqrt{3}$
	3	$-2P$	$-2P/\sqrt{2}$	$-2P/\sqrt{3}$
	1	0	0	$-2P/\sqrt{3}$
1/2, 0, 0	2	0	$P/\sqrt{2}$	$P/\sqrt{3}$
	3	P	$P/\sqrt{2}$	$P/\sqrt{3}$

The projections of the structural coefficients on the X, Y and Z axes (specified by their indices $l = 1, 2, 3$) for dipoles oriented along [001], [011], and [111] are presented in Table 2.

From the data of McKeehan [2] for the simple cubic lattice, one can determine the projected structural coefficients for the perovskite structure for dipoles oriented along [111]. These agree with the appropriate values in Table 2, obtained by independent means.

In the calculation of the component of the internal electric field, one has to keep in mind that the quantity $4\pi/3$ in Eq. (1) probably decreases by $\sqrt{2}$ and $\sqrt{3}$ times, respectively, in the case of dipoles oriented along [011] and [111].

In conclusion, the relation between the two designations of the structural coefficients [C_{ik} and $S_l(x, y, z)$] will be shown. For the orientation [001], the connection between the elementary matrix (3) and $S_l(x, y, z)$ is expressed by the following relations:

$$
\begin{aligned}
&S_z(0,\ 0,\ 0) \equiv C_{i1} = 0 \qquad (i = 1-5),\\
&S_z(1/2,\ 1/2,\ 1/2) \equiv C_{13} = C_{21} = 0,\\
&S_z(0,\ 1/2,\ 1/2) \equiv C_{24} = C_{43} = C_{35} = C_{53} = C_{14} = C_{41} = C_{15} = C_{51} = Q,\\
&S_z(1/2,\ 1/2,\ 0) \equiv C_{13} = C_{31} = C_{45} = C_{54} = -2Q,\\
&S_z(0,\ 0,\ 1/2) \equiv C_{33} = C_{32} = -2P,\\
&S_z(1/2,\ 0,\ 0) \equiv C_{34} = C_{42} = C_{52} = C_{25} = P.
\end{aligned}
$$

For dipoles oriented along [011] and [111] there exist relationships in the same way for all the projected coefficients, but the numerical values of the projections are necessary to obtain agreement with the data of Table 2.

2. Influence of Ionic Shifts and Tetragonal Lattice on the Structural Coefficients

Certain ferroelectrics ($BaTiO_3$, $PbTiO_3$, $KNbO_3$) below the Curie temperature have a tetragonal lattice, in which individual ions shift from the positions they occupied in the cubic lattice. For a small tetragonal distortion, measurable by the axial ratio c/a, and comparatively small ionic shifts, so that the perovskite structure can be said to be preserved, the structural coefficients may be expressed in the form $C_{lk} = \mathring{C}_{lk} + \Delta\mathring{C}_{lk}$. Then $\Delta\mathring{C}_{lk}$, the change in $\mathring{C}_{lk}$, is conditioned by the tetragonality of the lattice and the shift of the ions.

The shift of the ions in the cubic form of $BaTiO_3$ was considered by Kozlovskii [5], who showed that

$$\frac{\Delta\mathring{C}_{lk}}{\mathring{C}_{lk}} \approx 12\left(\frac{\delta}{r}\right)^2, \qquad (5)$$

where δ is the shift of the ions, $r = a/2$ is the shortest distance between ions. Hence, for $BaTiO_3$ ($\delta \approx 0.1$ A and $r \approx 2$ A) $\Delta\mathring{C}_{lk}$ comprises about 3% of $\mathring{C}_{lk}$. Therefore, for $BaTiO_3$ this correction can be neglected.

In $PbTiO_3$ the shift of the ions is much larger ($\delta \approx 0.5$ A) and $\Delta\mathring{C}_{lk}$, calculated by Formula (5), comprises as much as 75% of $\mathring{C}_{lk}$. However, in the formula the tetragonal distortion of the cell is not taken into account.

The structural coefficients for $BaTiO_3$ taking into account the tetragonality (c/a = 1.01) and the shift of Ti and O_I ions determined by Känzig [14] ($\delta_T = \frac{\delta_{Ti}}{c} = 0.0142$; $\delta_O = \frac{\delta_{O_I}}{c} = -0.0316$) were calculated by Hagedorn [7] by the Madelung method. He obtained expressions for the periodic functions $g_l(x)$, which represent values $4\pi/3 + S_z(x, y, z)$. Using these expressions, one can calculate the numerical values of the functions $g_l(x)$, and consequently, also $S_z(x, y, z)$ in the case of any shift of ions along the Z axis in the $BaTiO_3$ cell with the tetragonality c/a = 1.01.

The values of the functions $g_l(x)$, necessary for the description of the field in $BaTiO_3$ with shifted positions of the ions, are given in Table 3. For comparison are given corresponding values obtained by McKeehan for the cubic lattice, and also the values calculated by us for $PbTiO_3$ (see below).

The comparison of the values of the coefficients $S_z(x, y, z)$, calculated by Hagedorn, with the coefficients $S_z(x, y, z)$, calculated by McKeehan, shows that the tetragonal distortion of the cell and the shift of the ions in barium titanate change the structural coefficients but little. The difference is a couple of units in the first decimal place, i. e., 2-3% of the value of ($4\pi/3 + \mathring{S}_z$).

The differences between $g_1(0)$, $g_3(^1/_2)$ and $g_3(0)$ [equal to $4\pi/3 + S_z(^1/_2, ^1/_2, 0)$; $4\pi/3 + S_z(0, ^1/_2, ^1/_2)$, and $4\pi/3 + S_z(0, 0, 0)$, respectively] and the corresponding values $4\pi/3 + \mathring{S}_z(x, y, z)$ for the cubic lattice depends only upon the tetragonal distortion; but the difference between $g_3(^1/_2)$ and $g_3(^1/_2 + \delta_O)$ and $g_1(0)$ and $g_1(\delta_O)$ is due only to the ionic shifts. The comparison of the respective numbers shows that the effect of the tetragonality of the lattice and the shift of ions on the structural coefficients largely compensate each other. One can expect that by taking account of the lattice tetragonality and the ionic shifts in $PbTiO_3$ the difference of 75% between C_{lk} and $\mathring{C}_{lk}$ found above would be reduced.

The calculation of the structural coefficients for the tetragonal lattice of $PbTiO_3$ taking into account the ionic shifts was performed by the method of Madelung-Hagedorn. The periodic lattice of $PbTiO_3$ and the ionic shifts were taken from [13]: a = 3.904 A; c = 4.153 A; c/a = 1.064; $\delta_{Pb} = 0$; $\delta_{Ti} = -0.17$ A; $\delta_T = \frac{\delta_{Ti}}{c} = -0.0409$; $\delta_{O_I} = \delta_{O_{II}} = -0.47$ A; $\delta_O = \delta_{O_I}/c = -0.1132$; $|\delta_T - \delta_O| = 0.0722$.

The results of the calculation are given in the last three columns of Table 3.

The difference between the values of the structural coefficients for $PbTiO_3$ at room temperature and the values of $\mathring{C}_{lk}$ for the cubic lattice is larger than the difference between the analogous values for $BaTiO_3$. This difference is more important the smaller the absolute value of the coefficients. For the smallest coefficients in absolute magnitude the difference amounts to 20%, and for the largest coefficients equals 1%.

Thus, in fact, in the case of $PbTiO_3$ the effect of ionic shifting and the effect of tetragonality compensate each other considerably. Therefore, for a semiquantitative estimate of the field in $PbTiO_3$ one can use the values of the structural coefficients calculated for the ideal cubic lattice.

TABLE 3

Structural Coefficients for an Ideal Cubic Lattice and a Tetragonally Distorted Lattice

Cubic lattice		$BaTiO_3$ (tetragonal lattice with c/a = 1.01)			$PbTiO_3$ (tetragonal lattice with c/a = 1.064)			
x, y, z	$\frac{4\pi}{3}+S_z(x,y,z)$,* data of McKeehan (Ewald method)	x, y, z	$\frac{4\pi}{3}+S_z(x,y,z)$ calculation of Hagedorn		x, y, z	$\frac{4\pi}{3}+S_z(x,y,z)$ calculation of authors		$\Delta\% = \frac{S_z - \frac{4\pi}{3}+S_z}{\frac{4\pi}{3}+S_z}\cdot 100$
0,0,0	4.18879	0,0,0	$g_3(0)$	4.0617	0,0,0	$g_3(0)$	3.405	19
$\frac{1}{2},\frac{1}{2},\frac{1}{2}$	4.18879	$\frac{1}{2},\frac{1}{2},\frac{1}{2}+\delta_T$	$g_1\left(\frac{1}{2}+\delta_T\right)$	4.295	$\frac{1}{2},\frac{1}{2},\frac{1}{2}+\lvert\delta_T\rvert$	$g_1\left(\frac{1}{2}+\lvert\delta_T\rvert\right)$	4.809	14
$0,\frac{1}{2},\frac{1}{2}$	8.52266	$0,\frac{1}{2},\frac{1}{2}$	$g_2\left(\frac{1}{2}\right)$	8.642	$0,\frac{1}{2},\frac{1}{2}$	$g_2\left(\frac{1}{2}\right)$	9.230	8
		$0,\frac{1}{2},\frac{1}{2}+\delta_O$	$g_2\left(\frac{1}{2}+\delta_O\right)$	8.530	$0,\frac{1}{2},\frac{1}{2}+\lvert\delta_O\rvert$	$g_2\left(\frac{1}{2}+\lvert\delta_O\rvert\right)$	7.759	9
$\frac{1}{2},\frac{1}{2},0$	−4.47894	$\frac{1}{2},\frac{1}{2},0$	$g_1(0)$	−4.6223	$\frac{1}{2},\frac{1}{2},0$	$g_1(0)$	−5.405	20
		$\frac{1}{2},\frac{1}{2},\delta_O$	$g_1(\delta_O)$	−4.522	$\frac{1}{2},\frac{1}{2},\lvert\delta_O\rvert$	$g_1(\lvert\delta_O\rvert)$	−3.948	12
$0,0,\frac{1}{2}$	34.27084	$0,0,\frac{1}{2}+\delta_T-\delta_O$	$g_2\left(\frac{1}{2}+\delta_T-\delta_O\right)$	35.231	$0,0,\frac{1}{2}+\lvert\delta_T-\delta_O\rvert$	$g_2\left(\frac{1}{2}+\lvert\delta_T-\delta_O\rvert\right)$	33.885	1
$\frac{1}{2},0,0$	−10.85223	$\frac{1}{2},0,\delta_T$	$g_2(\delta_T)$	−11.026	$\frac{1}{2},0,\lvert\delta_T-\delta_O\rvert$	$g_2\left(\lvert\delta_T-\delta_O\rvert\right)$	−10.539	3

* All values of $4\pi/3 + S_z$ are given in units of the volume of the unit cell.

SUMMARY

The data on the structural coefficients of the internal field in ferroelectrics with the perovskite-type structure are examined and supplemented.

The structural coefficients C_{1k} for ferroelectrics of the perovskite type, the cell of which shows a small distortion ($\sim$ 1%), are distinguished from the coefficients $\mathring{C}_{1k}$ for the ideal cubic lattice only in the first decimal place, i. e., by no more than 2-3%. This makes it possible to use the values of $\mathring{C}_{1k}$ instead of C_{1k} for the calculation of the field.

In a tetragonally deformed lattice of the perovskite type the effect of the tetragonality of the lattice and the ionic shifts on the structural coefficients largely compensate each other. Therefore, even for $PbTiO_3$, in spite of its considerable tetragonal distortion and large ionic shifts, the difference between C_{1k} and $\mathring{C}_{1k}$ does not exceed 20%.

LITERATURE CITED

[1] G. I. Skanavi, "On the question of the high dielectric constant of some crystals," J. Expti.-Theoret. Phys. (USSR) 17, 5, 399 (1947); Physics of Dielectrics [in Russian] (1949).

[2] L. W. McKeehan, "Magnetic fields in unstrained cubic crystals," Phys. Rev. 43, 913 (1933); Phys. Rev. 72, 78 (1947).

[3] J. H. van Santen and W. Opechowski, "On a generalization of the Lorentz-Lorenz formula," Physica 14, 545 (1948).

[4] J. H. van Santen and F. de Boer, "High indices of refraction of barium titanate and other heteropolar titanium compounds," Nature 163, 4155, 957 (1949).

[5] V. Kh. Kozlovskii, "Effective field in barium titanate," J. Tech. Phys. (USSR) 21, 11, 1388 (1951).

[6] E. T. Jaynes, Ferroelectricity (Princeton University Press, 1953).

[7] R. Hagedorn, "Statisches Modell von Bariumtitanat bei Zimmertemperatur," Z. Physik 133, 394-421 (1952).

[8] P. P. Ewald, "Die Berechnung optischer und electrostatischer Gitterpotentiale," Ann. Physik 64, 253 (1921).

[9] E. Madelung, Z. Physik 19, 524 (1918).

[10] J. M. Luttinge and L. Tisza, "Theory of dipole interaction in crystals," Phys. Rev. 70, 954 (1946); Phys. Rev. 72, 257 (1947).

[11] W. Kinase, "On interaction among ions of $BaTiO_3$ crystal and on its 180° and 90° type domain boundaries," Progr. Theoret. Phys. 13, 5, 529 (1955).

[12] J. C. Slater, "The Lorentz correction in barium titanate," Phys. Rev. 78, 748 (1950).

[13] G. Shirane, R. Pepinsky, and B. C. Frazer, "X-ray and neutron diffraction study of ferroelectric $PbTiO_3$," Acta Cryst. 9, 131 (1956); Phys. Rev. 97, 4, 1179 (1954).

[14] W. Kaenzig, "Röntgenuntersuchungen über die Seignetteelektrizität von Bariumtitanat," Helv. Phys. Acta 24, 175 (1951).

Received May 31, 1957

L. Ia. Karpov Physicochemical Institute

THE PACKING OF CHAIN MOLECULES

II. THE LAYERS OF PARAFFIN MOLECULES

A. I. Kitaigorodskii

The parameters and symmetry of the possible layers of paraffin molecules are derived, based on the theory of close packing of molecules.

§1. The Pseudocells of the Layers

Crystals of paraffins are constructed by the superposition of layers of parallel molecules. In this report the structure of similar layers will be discussed, and in succeeding ones the superposition of layers leading to the formation of the crystal.

As was shown* in (I), the principles of organic crystallochemistry [1] lead to five possible packings of infinite chains. A layer of infinite chains has a period along the chain equal to 2.54 A (period of plane aliphatic zigzag) and is equivalent to a three-dimensional crystal.

Each of the five packings may therefore be characterized by a three-dimensional unit cell. Of the five packings described in (I), three have an orthorhombic cell, one a monoclinic and one a triclinic.

These cells may, it is understood, also be formed in molecular layers of finite length. However, the layers of paraffin molecules do not have a three-dimensional lattice and the cells formed are not cells of the crystal. In this case it is expedient to call them pseudocells. In the English literature [2] the term "subcell" is used in somehwat the same sense.

We assume that the packing principles for methylene groups in infinite chains and molecules of finite length are the same. This means that only the cells of layers of infinite chains, as brought out in (I), can occur in the form of pseudocells in the layers of paraffin molecules.

However, of the three types of structures with an orthorhombic pseudocell we shall examine only one, since one of the three indicated packings has a reduced packing density and is therefore of course rejected, and the other two are equivalent with respect to density**; however, in crystals of paraffins and related compounds we encounter only one of these variants, on which the examination will be based.

The following is characteristic for the close packing in question: the molecules, connected by symmetry operation 2_1, are turned with respect to one another by an angle close to a right angle. Attention is then turned to the location of the screw axes. If a cross section of the packing is drawn through the carbon atoms, then axis 2_1, which belongs to the pseudocell, will lie in this plane parallel to the long axis b_s. But there is also another set of axes 2_1, parallel to the axis of the pseudocell a_s, and these axes lie in the plane which passes between the CH_2 groups.

---

* See the author's paper "Concepts of Organic Crystallochemistry," Kristallografiia 2, 4, 456-465 (1957). [Soviet Physics – Crystallography, p. 454].

** In predicting the possible structure with the help of the theory of close packing, we are on solid ground. On the other hand, we do not have any general concepts permitting the determination of the energy advantage of one structure compared with others having the same density and symmetry.

The orthorhombic pseudocell is found very often with paraffins and related compounds. The variation in the dimensions of the pseudocell is extremely small.

We assume that $a_0 = 4.96$, $b_0 = 7.42$ and $c_0 = 2.54$ A.

The angle of inclination of the plane zigzag toward axis b_0 is determined in a series of experiments [3]. The value 42° is probably an average figure.

The packing of the methylene groups is determined by the contacts of the hydrogen atoms H_1, H_2 and H_3 (Fig. 1, a). The atom H_1 touches the two atoms H_2 lying in adjacent levels and the atom H_3 lying in the same level. The atom H_2 touches, in addition, the two atoms H_3. The distances H . . . H are very close: $H_2 \ldots H_2 = 2.6$; $H_1 \ldots H_3 = 2.7$ A and $H_2 \ldots H_3$ has an intermediate value.

Thus the intermolecular radius of hydrogen in the methylene groups of paraffins is $R_H = 1.33$ A (counting $R_{C-H} = 1.08$ A). We hope to return to the question of the large value of R_H in paraffins in a subsequent report.

Together with layers having an orthorhombic pseudocell, there occur layers of molecules of paraffins or related compounds which have an oblique-angled two-dimensional cell. However, up to the present time complete structural investigations of such crystals are lacking and the type of their pseudocell is unknown.

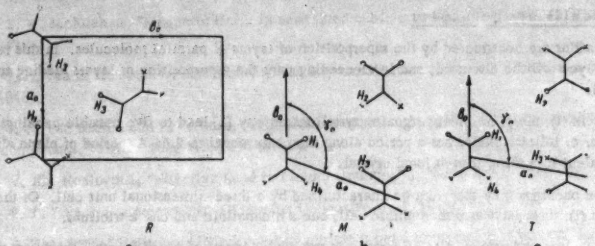

Fig. 1. The pseudocells of paraffins (schematic): R orthorhombic, M) monoclinic, T) triclinic. Axis Z faces the reader. The hydrogen atoms marked by symbol X lie higher by $^1/_2 c_0$ (= 1.27 A) than atoms marked by symbol O.

On the basis of the theory of close packing we derived in (I) two more types of packings of methylene groups – with monoclinic and triclinic pseudocells (see [1]).

The monoclinic pseudocell is determined first of all by the translation a_0, which is easily found from the condition that the atom H_3 should be at a distance of 2 R_H from the atoms H_1 and H_4. The arrangement of the three molecules, which determines the axis b_0, is found from the condition of equality to 2 R_H of the distances $H_3 \ldots H_1$ and $H_2 \ldots H_3$ (Fig. 1, b). We arrive at a pseudocell with the following parameters: $a_0 = 4.2$; $b_0 = 4.4$; $c_0 = 2.54$ A; $\gamma_0 = 111°$.

Finally, we find the last type of packing of methylene groups with the help of Fig. 1, c. The triclinic pseudocell is determined first of all by the translation a_0, but now this translation connects the molecules displaced on a level with respect to one another. Here this translation is determined by the equality to 2 R_H of the distances $H_3 \ldots H_1$ and $H_4 \ldots H_1$. The difference from the previous case consists in the fact that in the monoclinic cell the atoms H_3 and H_1 lie in one level, and H_3 and H_4 in different ones, and in the triclinic cell, conversely, H_3 and H_4 lie in the same levels, and H_3 and H_1 in different ones. The translation b_0 is determined according to the contacts $H_3 \ldots H_3$ and $H_3 \ldots H_1$. We arrive at a pseudocell with the following parameters: $a_0 = 4.3$; $b_0 = 4.8$; $c_0 = 2.54$ A; $\alpha_0 = 90°$; $\beta = 108°$; $\gamma_0 = 107°$.

The projection of a_0 on a plane perpendicular to c_0 equals 4.0 A, the angle between axis b and this projection differs from γ_0 by not more than half a degree.

§2. The Derivation of Possible Layers

Passing from the packing of infinite molecules to layers composed of molecules of finite length, we should take into account a new parameter of the structure, i. e., the angle of inclination to the plane which passes through the end groups toward the axes of the chains. If this angle equals 90°, then we shall speak of right layers. Other layers shall be called oblique.

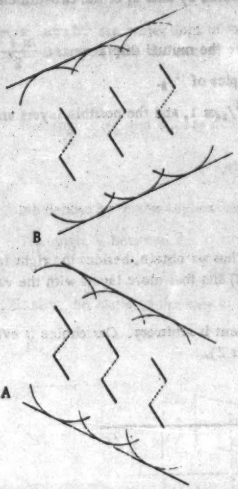

Fig. 2. Example of layers differing in the sign of the mutual displacement of the molecules. Layer B proves to be approximately 0.7 A thicker than A.

The character of the packing of the methylene groups in oblique layers will not differ from the character of the packing in a right layer, providing the mutual displacement translationally of identical molecules along the axis of the chain is of magnitude mc_0, where m is a whole number, and $c_0 = 2.54$ A is the distance between two methylene groups, located one above another. This idea was first expressed almost 20 years ago [4], in spite of the quite simple structural concepts existing at that time.

We shall designate by m the displacement of molecules translated by axis a, and by n the displacement of molecules translated by axis b. The two-dimensional cell of the layer is determined by the pseudocell and by the quantities m, n. Two-dimensional cells characterized by the symbols R[m, n], M[m, n] and T[m, n] are therefore possible.

It is not necessary to consider all the possible displacements of the chains. If the displacement of two adjacent chains exceeds one period c_0, then contacts of end groups with CH_2 groups arise. This would lead to a reduction in the density of packing, which is impossible.

Therefore, we shall limit consideration to layers in which the adjacent chains are not displaced, displaced by $^1/_2\, c_0$, or by c_0.

It is necessary to take into account the fact that layers differing by the signs of m and n are nonequivalent. Each pair of quantities m, n yield four different layers

$$m,\ n;\ \bar{m},\ n;\ m,\ \bar{n};\ \bar{m},\ \bar{n}.$$

This difference is illustrated in Fig. 2 in which are represented a series of molecules translated at an angle with the axis of the chain. These series differ only by the sign of the displacement. Thus, with identical packings of methylene groups and with identical inclinations of the axis of the chain with the plane which passes through the end groups, the oblique layers differ in the "form" of the surface of the layer. Displacing "upwards" along translations a and b, we see the methylene groups positioned differently.

After these general observations the possible layers may be enumerated.

Layers with T-pseudocell

All layers with such a pseudocell are oblique. If the plane ab of the two-dimensional cell of the layer coincides with the plane a_0b_0 of the pseudocell, then the symbols of such layers will be

$$T\,[^1/_2, 0) \quad \text{and} \quad T\,[\overline{^1/_2}, 0].$$

In layers with a T-pseudocell each molecule has 6 neighbors, translated by vectors $\pm\vec{a}_0$, $\pm\vec{b}_0$ and $\pm(\vec{a}_0 + \vec{b}_0)$ (counting, as usual, the angle γ obtuse). The condition that the displacement of any of these molecules must not be greater than unity permits only two more layers $T[^1/_2, \bar{1}]$ and $T[\overline{^1/_2}, 1]$.

Layers with M-pseudocell

Besides the right layer M [0, 0], the oblique layers M [1, 0] and M $(\bar{1}, 0)$ as well as M [0, 1] and M $[0, \bar{1}]$ are possible.

Layers with R-pseudocell

Each molecule of the layer has nearest neighbors of two sorts – connected by axis 2_1 of the two-dimensional cell and connected by the translation vector $\vec{t}_0$.

The molecules connected by axis 2_1 of the two-dimensional cell have the mutual displacement $\frac{m+n}{2}$. Thus, these neighbors can be displaced by a number of periods c_0, in multiples of $^1/_2$.

In such a case n = 0 or 1, m = 0 or 1, and $^1/_2 \cdot (m+n)$ equals zero, $^1/_2$, or 1, and the possible layers are worked out by the following variants of the values m, n:

$$m = 0,\ n = 0;\ m = 1,\ n = 0,$$
$$m = 0,\ n = 1;\ m = 1,\ n = 1.$$
$$m = 0,\ n = 2.$$

At the same time all signs are possible with the numbers m and n. Thus we obtain, besides the right layer R[00], the oblique layers R[01] and R[0$\bar{1}$], R[10] and R[$\bar{1}$0], R[02] and R[0$\bar{2}$] and four more layers with the values m and n equal to unity R[11], R[1$\bar{1}$], R[$\bar{1}$1] and R[$\bar{1}\bar{1}$].

It is understood that the choice of direction of the positive displacement is arbitrary. Our choice is evident from Fig. 1 (the positive displacement is along the positive direction of axis Z).

TABLE 1

Pseudocell	Layer	Cell of layer	α	β	γ
H	H[00]	$a=4.8$	90	90	0
	R[00]	$a=4.96$; $b=7.42$; $\gamma=90°$	90°	90°	0°
	R[0±2]	$a=4.96$; $b=9.0$; $\gamma=90°$	90°	55.5 124.5	34.5
R	R[±1.0]	$a=5.57$; $b=7.42$; $\gamma=90°$	63 117	90 71	27
$a_0 = 4.96$ $b_0 = 7.42$	R[0±1] R[±1.±1]	$a=4.96$; $b=7.85$; $\gamma=90°$ $a=5.57$; $b=7.85$ $\gamma=81.5$	90 63	109	19
		for $R[1,1]$ & $R[\bar{1},\bar{1}]$		71	31.5
$c_0 = 2.54$		$\gamma=98.5$ for $R[1,\bar{1}]$&$R[\bar{1},1]$	117	109	
M					
$a_0 = 4.2$	*M*[00]	$a=4.2$; $b=4.4$; $\gamma=111°$	90	90	0
$b_0 = 4.4$	*M*[±1.0]	$a=4.9$; $b=4.4$; $\gamma=107°$	59 121	90	32
$c_0 = 2.54$	*M*[0.±1]	$a=4.2$; $b=5.1$; $\gamma=107°$		60	
$\gamma_0 = 111°$			90	120	32
T	$T\left[\pm\frac{1}{2}.0\right]$	$a=4.3$; $b=4.5$; $\gamma=103°$	73 117	90	18
$a_0 = 4.3$ $b_0 = 4.5$ $c_0 = 2.54$	$T\left[\frac{1}{2}.\bar{1}\right]$ $T\left[\frac{\bar{1}}{2}.1\right]$	$a=4.3$; $b=5.2$; $\gamma=109°$	73	120	
$\alpha_0 = 90.\beta_0 = 107.$ $\gamma_0 = 103$			117	60	36

In Table 1 are given the geometric parameters of the layers, namely, the dimensions of the cell of the layer and the angles φ_a, φ_b and φ_{c*}, formed by the axis of the chain (direction of axis Z, assumed in Fig. 1) with the axes a, b and the normal to the plane ab.

The lengths of the axes are found by the formulas

$$a = \sqrt{a_\perp^2 + m^2 c_0^2}, \qquad b = \sqrt{b_\perp^2 + n^2 c_0^2}$$

where $a_\perp$ and $b_\perp$ are projections of the periods of the cell on the plane perpendicular to the chain, equal to a_0 and b_0 in all cases, with the exception of layers with the T-pseudocell, where

$$a_\perp = \sqrt{a_0^2 - \left(\frac{1}{2} c_0\right)^2}.$$

The angles φ_a and φ_b are determined by the formulas

$$\operatorname{ctg} \varphi_a = m \frac{c_0}{a_\perp}, \qquad \operatorname{ctg} \varphi_b = n \frac{c_0}{b_\perp}.$$

We denote by ϵ the angle between $a_\perp$ and $b_\perp$. In the R-cell $\epsilon = 90°$, in the M-cell $\epsilon = \gamma_0$.

The angle γ between the vectors a and b of the cell of the layer is found from the expression

$$\cos \gamma = \cos \varphi_a \cdot \cos \varphi_b + \sin \varphi_a \cdot \sin \varphi_b \cdot \cos \varepsilon$$

and, finally, the angle of the axis of the chain with the normal of the layer φ_{c*} from the formula

$$\operatorname{tg}^2 \varphi_{c*} = \frac{1}{\sin^2 \varepsilon} (\operatorname{ctg}^2 \varphi_a + \operatorname{ctg}^2 \varphi_b - 2 \operatorname{ctg} \varphi_a \cdot \operatorname{ctg} \varphi_b \cdot \cos \varepsilon).$$

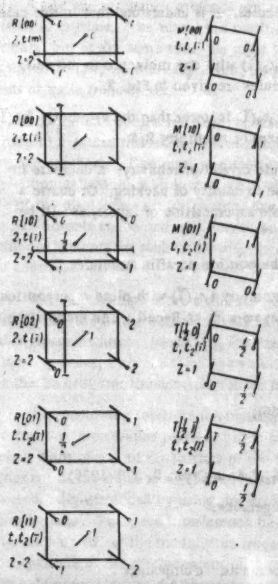

Fig. 3. Diagrams of the symmetry of the possible layers of paraffin molecules. The end groups are marked by a large dot; the figures 0, 1/2, 1 and 2 indicate the "level" of the end group.

It should be noted that in spite of the closeness of the dimensions of some of the cells (for example, M [1, 0] and M [0, $\bar{1}$]), they correspond to different types of structure differing by the character of the packing of the molecules. In Table 1 we have also inserted a hexagonal layer constructed of rotating or statistically randomly distributed molecules. There can be only one such layer. The diameter of the cylinder, in which, on the average, the molecule is inscribed, should have a "mean" value between the greatest and the least diameter, i. e., something near 4.8 A.

§ 3. The Symmetry of the Layers

The symmetry of a layer is determined not only by its geometric parameters but by the symmetry of the molecule.

If an aliphatic chain is stretched out into a plane zigzag, then with an even number of carbon atoms the molecule has the symmetry $\frac{2}{m}$, and with an odd number of C atoms—the symmetry mm. In accordance with the principle of close packing (see [1]), a molecule of symmetry $\frac{2}{m}$, becoming a part of the crystal, retains in it a center of inversion, and a molecule of symmetry mm — one of its own planes.

It is evident that in the crystal, the plane of symmetry passing along the molecule is lost. The preservation of the plane of symmetry perpendicular to the chain of the odd paraffins leads to the possibility of close packing of parallel chains. The loss of both planes of symmetry is, as is well known, not very likely. But if so, then we come to the following conclusion. The odd paraffins can form only right layers R[00], since the remaining layers cannot have the symmetry of a mirror plane.

All the remaining layers, enumerated in Table 1, will, generally speaking, be applicable to centrosymmetrical molecules. Thus the following becomes apparent: even paraffins, in contrast to odd ones, should have a great variety of structures.

The right layers R[00], formed by molecules of an odd paraffin, have the symmetry $2_1t(m_{\parallel})$ (in our notation, see [1]).

With this it is emphasized that the mirror plane of symmetry passes perpendicular to the axes of the chains in the middle of the layer. Into this plane fall axes 2_1, parallel to the long axis of the cell.

The right layers R[00], composed of molecules of an even paraffin, have the symmetry $2_1t(\bar{1})$. This means that the plane can pass through the center of inversion of the molecules and that into this plane fall axes 2_1, parallel now to the short axis of the cell.

Because of the presence of two systems of axes 2_1, parallel to axes a_0 and b_0, the oblique layer composed of centrosymmetrical molecules preserves the monoclinic symmetry if m = 0 and n = 2, and also when m = 1 and n = 0. In these cases the axes 2_1 will also lie in the planes which pass through the center of symmetry.

In the remaining cases the layer loses the axis of symmetry 2_1. At the same time the molecules in the center and at the vertex of the cell cease to be symmetrically related. This does not imply the presence of an arbitrary displacement along the chain between the symmetrically unrelated molecules. If there had been such a displacement, then the crystal would not only have lost axis 2_1, but also the center of symmetry, which is unlikely. In order that a layer might preserve the center of inversion, the centers of inversion of all the molecules should fall in the same plane. Therefore, the displacement of "average" molecules in the case of triclinic layers also remains equal to $\frac{m+n}{2}$.

Layers with such cells, however, can also yield nonsymmetrical molecules. It is understood that in this case the layer does not have symmetry, aside from translation.

As regards layers with M- and T-pseudocells, they all yield layers $t_1t_2(\bar{1})$ with one molecule in the cell. Diagrams illustrating the symmetry of the possible layers of paraffin molecules are given in Fig. 3.

One problem remains to be commented on further. The symmetry $t_1t_2(\bar{1})$ is lower than the symmetry $2_1t(\bar{1})$; thus should the consideration be limited only to layers which contain the axes of symmetry 2_1?

Here it is necessary to consider one of the fundamental rules of organic crystallochemistry: a decrease in symmetry is energetically advantageous if it is accompanied by an increase in density of packing. Of course a single layer – oblique or right – occupies the same volume. However, in the superposition of layers, as will be seen below, the oblique layers permit a gain in the density of packing.

On the closest superposition of the layers we have derived, we find the possible paraffin structures.

According to the rules of organic crystallochemistry, the layers of symmetry $t_1t_2(\bar{1})$ with close superposition lead to triclinic crystals. The orthorhombic crystals can yield only right layers with an R-cell. The monoclinic crystals are formed by right and oblique layers of symmetry $2_1t(\bar{1})$.

LITERATURE CITED

[1] A. I. Kitaigorodskii, Organic Crystallochemistry [in Russian] (1955).

[2] V. Vand, Acta Cryst. 1, 109, 290 (1948).

[3] H. M. M. Shearer and V. Vand, "The crystal structure of n-$C_{36}H_{74}$," Acta Cryst. 9, 379 (1956).

[4] T. Schoon, Polymorphe Formen Kristalliner Kohlenstoffverbindungen, usw.

Received May 15, 1957

Institute of Heteroorganic Compounds

APPARATUS FOR MEASURING VERY SMALL DISPLACEMENTS OF OSCILLATING CRYSTALS

A. A. Fotchenkov

Directions are given for measuring very small displacements (to 0.05 A) working on the principle of modulated interferometry [1, 2]. The apparatus is intended for measuring the piezoelectric and electrostrictive coefficients of crystals in the temperature range −20 to +100°C at frequencies from 20 to 26,000 cycles.

The results obtained on measurements of the piezoelectric modulus d_{11} of quartz are in good agreement with the results of measurements by other methods.

Static and resonance methods are at present the most widespread ones for measuring the piezoelectric coefficients of crystals. The resonance method, permitting the measurement of adiabatic coefficients, is the most accurate, but at the same time the most laborious method. Furthermore, resonance methods cannot always be employed at low, we shall say audio, frequencies, since crystals of large dimensions are required for measurements at these frequencies.

The method considered here, of direct measurement of the displacements in the audiofrequency range, can be used to measure the isothermal coefficients of crystals which, even for linear piezoelectrics, slightly differ from the adiabatic. One must also take into account that, for the characteristics of those or other crystals such as electromechanical transducers, particularly audio and ultrasonic emitters, it is important to know the magnitude of the displacements which arise due to the superposition of an electric field, that is, to know the piezoelectric coefficients connected with just these conditions of the function of a transducer. The calculation of the values of the coefficients for such transducers from the measurements of other coefficients is always connected with certain additional errors.

Still more complicated is the problem of measuring electrostrictive coefficients. While for ferroelectric crystals, because of the comparatively large values of these coefficients, their measurement can be carried out (although not without difficulties), for linear dielectrics the measurements of the electrostrictive coefficients are, up to the present, impractical. The value of such measurements, however, cannot be overrated, since they enable the investigator to understand more fully the processes of polarization of dielectrics.

The modulated interference method of measuring the amplitudes of small displacements is based on the fact that the interference pattern, which is obtained from a Michelson interferometer, is modulated by a periodic displacement of one of the mirrors of the interferometer and is then analyzed by a photoelectrically sensitive instrument at the input to the narrow bandwidth filter amplifier, tuned to the modulation frequency. The mirror is periodically displaced by using the inverse piezoelectric effect or the electrostriction of a crystal, to which this mirror is stuck. Thus, the interference bands observed in the field of view of the interferometer will be displaced by an amount Δl at the modulation frequency Ω. According to the size of this displacement, one can estimate the magnitude of the displacement of the mirror. If, however, the interference is analyzed by a photomultiplier, a variable component of the photocurrent at the modulation frequency will appear across its anode load. After amplification and detection of this variable component, the readings of the output instrument will be proportional

to the mirror displacements. Knowing the parameters of the electrical parts of the apparatus, one can determine the quantity $(\Delta l)_{max}$ and hence both the amplitude of the change in path difference of the two interfering light beams l_0 and, consequently, the amplitude of oscillation of the crystal under investigation.

From an examination of the theory of the method, given by I. L. Bershtein [2, 5], the quantity l_0 is defined by the expression

$$l_0 = \frac{(\Delta l)_{max}\,\lambda}{\pi\,(I_{max} - I_{min})}, \qquad (1)$$

where $(\Delta I)_{max}$ is the amplitude of the variable component of the photocurrent, λ the wavelength of the monochromatic light, I_{max} and I_{min} the maximum and minimum values of the steady component of the photocurrent (corresponding to maximum and minimum brightness of the interference pattern).

Analyzing the limit of possibilities of the method, which is limited by the level of electrical fluctuations (basically the ripple effect of the photomultiplier) the minimum detectable value l_{0min} is defined by the expression [3, 4]

$$l_{0min} = \frac{1.4 \cdot 10^{-10}}{m} \sqrt{\frac{\Delta f}{I_1}}\,\lambda. \qquad (2)$$

Hence, it is clear that the narrower the admission band of the filter amplifier and the greater the intensity of the interfering light pencils, the higher the resolving power of the method, that is, the smaller the amplitudes of the crystal oscillations that can be measured. By using a cineprojector as a light source and simple optical apparatus, the smallest detected amplitude of displacement of a crystal was equal to a hundredth part of an A.

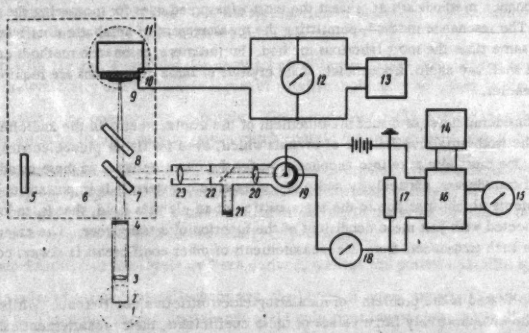

Fig. 1. Block diagram of the apparatus. 1) Illuminator (cineprojection lamp 30 v, 400 w); 2) inlet slit; 3) lens; 4) interference light filter; 5) moving mirror of the interferometer; 6) Michelson interferometer; 7, 8) plane-parallel glass plates; 9) mirror, fixed to the sample under investigation; 10) sample under investigation; 11) thermostat; 12) vacuum tube voltmeter LB9-2; 13) audio generator 3G-2A; 14) stabilized rectifier USV-2; 15) microammeter at constant current of 75 μa; 16) filter amplifier; 17) load resistance; 18) microammeter at constant current of 50 μa; 19) photomultiplier FEU-17; 20) focussing lens; 21) control screen; 22) regulating slit diaphragm; 23) lens.

The block diagram of the apparatus is shown in Fig. 1, the over-all view in Fig. 2. The Michelson interferometer, built with the object of investigating the inverse piezoelectric effect and the electrostriction of crystals, forms the basic element of the optical part of the apparatus. The interferometer contains two mirrors 5 and 9 and two absolutely identical plane-parallel glass plates 7 and 8. Plate 7 produces two coherent beams of light while

Fig. 2. View of the instrument.

plate 8 acts as a compensator. A high power cineprojection lamp 1 is used as a light source. The entering light beam, cut down by the slit 2, is focussed by lens 3 onto the plane of mirror 9. To obtain monochromatic light, the light beam passes through the interference light filter 4 which lets through light in the range 5100-5290 A. The interference pattern, localized in the plane of mirror 5, is enlarged exactly five times by lens 23, so that it can be observed visually on the control screen 21. The regulating slit diaphragm 22 isolates the desired band from the full interference pattern and lens 20 focusses it onto the cathode of the photomultiplier 19 in the reduced view. For protection against extraneous light, the interference pattern is projected inside metal tubes which are tightly joined to the photomultiplier housing. The load resistance 17 and the microammeter 18 for measuring the constant component of the photocurrent are placed across the anode of the photomultiplier. The anode current of the photomultiplier is fed to the load resistance via a coaxial cable, the capacity of which is equal to 60 μμf. The modulation frequency voltage from the audio generator 13 is fed onto the specimen under investigation 10, which is fastened to a massive support, placed in the thermostat 11, permitting measurements in the temperature range −20° to +100°C. The variable voltage, originating as the variable component of the photocurrent on the load resistance, is fed to the input of a narrow bandwidth filter amplifier 16 with an admission bandwidth of 10 kilocycles in the frequency range 20-26,000 cycles, tuned to the modulation frequency. After detection, the amplified modulation frequency voltage is measured by the constant current instrument at output 15. The voltage is fed from the rectifier 14, with electronically stabilized output voltage, onto the anodes and the heater of the filter amplifier tube.

The process of measuring the piezoelectric and electrostrictive coefficients of crystals consists of the following. The interferometer is tuned for observing bands of equal pitch. For this, mirror 5 can be moved along the ray path by screws with coarse and fine adjustments and, by adjusting screws, can be turned through small angles about the vertical and horizontal axes. The particular interference band with zero path difference is isolated by the regulating diaphragm 22 and, by turning the compensator 8 it is displaced in the field of view by values of exactly $\pm\frac{\lambda}{4}$. Thus the intensity will change from I_{max} to I_{min}. These quantities are measured in the microammeter in the anode of the photomultiplier. The values I_{max} and I_{min} are essential for calculating the displacement of Formula (1). Besides this, by the successive overlapping of each of the light beams the quantities I_1 and I_2 are determined and the relation $I_1 + I_2 = \frac{I_{max} + I_{min}}{2}$ verified. After measurement of the quantities I_1, I_2, I_{max}, I_{min}, the final setting of the path difference, for which the photocurrent equals $I_0 = I_1 + I_2$, is made. When fed the modulated voltage from the audio generator, the specimen will oscillate with mirror 9 at the modulation frequency, whence the inverse piezoelectric effect can be calculated, or with double the frequency for the calculation of the electrostrictive effect. Thus the intensity of the interferometer pattern falling on the photocathode will vary within certain limits and appear in the anode circuit of the photomultiplier as the variable component of the photocurrent. In the output impedance Z the latter causes a drop in voltage, the amplitude of which on the grid of the first tube is equal to

$$(\Delta I)_{\max}\frac{ZR}{|\overline{Z}+R|}. \tag{3}$$

After amplification, this voltage is detected by a linear detector giving a reading α_1 in the output instrument equal to

$$\alpha_1 = B(\Delta I)_{\max}\left|\frac{ZR}{\overline{Z}+R}\right|, \tag{4}$$

where B is the constant of the filter amplifier.

Beyond this the light overlaps and the filter amplifier is switched over to calibration. The calibrating voltage U_k at this modulation frequency acts across the calibration resistance R at the input of the system. The voltage amplitude on the grid of the first tube is equal to

$$\frac{\sqrt{2}U_k Z}{|\overline{Z}+R|}. \tag{5}$$

The output instrument thus gives a reading α_2, equal to

$$\alpha_2 = B\frac{\sqrt{2}U_k Z}{|\overline{Z}+R|}. \tag{6}$$

From (4) and (6) we obtain

$$(\Delta I)_{\max} = \frac{\sqrt{2}U_k}{R}\cdot\frac{\alpha_1}{\alpha_2}. \tag{7}$$

Substituting (7) in (1) we obtain the final calculated formula for determining the amplitude of displacement of the specimen:

$$\frac{l_0}{2} = \frac{\lambda U_k}{\sqrt{2}\pi R(I_{\max}-I_{\min})}\cdot\frac{\alpha_1}{\alpha_2}. \tag{8}$$

The quantities λ and R were constant for all experiments; the quantities $I_{\max}-I_{\min}$, U_k, α_2 constant over the series of observations. This enables each particular measurement to be carried out quickly and the results of the series of measurements to be easily treated. Substituting in (8) the values for $\lambda = 5190$ A and $R = 1.82\cdot 10^6$ ohms, we obtain the working formula for calculating the amplitude of displacement of the specimen:

$$\frac{l_0}{2}\,[\text{A}] = 0.637\frac{U_k[\text{mv}]}{(I_{\max}-I_{\min})[\mu\text{A}]}\cdot\frac{\alpha_1}{\alpha_2}. \tag{9}$$

The piezoelectric modulus d_{11} of a single crystal of quartz was used to check the working of the apparatus. Onto the X-section specimen of diameter 18 mm and thickness 2 mm were attached electrodes by the fused silver method, and to them were attached copper wire conductors of 0.1 mm diameter. A small mirror is stuck to one surface of the specimen, the other being stuck to the crystal holder – a brass cylinder, tightly screwed to a massive brass parallelepiped placed in the thermostat of the interferometer. The amplitude of displacement of the surface perpendicular to the X axis is measured by placing an electric field along this axis. Hence $l_0/2 = \Delta x = d_{11}E_x\cdot x = d_{11}U_{\text{ampl}}$, and

$$d_{11}[\text{CGS}] = \frac{\frac{l_0}{2}}{\sqrt{2}U_{\text{eff}}} = 0.637\frac{V_x[\text{mv}]\cdot 300\cdot 10^{-8}}{\sqrt{2}\,U_{\text{eff}}[\text{v}](I_{\max}-I_{\min})_{[\mu\text{A}]}}\cdot\frac{\alpha_1}{\alpha_2}. \tag{10}$$

The piezoelectric modulus d_{11} of quartz was measured by placing an effective voltage of 100 v at 3000 cycles across the specimen. The magnitude of the displacement was of the order of 3.1 A. (The very minimum size

of the displacements that can be measured by the apparatus depends on the level of electrical and acoustical disturbances. For the known disturbances the apparatus permitted the measurement of amplitudes of crystal displacements exceeding 0.5 A and for lesser displacements at nighttime 0.05 A.) Our measurements gave a value of the piezomodulus of quartz of $d_{11} = (6.57 \times 0.07) \cdot 10^{-8}$ (CGS). The value of the piezomodulus was determined as the mean of the results of several (4-5) repeated measurements on one and the same specimen, but for repeated stickings of it on the crystal holder. The relative error of measurement was in this case of the order of 1%. For steady sticking the repeated measurements gave a relative error of exactly 0.5%. Statistical measurements by the electrometer on the very same specimen gave a value of d_{11} for quartz as $6.65 \cdot 10^{-8}$ (CGS), which is in good agreement with the results above.

As can be seen from the given data, the apparatus described can be used to determine the piezoelectric and electrostrictive coefficients of crystals and their frequency and temperature dependence, for the investigation of the processes of polarization of dielectrics and phase transitions of ferroelectrics.

I convey my deepest thanks to I. S. Zheludev for help and guidance in this work and also V. A. Shamburov and co-workers of the Gor'kii Institute of Scientific Research in Radio Physics, to I. L. Bershtein and N. M. Borovitskaia for help rendered in the preparation of the apparatus.

LITERATURE CITED

[1] G. S. Gorelik, "On the application of modulation methods in optical interferometry," Doklady Akad. Nauk SSSR 83, 4, 549-552 (1952).

[2] I. L. Bershtein, "On the measurement of very small changes in path difference of two light waves," Doklady Akad. Nauk SSSR 94, 4, 655-658 (1954).

[3] I. L. Bershtein, Letter to the editor, A review of "Modulation Interferometry," UFN 37, 4, 631-633 (1953).*

[4] N. O. Chechik, "The application of photomultipliers in spectral analysis," UFN 37, 1, 74-113 (1949).*

[5] I. L. Bershtein, Thesis for doctorate, IRE (1955).

Received May 24, 1957

Institute of Crystallography, Academy of Sciences USSR

* Uspekhi Fiz. Nauk.

THE INFLUENCE OF DEFORMATION CONDITIONS ON THE MECHANISM OF THE FORMATION OF SLIP BANDS

E. V. Kolontsova and I. V. Telegina

This is a study by an x-ray method of the structure of the slip bands in Sn monocrystals deformed by stretching. The influence of the original orientation of the sample and the rate of deformation on the external shape and structure of the slip bands was analyzed. It was established that, under definite conditions of deformation, a twinning of the mother crystal is observed at the boundary of the slip bands.

As several authors [1-4] have shown in their studies, a completely definite orientation of the sample and the presence of bending moments during deformation are essential for the formation of sharply defined slip bands in metallic and ionic crystals. The original orientation must be such that at the very beginning of deformation the processes of gliding and twinning are obstructed, or, in other words, the magnitudes of the critical shear stresses along the corresponding gliding and twinning surfaces must increase greatly.

It is known that the orientation of the crystal changes during deformation and, as a result, the significance of the critical shear stresses increases. It seemed essential to us to trace the influence of the original orientation of the crystal on the formation of the slip bands during deformation, when conditions favorable for their appearance arise in a sample which has a sufficiently well defined plasticity.

With this idea in mind, we carried through the stretching of tin monocrystals of different orientation up to the ultimate possible deformations (of the order of 300-350% elongation). The samples were cylindrical and the stretching force was applied along the axis of the cylinder.

Our experiments showed that clearly defined slip bands were observed at any original crystal orientation up to that most favorable for gliding, when the glide surface and the directions of gliding are at a 45° angle to the direction of the applied force. The stage at which the slip bands appear depends essentially on the original crystal orientation, while the number occurring in a unit of length is basically determined by the number of defects on the surface of the sample. Deep etching of the crystal surface before deformation decreases the concentration of slip bands twentyfold.

The external form of the crystal after deformation – the shape of the slip bands and the clearness of the break of the surface at the slip boundary – depends on the rate of deformation: when the deformation rate is slow the contours of the slip bands are less well defined.* The plane of the "ribbon" (a sample of cylindrical shape becomes ribbon-like after deformation) retains its orientation along the whole length of the sample. A change in orientation of the plane of the ribbon is observed at the boundaries of the slip bands in the monocrystals that were stretched rapidly. In agreement with this, etching of the crystal surface reveals regions of the crystal with a new orientation derived from the slip bands. The dimensions of these regions depend on the rate of deformation. The greater the rate, the larger their dimensions. The linear dimensions of the regions of the crystal with a new orientation reached 10 mm. Much smaller ones, in terms of the grain size of the new orientation (not larger than 0.05 mm), are observed within the slip bands and in monocrystals slowly stretched.

* The rate of deformation was evaluated by the length of time it takes for a crystal to stretch until rupture. The slow rate corresponded to 1 min, the rapid rate to part of a second. The average elongation of the samples was 60-70 mm when the original length was 20-25 mm.

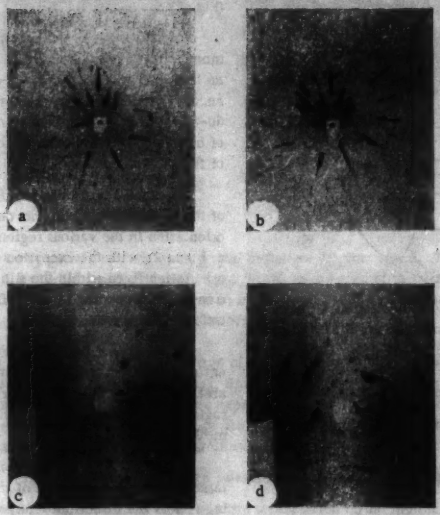

Fig. 1. X-ray patterns of a tin monocrystal stretched slowly; a) in the area of the slip band; b) between the slip bands; c) within the slip band, in the region adjacent to the sharply curved surface of the crystal; d) in the central part of the slip band at orientation 1, c. The orientation of the crystal is shown in Fig. 2.

To determine the new orientations which arose during deformation, and the structure of the slip bands, x-ray photographs were taken by the Laue method (using beams of cross section from 15 μ to 1 mm in diameter) of various regions of the crystal: within the slip bands, at their boundaries and between the bands. The position of the x-ray beam was fixed with the aid of a special device which directed the beam at the chosen region of the crystal with an accuracy of up to 10 μ.

On the basis of the x-ray data, it can be concluded that complex gliding is the origin of the slip band formation observed at a low rate of deformation in tin, and that its mechanism can be described according to Barrett [1], using the notion of dislocations. The smooth change in orientation observed within the slip band also follows essentially the laws previously stated in the literature [3], i. e., in tin one also observes within the slip bands an S-shaped twist of regions of the crystal around a direction approximately perpendicular to the glide direction [001] (± 5°) and approximately parallel to the gliding plane (110) — accurate to ± 15°.

The angle of deviation depends on the rate of deformation. For the majority of the crystals studied, the axis of fundamental twist coincided approximately with the direction [530]. The maximum angle of twist was 30-45°. Additional twists of approximately 5-10% from the fundamental twist angle are observed around the glide direction and the normal to the glide plane.

The axes of twist in the upper and lower parts of the slip band may be not completely parallel (the angle of deviation is of the order 2-3°) and, as a result, the orientation of the crystal is not always completely restored.

The turning of the lattice which occurs within the slip bands contributes to the realase of the inner stresses inside the slip bands near their boundaries. This can be deduced from the clearness of the spots on the x-ray patterns obtained with a 15 μ pinhole system from the regions adjacent to the sharply curved surface of the crystal

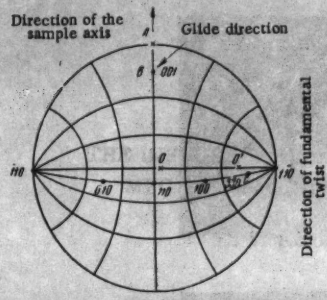

Fig. 2. Gnomostereographic projection of a tin monocrystal deformed 300% by elongation. O) Direction of the initial x-ray beam for 1, a and 1, b; O') for 1, c and 1, d. A is the sample axis, B is the glide direction, C is the axis of fundamental twist.

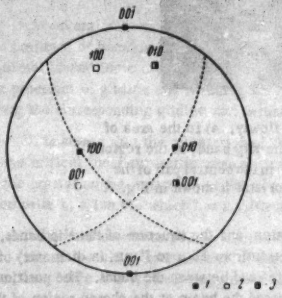

Fig. 3. Mutual arrangement of the new orientations and the orientation of the mother crystal; 1) corresponds to the mother crystal, 2, 3) correspond to the new orientations. The dotted lines are the planes with poles (03$\bar{1}$) and (30$\bar{1}$).

inside the band, and from the regions outside of the band (Fig. 1).*

As the x-ray pattern shows (with a 30 μ beam), the monocrystal in the central part of the slip band is broken up into a series of blocks twisted with relation to one another by 15-20°. The collection of orientations covers 50-60° (Fig. 1, c). The widening of the angular range of orientations is proportional to the increase of the angle of fundamental twist.

X-ray photographing confirms the monocrystallinity of the whole sample and the constancy of the crystal orientation in the various regions of the sample (see Figs. 1, a, b and 2), with the exception of the small areas of new orientation fixed within the slip band. The new orientation is not connected in any definite way with the orientation of the mother crystal.

A tin crystal deformed at a very high rate has an entirely different structure. Within the slip bands, in the area adjacent to the sharply curved crystal surface, large regions appear quite different in orientation from the mother crystal.

As calculation shows, new orientations can be obtained from the orientation of the mother crystal by turning it near the directions [100] and [010] by an angle of 64° (Fig. 3). It is apparent from the figure that these new orientations are not arbitrary with respect to the mother crystal; the orientation of the mother crystal and the new orientations are symmetrically related to a plane of the type (301).

Acceleration of the deformation causes an increase in the volume of the regions of the crystal with a new orientation. Within the limits of speed of deformation possible under our conditions, a new orientation is observed almost throughout the crystal; moreover, an additional elongation of the sample is possible (50-100% more) by gliding in the separate regions of the crystal with a new orientation.**

These facts, taking into account the fact that the formation of slip bands at high speeds is always accompanied by a characteristic sound, show that conditions within the slip bands are such that deformation by twinning is possible. Actually, the (301) plane in tin crystals is the mechanical twinning plane [5].

The sharpness of the reflections on the x-ray patterns obtained from the twinned regions of the crystal shows that the twinning process contributes to the release of lattice stresses (Fig. 4, a, b).***

* Due to the difficulty of reproducing these patterns on Fig. 1, those obtained with 0.5 mm and 0.15 mm pinholes are given, inasmuch as they already show the increase in clearness of the spots from the regions of the crystal located at the band boundary.

** A 400% elongation was performed in a tenth part of a second.

*** In case the new orientation proves advantageous for gliding, the x-ray patterns show the presence of well-defined asterism also in the regions of the crystal with a new orientation.

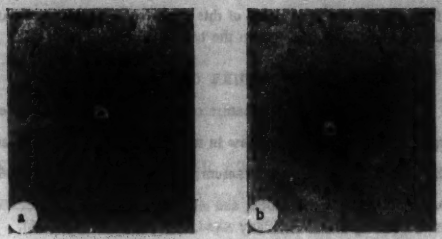

Fig. 4. X-ray pattern of a tin monocrystal deformed at great speed. The arrows on Fig. 4, a mark the reflections of Fig. 4, b. a) In the area of the slip band; $[110] \parallel$, a $[001] \perp$ to the x-ray beam; b) in the region of the crystal adjacent to the slip band at the same orientation of the sample.

We were not able to trace in detail the transition of the mother crystal to the twinned orientation, nor to study the inner structure of the slip band in tin crystal, since x-ray photography of the inner regions of tin crystals by means of a fine beam demands exceptionally long exposures. But x-ray photography with a coarse beam and with a fine beam for regions of the crystal adjacent to the surface makes impossible any definite conclusions concerning the laws of transition from one crystal orientation to another.

Transparent Cs and Tl halide crystals are more suitable for the study of the fine structure of slip bands.

As has already been said [6, 7] a sharp change in the orienatation of the mother crystals is observed in some samples of CsI, CsBr and TlBr—TlI crystals deformed by pressure near the sharply curved surface of the crystal at the slip band boundary, as well as in tin crystals.

Depending on the degree of deformation and the rate of loading of the sample, the dimensions of the area in which a new orientation is observed can change; in which case, according to Klassen-Nekhliudova's and Urusovskaya's [8] data, only the formation of slip bands with clear contours is accompanied by the sound characteristic of twinning. In addition, within clearly defined slip bands, it is possible that not just one definite orientation appear, but several, arbitrarily oriented in relation to the mother crystal [7]. It is true that in the case of tin all the new orientations arrange themselves with mirror symmetry in relation to planes of the type (301), whereas in CsI and CsBr crystals there are at least two families of crystallographically different planes of the type (501) and (11 n) (n = 3-5), which can be considered as twinning planes [6, 7].

Although it is impossible to make a unique choice of the twinning plane in Cs and Tl halide crystals, one can assume that the twinning process plays a part in the formation of slip bands in metallic as well as in ionic crystals, inasmuch as all the new orientations, observed within the slip bands in Sn, CsI, and CsBr crystals, join with the mother crystal across well-defined equivalent crystallographic planes. Moreover, twinning is observed when resting of the crystals during deformation does not remove the stresses necessary for twinning. Such stresses arise within the slip bands in the regions of the crystals adjacent to the sharply curved surface of the sample.*

Barrett's [1] conclusion that a complex gliding is the basis of the mechanism of formation of slip bands, but that twinning plays no part, is derived from the fact that the metallic crystals, which were the objects of study in his published works, rest well at room temperature, and that the rate of deformation was low.

The structure of the slip bands which arise at high rates of deformation and under nonhomogeneous stresses is better described by the scheme proposed by Orowan [2], than by that by Barrett [1], whereby the length and the direction of the line along which the glide directions deviate sharply from the original direction depend essentially on the sample and the conditions of deformation [6, 7]. Our experiments show that this line is the trace of

* Besides the twinning, conditions are created within the slip bands favorable to recrystallization at room temperature, even at low rates of deformation (Fig. 1, c).

the twinning plane. Thus, for CsBr crystals the indices of this direction, [$\bar{1}31$] determined optically, correspond to those of the twinning plane ($\bar{1}14$), determined from the Laue pattern.

LITERATURE CITED

[1] J. B. Hess and C. S. Barrett, "Structure and nature of kink bands in zinc," J. Metals 9, 599 (1949).

[2] E. Orowan, "A type of plastic deformation new in metals," Nature 149, 643-646 (1942).

[3] F. D. Rosi, "Mechanism of plastic flow in titanium," J. Metals 6, 1, 58-69 (1954).

[4] A. T. Zemtsov, M. V. Klassen-Nekhliudova, and A. A.Urusovskaia, "Concerning the complex development of plastic deformation of monocrystals," Doklady Akad. Nauk SSSR 91, 4 (1953).

[5] E. O. Hall, Twinning and Diffusionless Transformations in Metals (London, 1954).

[6] E. V. Kolontsova, I. V. Telegina, and G. M. Plavnik, "Concerning the structure of the slip bands of some ionic crystals," Kristallografiia 1, 4, 419-424 (1956).

[7] E. V. Kolontsova and I. V. Telegina, "Concerning the mechanism of slip band formation," submitted for publication in Doklady Akad. Nauk SSSR.

[8] M. V. Klassen-Nekhliudova, and A. A. Urusovskaia, "The influence of nonhomogeneous stress conditions on the mechanism of plastic deformation of Tl and Cs halides," Kristallografiia 1, 4, 410-418 (1956).

Received February 22, 1957

M. V. Lomonosov Moscow State University

ON THE MORPHOLOGY OF SPHERULITIC GRAPHITE IN HIGH-STRENGTH CAST IRON

Dr. I. Ezhek, Doctor of Engineering I. Koritta, and Candidate of Technical Sciences K. Lebl'

INTRODUCTION

Graphite in cast iron is of great interest to foundry technologists. The form of segregations and the number and mutual distribution of graphite grains in gray cast iron substantially affect its mechanical properties and the physical and, in part, chemical properties of castings. Although the methods and processes leading to the separation of graphite in the form of grains instead of flakes and plates, i. e., in the form which endows cast iron with unusual strength and plasticity, are well known; the morphology of these nonmetallic inclusions is not quite clear as yet and is of great scientific interest.

During the past decade it became possible to produce high-strength cast iron with inclusions of spherulitic graphite, and much attention has been devoted to x-ray studies of the inclusions. The present work reports the results of electron microscope study of these inclusions in gray high-strength and malleable cast iron.

Preparation of Polished Sections and the Technique of Making Replicas

The polished sections used in this work were made in the following way. Preliminary polishing was done on metallographic papers of the Swiss brand SIA and continued with successively finer diamond dust suspended in glycerine and spread over photographic paper. Finally, the sections were polished for 1 to 3 min on a lap covered with velvet and moistened with a water suspension of P. F. Dulardin's Tonerde Alumina Nos. 1, 2 and 3.

The finished sections were gently etched with nitol for twenty seconds, and after they were thoroughly dry a drop of 1% solution of collodion in amyl acetate was applied to their surfaces. If the solution is allowed to flow freely over the surface of a section, a very thin (600-800 A) collodion replica is formed. The replica was covered with gummed tape and carefully removed from the section. It was then placed on the surface of hot water, the glue on the tape dissolved and the replica floated free. After careful washing, the replica was laid on 0.1 mm mesh of phosphorus bronze. To increase contrast, the replica was placed in a vacuum at an angle of 20° and tinted with vaporized chrome. The investigations were carried out on the Tecla electron microscope. This instrument is an electromagnetic microscope made in Czechoslovakia and has a resolving power of 100 A.

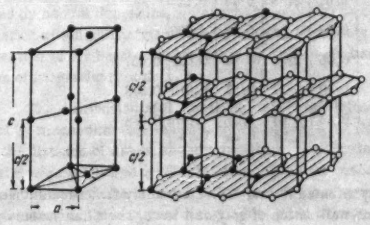

Fig. 1. Diagram of graphite structure.

Flaky Graphite

Graphite crystallizes in gray cast iron with the usual hexagonal structure. Individual atomic layers are held together by metallic bond. From the position of atoms in the unit cell (Fig. 1) it follows that the flaky form is the natural form of graphite inclusions. As the melt cools, particles of graphite grow along the basal surfaces. It is well known that the weak forces between the individual atomic layers make graphite an excellent lubricant.

Fig. 2. Structure of an eutectic graphite lamella (× 8000).

Fig. 3. A "twinned" graphite lamella (× 8000).

Fig. 4. Orientation of elementary plates in a lamella (× 8000).

Fig. 5. Graphite lamella attached to the phosphite eutectic (× 8000).

Chemical Composition of Investigated Samples (%)

Material	C total	C bound	Mn	Si	P	S	Mg
Gray cast iron	3.82	0.49	0.61	2.48	0.42	0.11	—
Gray cast iron (modif. by ferrosilicon)	2.98	0.52	0.68	1.71	0.33	0.098	—
High-strength cast iron I	3.08	0.66	0.55	2.69	0.19	0.020	0.051
High-strength cast iron II	3.42	0.18	0.42	2.32	0.17	0.019	0.073
High-strength cast iron III	3.17	0.40	0.49	2.84	0.21	0.016	0.068
Malleable cast iron	2.82	—	0.42	1.08	0.24	0.14	—

Graphite plates form from individual small suitably oriented flakes. The elementary flakes reach their maximum size in graphite formed during hypereutectic crystallization of gray cast iron. Their dimensions and distribution in the graphite lamellae in eutectic crystallization are clearly shown in Fig. 2. The primary plates

separated directly from the melt are straighter and stronger than the slender and bent lamellae of graphite of eutectic crystallization. An interesting case of "twinning" of plates is shown in Fig. 3. The details of branching of the plates and orientation of individual graphite flakes are shown in Fig. 4. Finally, an interesting specimen is shown in Fig. 5, in which the plate of graphite is followed directly by the triple phosphide eutectic (steadite). The basic structure of a sample of gray cast iron was ferrite-pearlitic and its composition is given in the table above.

Graphite in High-Strength Cast Iron

Spherulitic graphite consists of crystallites growing from a center. They have the form of many-faced pyramids or cones whose bases are parallel to the flakes of graphite or to the basal planes of its crystal lattice oriented approximately at right angles to the diameter of the crystal aggregate (graphite grains). The atomic

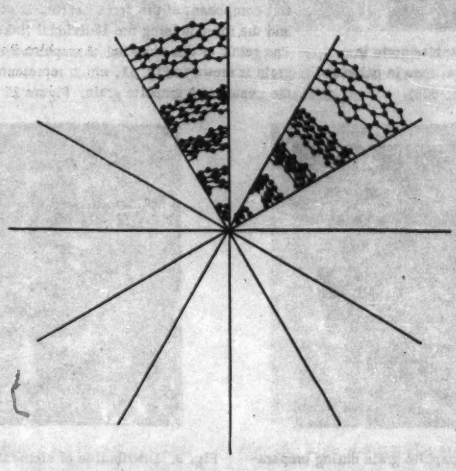

Fig. 6. Diagram of the distribution of carbon atoms in a graphite grain from high-strength cast iron.

structure of a graphite grain is shown diagrammatically in Fig. 6. Observation of a polished section of such a grain in polarized light reveals the radiated arrangement of crystallites (Fig. 7). The radial structure of the grains becomes apparent at the very beginning of preparation of a polished section (Fig. 8). The graphite grains grows in the direction least advantageous from the point of view of expended energy because its growth does not proceed by natural deposition of carbon atoms on the basal planes of the lattice. This is the reason for slower crystallization of spherulitic graphite as compared with platy graphite [3]. The decrease in the rate of growth in the direction of the basal surfaces makes it possible to change physical and chemical properties of the melt by addition of magnesium, cerium, etc.

The distribution of flakes in individual crystallites of spherulitic graphite in high-strength cast iron modified by magnesium (see table) is shown in Fig. 9. A detail of structure of a graphite grain in a polished section at the distance of approximately one-third of the grain radius from its center is shown in Fig. 10. The centers of grains were studied with special care. As in the preceding investigations by the VUMT [4], no "nuclei" were found, even with the high magnifications of the electron microscope. Therefore, it may be supposed that the appearance of the structure of a graphite grain as seen under an optical microscope depends on the distance of the surface of the polished section from the center of the grain, on the method of preparation of the polished section

Fig. 7. Section of a graphite grain in high-strength cast iron as seen in polarized light in the dark field (× 600).

and, partly, on the type of basic structure of the cast iron which encloses the grain. The last factor is important in the study of the peripheral parts of the grain.

After testing a series of samples of differently prepared cast iron with spherulitic graphite (see table), it may be considered as proved that the "nuclei" are optical illusions produced by the difference in reflectivity of the radially arranged faces and the almost nonreflecting center, where individual flakes of graphite are usually torn out, so that these areas do not react to polarized light. The plucking out of graphite flakes occurs when the angle between the surface of the polished section and the gliding plane of the crystallite reaches a certain minimum value so that the tangential component of the force exerted in polishing becomes dominant and the force holding the individual flakes together is exceeded. The result of this plucking of graphite flakes from the center of a grain is shown in Fig. 11, which represents a section passing through the center of a graphite grain. Figure 12 shows the disordered struc-

Fig. 8. Structure of a graphite grain during preparation of a polished section after it has been polished on paper No. 300 (× 800).

Fig. 9. Distribution of elementary flakes in granular graphite (× 8000).

Fig. 10. Detail of structure of a graphite grain above its center (× 8000).

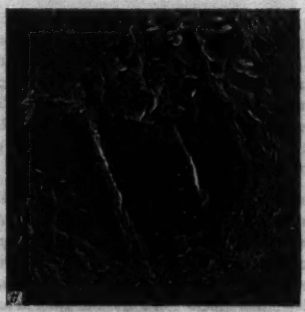

Fig. 11. Graphite layers exposed in the center of a grain (× 800).

Fig. 12. Complex structure of a graphite grain above its center (× 8000).

Fig. 13. Structure of high-strength cast iron with dominantly pearlitic metallic groundmass (observations were made in partially polarized light) (× 600).

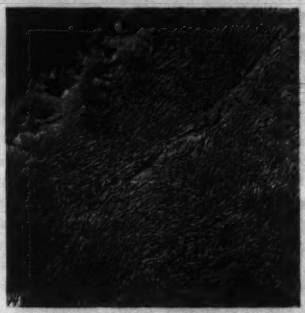

Fig. 14. Edge of a graphite grain in cast iron after annealing (× 16,000).

Fig. 15. Edge of a graphite grain in a casting (× 8000).

ture of a graphite grain at the point over its geometric center. The authors doubt the correctness of the idea that nuclei appear in the upper part of a grain [5]. This is probably another optical illusion.

The next question to be touched upon is that of the origin of the so-called double boundary of a graphite grain (Fig. 13) which, in the opinion of some writers [6], forms as the result of diffusion of carbon into the grain, especially in ferrite annealing. We have shown that this double boundary (Fig. 13, along the periphery) is found more frequently on grains included in ferrite, i. e., in castings which have bene subjected to prolonged annealing. In these cases, the edges of grains do show an orientation of individual graphite plates differing from the usual (Fig. 14). Of course, here also the preparation of the polished sections plays an important role, for the strong cohesion between graphite and ferrite at the boundary must be taken into consideration [4]. In cast iron samples from castings and with spherulitic graphite and ferrite-pearlite structure no special orientation on the boundaries is observed (Fig. 14).

Carbon Separated in Annealing

We included among the subjects for investigation several samples of malleable cast iron with black fracture. In these castings graphite is in the form of considerably disordered grains (see graphite plates in the carbon grains of Fig. 15). It is not necessary to postulate the presence of numerous centers of crystallization in these samples, but here also, in spite of all our efforts, we have failed to detect a "nucleus."

SUMMARY

An investigation of segregations of graphite in gray high-strength and malleable cast iron showed differences in the mutual orientation of separate graphite plates in these materials.

It has been confirmed that the segregations of graphite in the high-strength cast iron are in the form of ideal spheres. The form of segregations is determined by the mechanism of anomalous crystallization of graphite in the direction normal to the basal planes on the crystal lattice. No "nuclei" have been found in the centers of grains, even with maximum magnifications of an electron microscope and careful preparation of replicas. Therefore, the "nuclei" which can often be seen with an optical microscope when the section is cut through the center of a grain must be considered as optical illusions. Surface layers of grains of spherulitic graphite were studied also in cast iron with ferrite annealing.

It has been established that separate elementary plates of graphite in the carbon of annealing are usually 5 to 50 times as large as in the cast iron with spherulitic graphite and so far as the order of magnitude is concerned, they are of the same size as the graphite flakes in gray cast iron.

LITERATURE CITED

[1] Scheil and Hütter, Arch. Eisenhüttw. 24, 237 (1935).

[2] Gröber and Hanemann, Arch. Eisenhüttw. 11, 199 (1937/38).

[3] Dumphy and Pellini, Memoires du CF 13 (1951).

[4] Králová and Klában, Práce Ceskoslov Vyzhumu Slevarenskeho 2 (1955).

[5] Wittmoser, Arch. Eisenhüttw. 24, 431 (1953).

[6] Rehder, Trans. Am. Foundrymen's Assoc. 58 (1950).

[7] Hughers, Foundry Trade J. 1882, 349 (1952).

[8] De Sy, Rev. Min. Met. 8 (1952).

Received December 9, 1956

Scientific Research Institute of Materials and Technology, Prague

AN INVESTIGATION OF PHASE EQUILIBRIA IN A PART OF THE SYSTEM $H_2O-SiO_2-Na_2CO_3$ AT HIGH TEMPERATURES AND PRESSURES

V. P. Butuzov and L. V. Briatov

The solubility of quartz in aqueous solutions of sodium carbonate at high temperatures (300-400°) and pressures (up to 1500 atmos) has been determined as well as the conditions of the splitting of the solution into two phases: the heavy phase with a high content of SiO_2 (35-50%) and the light phase with a small content of SiO_2 (up to 3%).

During the last decade much attention has been devoted to the development of methods of growing of single quartz crystals [1-4]. Quartz is grown from aqueous solutions containing sodium carbonate or sodium hydroxide, at high temperatures (300-420°C) and high pressures (300-1200 atmos). A number of investigators have studied the system $H_2O-SiO_2-Na_2O$ in order to determine the conditions of growth of single quartz crystals and the behavior of the system in the unexplored region of high temperature and pressure. Morey and Hesselgesser [5] studied the dependence of the behavior of the system at 400°C on pressure (up to 2500 atmos); Tuttle and Friedman [6] studied the same system at 200°, 300° and 350° at the pressure of saturated vapors of the compounds under investigation, and later Friedman [7] investigated the system at 400 and 450°C. Friedman did not measure pressure in his experiments. The available data on the behavior of the system $H_2O-SiO_2-Na_2O$ are insufficient for a physicochemical characteristic of the conditions of growing single quartz crystals because the studies of Morey and Hesselgesser make it possible to judge only of the effect of pressure on the system, while the data of Tuttle and Friedman do not throw light on the effect of pressure. Besides, the measurements and conclusions of the different authors are discrepant.

An aqueous solution of sodium carbonate is mot frequently used as the solvent of quartz. No complete investigations of the system $H_2O-SiO_2-Na_2O$ at high temperatures and pressures has been made up to now. There are works [8, 9] on the solubility of quartz in aqueous solutions of sodium carbonate at high temperatures and pressures, but their data are also insufficient for determining the conditions of growth of single quartz crystals. For this reason we have investigated a part of the system $H_2O-SiO_2-Na_2O$ at high temperatures and at pressures higher than the pressures of the saturated vapors of the system.

Method of Investigation

The solubility of quartz in unsaturated solutions of sodium carbonate was studied in the following way. A definite amount of the aqueous solution of sodium carbonate of a given concentration was poured into a stainless steel autoclave and a weighed block of quartz was introduced into it. The ratio of the volume of solution in the autoclave to the volume of the autoclave (minus the volume of the quartz block) at room temperature will be called the charge of the autoclave. The autoclave was hermetically sealed and placed in a furnace where it was heated to a definite temperature and held at that temperature for the period of time required to establish equilibrium. The autoclave was then taken out of the furnace and quickly placed in a tank with flowing water where in one to two minutes it was cooled to room temperature. After it cooled the autoclave was opened. As we have shown earlier [10], the solubility of quartz cannot be determined from the loss of weight by the quartz block, since under certain conditions the solution in the autoclave splits into a solution with a few percent of

SiO_2 and a solution containing almost 50% of silica by weight. The latter solution we call the heavy phase. Friedman [8] did not consider the appearance of this phase, and his data on the solubility of quartz are incorrect.

In the presence of the heavy fraction in the autoclave we determined the solubility of quartz in the following manner. The quartz block was fastened near the cover of the autoclave. The autoclave was placed in the furnace in inverted position and the heavy fraction accumulated in its lower part, on the cover. The autoclave was chilled in this position and then reversed and opened. Thus we sharply cut the time for the reaction of the heavy fraction with the rest of the solution. To prove that no noticeable reaction took place when this procedure was used, the autoclave was heated in the furnace in inverted position and on being taken out was quickly reversed and then chilled. The heavy phase had no time to flow downward, but solidified on the cover and did not react with the rest of the solution. The data obtained in both cases show satisfactory agreement of the results characterizing the composition of the heavy phase. After the autoclave was opened the solution was poured off and its SiO_2 content determined gravimetrically; the content of Na_2CO_3 in it was determined volumetrically. The heavy phase after cooling was represented by glass and was analyzed for H_2O, SiO_2 and Na_2O.

Results of Experiments

Figure 1 presents the data on the relation between the solubility of quartz* and the amount of 5% solution of sodium carbonate in the autoclave in the form of isotherms. The solubility was obtained by determining the amount of SiO_2 in solution and then calculating the amount of SiO_2 per liter of solution at room temperature. The

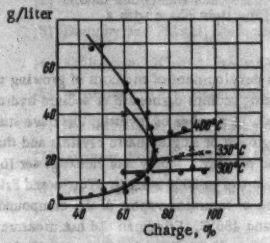

Fig. 1. Isotherms of solubility of quartz in 5% solution of sodium carbonate. ——) Solubility curves; ——) loss in weight due to formation of the heavy phase in the autoclave.

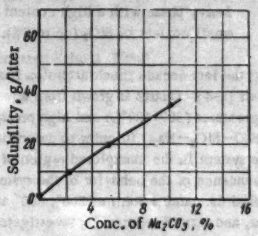

Fig. 2. Relation between solubility of quartz and concentration of sodium carbonate in the solvent with 80% charge and 350°C.

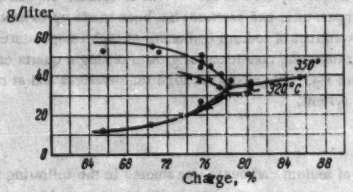

a

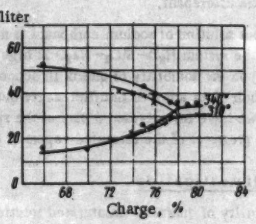

b

Fig. 3. Isotherms of solubility of quartz in 10% solution of sodium carbonate. ——) Solubility curves, ——) loss of weight with formation of heavy phase in the autoclave.

* When we speak of the solubility of quartz we mean its solubility in the initial solution, not in the heavy phase.

TABLE 1

Compositions of Coexisting Phases (in wt%)

T, °C	Conc. Na_2CO_3	Charge, %	Solution			Heavy phase		
			H_2O	SiO_2	Na_2CO_3	H_2O	SiO_2	Na_2O
300	0	80	99.92	0 08	—	—	—	—
300	5	80	94	1.2	4.8	—	—	—
300	10	80	88	2.7	9.3	—	—	—
350	0	75	99.87	0.13	—	—	—	—
350	5	75	93.5	1.9	4.6	—	—	—
350	10	80	87.5	3.3	9.2	—	—	—
350	5	70	94.1	1.5	4.4	47	40	13
350	10	75	89.5	2.4	8.1	38.8	34.1	27.1
350	10	65	93	1.0	6	40.8	35	24.2
400	0	75	99.78	0.22	—	—	—	—
400	5	75	92.5	2.7	4.8	—	—	—
400	5	60	96.5	1,0	2.5	26.4	49,5	24.1

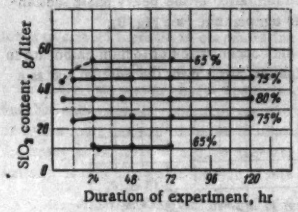

Fig. 4. The speed of attainment of equilibrium in the process of solution of quartz in 10% solution of sodium carbonate at 350°C. Upper curves, corresponding to 65 and 75% charge, give amount of SiO_2 in the solution and in the heavy phase. Lower curves, corresponding to 75 and 80%, indicate amount of SiO_2 in the solution.

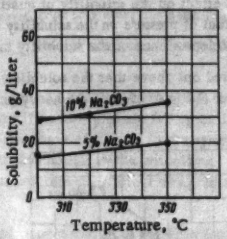

Fig. 5. Relation between temperature and solubility of quartz in sodium carbonate solutions of different concentration with 80% charge. The curves are based on many more points than are shown on the graph.

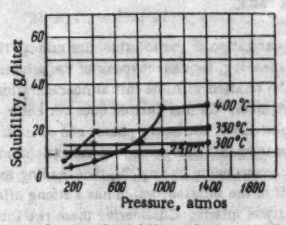

Fig. 6. Isotherms of solubility of quartz in 5% solution of sodium carbonate in relation to pressure.

shape of the 300° isotherm shows that a slight increase in solubility occurs when the charge of the autoclave is increased. If the temperature is raised to 350°C, then with the charge of over 72% the same relation is observed between the solubility of quartz and the charge. With charges less than 72%, the solubility curve shows a break due to the appearance in the system of a heavy phase and the solubility curve bends sharply downward, i. e., the solubility of quartz depends significantly on the charge. The loss in weight per unit volume of the solvent with decrease in charge rises sharply upward. An analogous relation is observed at 400°C.

Increase in concentration of sodium carbonate in the solution at constant temperature and charge leads to increase in solubility of quartz if the heavy phase does not form in the system (Fig. 2). An analogous relation for dilute alkaline solution was noted by Wyart and Sabatier [11].

Figure 3 shows the isotherms of solubility of quartz in 10% solution of sodium carbonate. In this case also the solubility of quartz in the presence of the heavy phase depends on the charge of the autoclave. It may be supposed that the heavy phase is an intermediate product of the solution process and that its presence in our experi-

ments indicated that the system had not reached equilibrium. We have conducted experiments which showed that equilibrium in the system is attained in 24 hr (Fig. 4). As a rule we left the autoclaves in the furnace for 3-5 days, which fully guaranteed the attainment of equilibrium in the system.

In the temperature interval 300-400°C with charges which do not give rise to the heavy phase the dependence of solubility of quartz on temperature is large enough, but the temperature coefficient of solubility of quartz is practically independent of the concentration of sodium carbonate (Fig. 5).

As can be seen from our data (Figs. 1 and 3), in a broad selection of charges with either 5 or 10% solution of sodium carbonate, the dependence of the solubility of quartz on temperature is slight in the presence of the heavy phase.

The compositions of coexisting phases are given in Table 1. The data on solubility of quartz were taken from the work of Kennedy [12].

DISCUSSION OF RESULTS

The experiments performed have shown that pressure, unless there is precipitation of the heavy phase in the system, has little effect on the solubility of quartz. This agrees with the results obtained by Adams [13], who investigated the effect of pressure on the solubility of NaCl. However, the formation of the heavy phase substantially changes the dependence of the solubility of quartz on pressure and temperature (see Fig. 6).

It was pointed out above that the solubility of quartz depends on the concentration of sodium carbonate in the solution. After the formation of the heavy phase, part of the Na_2O passes into it from the solution and as a

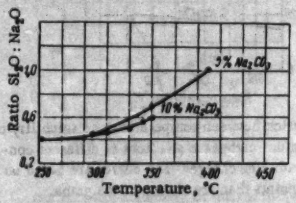

Fig. 7. Dependence of the SiO_2: Na_2O ratio in sodium carbonate solutions of different concentration on temperature.

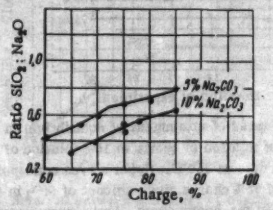

Fig. 8. Dependence of the SiO_2: Na_2O ratio on the charge of sodium carbonate solutions of different concentrations at 350°C.

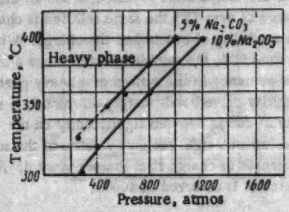

Fig. 9. P-T diagram of the field of existence of the heavy phase for solutions with different sodium carbonate concentrations.

result the concentration of the solution diminishes. Therefore, strictly speaking, we cannot speak of the solubility of quartz in the solution with the initial concentration of sodium carbonate. Carbon dioxide does not enter into the composition of the heavy phase, and so its amount in the solution increases with respect to the stoichiometric composition corresponding to Na_2CO_3, thus leading to the decrease in pH of the solution, which has a strong effect on the solubility of quartz. Considering these two factors (decrease in the concentration of sodium carbonate in the solution and decrease in its pH due to excess of CO_2), the strong decrease of solubility of quartz in the solution which coexists with the heavy phase becomes understandable.

The solubility of quartz increases with temperature (when the heavy phase is absent from the system) and so does the SiO_2: Na_2O ratio in the solution. The higher the concentration of Na_2CO_3, the lower the SiO_2: Na_2O ratio (Fig. 7). Since decrease of the charge leads to the formation of the heavy phase, there results a sharp de-

crease in the SiO_2: Na_2O ratio (Fig. 8). The value of the SiO_2:Na_2O ratio in the heavy phase ranges from 2-5, and the higher the temperature, the higher the value of the ratio. No exact relationship between SiO_2:Na_2O ratio and the charge and temperature has been established.

The field of existence of the heavy phase is determined by temperature, charge and concentration of sodium carbonate in the initial solution. Temperature change at a given concentration of sodium carbonate in the initial solution does not lead to a change in the maximum value of the charge at which the heavy phase ceases to exist while an increase in concentration of sodium carbonate in the initial solution shifts the heavy phase field toward higher charges. The higher the temperature, the higher the pressures at which the heavy phase can exist (for a given concentration of sodium carbonate in the initial solution) and the higher the concentration of sodium carbonate, the higher the pressure needed to form the heavy phase (Fig. 9).

These experimental data are of great interest to technologists engaged in growing single quartz crystals.

SUMMARY

1. The quantitative composition of the phases in equilibrium at high temperatures (300-400°C) and pressures (up to 1500 atmos) in a part of the system $H_2O-SiO_2-Na_2CO_3$, rich in water, has been determined.

2. It has been demonstrated that increase in concentration of sodium carbonate (up to 10%) in the solution leads to a rapid increase in concentration of sodium carbonate.

3. The dependence of the solubility of quartz on pressure and temperature has been determined. It has been shown that pressure has a slight effect on solubility of quartz if no heavy phase is formed in the autoclave, but that under certain conditions pressure has a strong effect on the phase equilibria in the system. The solubility of quartz increases with increase in temperature if the heavy phase is absent in the autoclave. The presence of the heavy phase leads to a sharp decrease in the value of the temperature coefficient of solubility of quartz and sometimes to a change in the sign of this coefficient.

4. Within the studied interval of temperature, pressure and concentration of sodium carbonate, the boundary of the existence of the heavy phase has been determined.

In conclusion, the authors express their gratitude to E. N. Emel'ianova, who took part in the experimental work.

LITERATURE CITED

[1] N. N. Sheftal', First Soviet Experiments in Growing of Quartz [in Russian] (Izd. AN SSSR, 1955).

[2] A. C. Walker and E. Buchler, "Growing large quartz crystals," Ind. Eng. Chem. 42, 7, 1369-1375 (1950).

[3] A. C. Walker, "Hydrothermal growth of quartz crystals as related to phase considerations," Ind. Eng. Chem. 46, 8, 1670-1676 (1954).

[4] I. Franke, "Production de grows cristals artificiel de quartz," Bull. Soc. Miner. Crist. 77, 1102-1115 (1954).

[5] G. Morey and G. Hesselgesser, "The system $H_2O-Na_2O-SiO_2$ at 400°C," Coll.: Experimental Investigations in Petrography and Ore Deposition [Russian translation] (IL, 1954).

[6] O. F. Tuttle and I. I. Friedman, "Liquid immiscibility in the system $H_2O-SiO_2-Na_2O$," Coll.: Problems of Physical Chemistry in Mineralogy and Petrography [Russian translation] (1950).

[7] I. I. Friedman, "Liquid immiscibility in the system $H_2O-Na_2O-SiO_2$," J. Am. Chem. Soc. 72, 10, 5470-5474 (1950).

[8] I. I. Friedman, "The solubility of quartz in sodium carbonate solutions at high temperature," J. Am. Chem. Soc. 70, 8, 2649-2650 (1948).

[9] I. Franke, "Cristallisation du quartz dans des solutions de carbonate de soude," Bull. Soc. Miner. Crist. 75, 10-12, 591-598 (1952).

[10] V. P. Butuzov and L. V. Briatov, "On growing quartz crystals," Coll.: Growth of Crystals [in Russian] (Izd. AN SSSR, 1957).

[11] I. Wyart and G. Sabatier, "Solubilite du quartz, dans des solutions de sels alcalins sans pression au dessus de la temperature critique," Compt. rend. 240, 32, 2157-2159 (1955).

[12] G. C. Kennedy, "A portion of the system silica–water," Econ. Geol. 45, 7, 629-654 (1950).

[13] L. H. Adams, "Equilibrium binary systems under pressure," J. Am. Chem. Soc. 53, 3769-3813 (1931).

Received May 5, 1957

Institute of Crystallography, Academy of Sciences, USSR

ILLARION ILLARIONOVICH SHAFRANOVSKII

(ON THE OCCASION OF HIS 50TH BIRTHDAY)

Illarion Illarionovich Shafranovskii holds a special place in the science of crystals. A mineralogist by education and a crystallographer by vocation, he combines in his works the interests of these two sciences.

Shafranovskii's scientific activity began in 1930 with a professorship in crystallography at the Leningrad Mining Institute, under the direction of Professor A. K. Boldyrev – a student of the brilliant E. S. Fedorov – at the end of the course at Leningrad University where he studied crystallography with another student of Fedorov's, Professor O. M. Ansheles. I. I. Shafranovskii has been teaching crystallography since 1931 (at one time also mineralogy). A doctor of geological and mineralogical science and a professor, he has been directing the department of Crystallography at the Mining Institute since 1945.

Shafranovskii shows diversified scientific interests, but the guiding theme of his creativity is the problem of the interaction between mineral crystals and the environment in which they form. In working on this basic problem he touches upon many other subjects. He summarized his many years of study of natural crystals in a two volume monograph "Crystals of Minerals" (1957), in which natural crystal formation is given the most detailed and thorough analysis.

In the first years of his work, and partly in subsequent ones, Shafranovskii has been studying the morphology of the crystals of a series of minerals from different localities of the Soviet Union, noting especially the connection between the shapes of the crystals and the conditions of their formation, i. e., touching upon one of the most interesting and practically important problems of crystal genesis in mineralogy – typomorphism of minerals.

However, besides his interest in ordinary crystals with plane faces, Shafranovskii is attracted by the complications in crystal formation, and devotes much time and energy to the study of rounded crystals of minerals, framework formation, various deformations of growth and the dissolution of crystals and of crystalline concretions. He contributed especially to the morphology of the rounded diamond crystals which do not easily lend themselves to analysis.

The monograph on the crystallography of this mineral and the well-known popular-scientific book "Diamonds" (1953) are products of his pen.

While collecting descriptive material, Shafranovskii also turns to the development of the causes which influence the formation of crystals, including those that deviate from ideal growth. Shafranovskii's systematic application of P. Curie's idea concerning the influence of the symmetry of the environment on the morphology of crystals (1954) and on crystal formation is of great significance in the study of crystal genesis and genetic mineralogy.

Equally important to genetic mineralogy is the examination of the question of the influence of the chemical composition of the environment on the shape of crystals. I. I. Shafranovskii together with V. I. Mikheev examined the behavior of crystal structures in chemically different environments (1948) having observed the dynamics of the phenomena on sphalerite, halite and corundum.

Penetrating more deeply into the fine peculiarities of crystal structure, I. I. Shafranovskii made substantial progress in the theory of crystal forms, deriving all possible structural morphological variants of the simple forms, which turned out to number 1403 (1948).

An entirely new division of crystallography was discovered by I. I. Shafranovskii in collaboration with V. I. Mikheev: in studying crystal edges and comparing with simple face forms, the simple edge forms were established – the correspondence of equal crystal edges, derived with the aid of the elements of symmetry (1955). Thus the structural morphological differences of simple forms, and the edge forms as well, were immediately given a very interesting morphological and genetic explanation.

There are many interesting and important scientific aspects in Shafranovskii's numerous studies, of which about 200 have been published. No other scientist has contributed as much toward the study of the history of Russian crystallography and mineralogy. With his particular appreciation of E. S. Fedorov and his scientific heritage, Shafranovskii was the first to give a complete survey of his accomplishments, thus revealing his hitherto unknown personality. Shafranovskii's (and G. M. Popov's) text on crystallography that has gone through countless editions, is used not only by Soviet but also by Chinese students. He excels in popularizing science, thus disseminating scientific knowledge among the masses through the medium of his interesting articles and books. His ideas and accomplishments are also widely known abroad.

D. P. Grigor'ev

LETTER TO THE EDITOR

CONCERNING THE COURSE IN GEOMETRIC CRYSTALLOGRAPHY FOR PHYSICISTS

N. V. Belov

Crystallography, as is known, lies in the middle of the triangle: physics—chemistry—mineralogy. Until recently — due to historical causes — it has been closest to the mineralogical apex, but in the last few years has shifted toward the physical one, which has found its outward expression in the transfer of the Institute of Crystallography to the physical-mathematical division of the Academy of Sciences, and its internal expression by filling the majority of the institute laboratories with young physicists.

Correspondingly, in the higher institutes of learning the course in crystallography shifts from the departments of geology to the physicomathematical ones, and from the elementary course for first-year students to the courses for the second-year students, to whom, of course, it cannot be given as it was meant to be for first-year students in geology.

Thus, Miller indices cannot be introduced as a smart innovation, and the name of the Cambridge professor can be mentioned with gratitude only in a historical survey, inasmuch as the indices themselves become mere coefficients in the equation of the plane-crystallographic face. We must justify the fact that in crystallography for the most part coordinate axes, or the corresponding data, are taken to have oblique angles and different scales, that, in crystallography tradition, in the equation for the plane $Ax + By + Cz = D$ the coefficients A, B, C, are substituted by h, k, l, leaving the right-hand term indefinite, i. e., it is considered to be not some one definite plane, but the whole family of hkl planes parallel to one another. Subsequently, it will be shown in microcrystallography that for crystallographic faces not only the coefficients hkl are whole numbers but, after introducing absolute scales, that all possible values of D will also become whole numbers.

The formulas relative to zones and the angles between faces and edges are all derived from the corresponding expressions of oblique angle geometry, predominantly in the vector form. It must be categorically forbidden to say that in the hexagonal system the faces have not three but four indices. In three-dimensional space any plane is characterized by three index coefficients, and only three indices can be used in calculating volumes, in finding lines of intersection, in the formulas for angles, etc. The introduction of the fourth index must always be considered as a temporary expedient to simplify the solution of some problems having reference to symmetry in cases when a three-fold or six-fold axis enters the symmetry complex of the crystal. Thus, in operating on an hkl face by a three-fold axis it is convenient to introduce the 4th index, which corresponds to the intersection of the face with the u axis, located in the xy plane symmetrically related to the two other axes, and then a cyclical permutation at once makes three out of one face: $hkil$, $ihkl$, $kihl$. But, as has been said before, when it is necessary to apply the face symbol for some calculation (this is especially important in determining intercepts) the fourth index must be immediately discarded, which can be carried out on the basis of the simplest case of $h + k + i = 0$, which allows one to substitute $-(h + k)$ for the letter i. At the very least, the search for the fourth index for an edge (cf. [1]) is senseless. If the face-plane has to intersect all the three xyu axes (or be parallel to one of them), then, for the point (of the edge), the coordinates along only two horizontal axes are always sufficient, and along the additional fourth (u) the index naturally must be 0. If we operate on the point by the three-fold axis, we must write down this 0 and we get: mn0p, 0mnp, n0mp. We eliminate the undesirable nonzero magnitude at the third place of the symbol by means of a very simple theorm (Fig. 1); if a section of equal length is added to the coordinates along each horizontal axis, then the location of the point will not change. Corresponding additions are made in such a way as to leave 0 at the third position of the symbol: mn0p, n, m − n, 0, p,

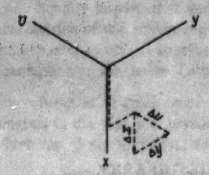

Fig. 1. Concerning the basic theorem of operating on a point by a three-fold axis.

n – m, m, 0, p. After this it remains only to destroy the third position of the third position of the symbol (forget the fourth axis!) and the operation of the three-fold axis is completed.

These various methods of using the symmetry when operating on faces, on the one hand, and on points (edges) on the other, are characteristic only of three-fold axes. With two- and four-fold axes the laws of operation are similar for both the faces and the points, and in this case, it is sometimes advantageous to introduce additional axes. Thus (according to Fedorov) in the case of the four-fold axis it is useful to introduce two more horizontal axes in addition: u, parallel to x, but having the reverse direction, and v connected in the same way with y. Then, by cyclic substitution we find the symbols of four points (or faces) connected by the four-fold axis: mn00p, 0mn0p, 00mnp, n00mp. It is easy to see that the magnitudes which appeared temporarily at the 3rd and 4th places of the symbol can be destroyed, by adding equal amounts to the first and third coordinates, and correspondingly to the second and fourth, after which we get (discarding the zeros at the third and fourth places) mnp, $\overline{m}$np, $\overline{mn}$p, n$\overline{m}$p.

In deriving the classes of symmetry having several higher-order axes (of order higher than 2), their detailed consideration by spherical triangles is superfluous. This matter is solved by the basic theorem, which states that the combinations of axes can only be such as characterize regular bodies, i. e., the groups T = 23, O = 432 and I = 532. In crystallography the last is excluded according to the "basic law," and thus only the two higher groups of axes remain.

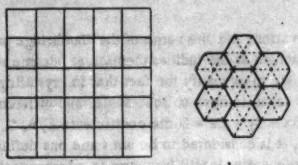

Fig. 2. Regular polyhedra with an infinite number of finite faces: a) the square net, b) the hexagonal net (triangles).

It should be noted that the same theorem applies to all cases of symmetry groups with more than one axis. In addition to the well-known five regular bodies, all the n-sided prisms are such, if they are considered to be infinite and as having two vertices at infinitely remote points. The axial groups will be: 622, 422, 32 – these are the crystallographic cases – and the infinite number of noncrystallographic ones: 822, 1022, . . ., 52, 72, . . ., etc.

A second group of degenerate regular bodies are the n-gonal "two-face" -dihedra, each of which is composed of the two planes of the pinacoid, that meet at infinity in the edges of the infinitely large regular n-gon. If prisms have n faces, n edges and two vertices, then the dihedra have two faces, n edges and n vertices; in both cases Euler's theorem f + v = e + 2 is strictly applicable. The mathematical concept of dihedra always coincides with the n-gonal pinacoid, and it must be conceded that the substitution in the "classification of the Fedorov Institute" (not done by Fedorov, however) of Fedorov's term doma (roof) by (antimathematical) dihedron is not a very fortunate one.

The orthorhombic pinacoid is simultaneously the limiting case of both kinds of regular bodies: of the digonal prism and of the digonal dihedron. In both forms the two pinacoidal faces meet at infinity along the regular (spherical) bi-angle (fuso).

Two more limiting regular polyhedra play a substantial role in crystallography – these are the polyhedron with an infinite number of square faces and the polyhedron with the infinite number of regular triangles. The first one is clearly an infinite plane net with square meshes, the second one is hexagonal, since each six triangles obviously can be combined into a hexagon (Fig. 2).

There are four axes of the 3rd order in the cubic system. If the operation on points by the axis which passes through the octants xyz, $\overline{xyz}$, seems very simple: mnp, pmn, npm, then it seems difficult when it is caused by the remaining three axes. The difficulty disappears if the concept of transformed operations from group theory is used, which is symbolized as follows:

$$B = L^{-1} AL.$$

If we know how to rotate (as has just been shown) around one three-fold axis (A) then, in order to turn around another analogous one (B), it is sufficient to shift the coordinate axis in such a way (L^{-1}) as to get B in the position of axis A; the rotations are performed according to a certain rule and we return again to the former system of coordinates (L). Thus, in order to carry out the rotation of the point mnp around the axis of the octant $\bar{x}yz$, the axes of coordinates are interchanged, $\bar{m}np$ is obtained, and the rotations result in $\bar{m}np$, $p\bar{m}n$, $np\bar{m}$. Returning to the former system of coordinates, mnp, $p\bar{m}n$, $\bar{n}p\bar{m}$ is ultimately obtained.

It is not difficult to show that in order to have the rotation of the second axis in the same direction (left or right) as the rotation around the first axis, then the (half) axis in the xyz octant must be combined with the (half) axis in the octant not with one, but with two negative axes.

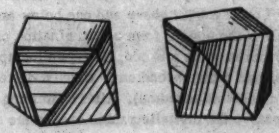

a b

Fig. 3. Twisted cubes: right (a) and left (b).

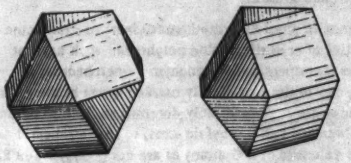

a b

Fig. 4. Coordination figures with 12 vertices: a) archimedes cubo-octahedron, b) hexagonal cubo-octahedron.

The author himself is very unfavorable to the system of notation for crystalline forms which bears the name of the system of the Fedorov Institute and which is contrary to Fedorov's own system, but appears in the "International Tables." Why, for the sake of preserving the purity of the Greek language (!) such a convenient (Fedorov's) term as bipyramid was replaced by dipyramid, which is confused with the di-n-gonal pyramid? Why are the trigontritetrahedron, trigontrioctahedron and trigontetrahexahedron better than (Fedorov's) pyramidal tetrahedron, octahedron and cube? Why must the term hexahedron replace the simple word cube? In principle, it is incorrect to denote the 24-face deltohedron by the tetragontrioctahedron, since the interstitial shape between the cube and the octahedron is often a tetragontetrahexahedron. The characteristic name for the 24-face deltohedron is 1) neutral in the context indicated and 2) suggests at once the characteristic shapes of the faces of this form. The same can be said of the 12-face deltohedron (Fedorov's) called a tetragontritetrahedron by the (Fedorov) Institute. The term gyrohedron conveys much better the peculiarities of the general form of class 432, than the term pentagontrioctahedron; moreover, this same form, depending on the indices, can be better described as a pentagontetrahexahedron.

It has already been mentioned how theoretically unsatisfactory was the substitution of doma by dihedron. In teaching, it is very convenient to use Fedorov's term (in parentheses) for orthorhombic tetrahedron-digonal trapezohedron, and for the orthorhombic bipyramid – digonal bipyramid (also in parentheses).

It is comforting to know that the attempt by the Fedorov Institute to substitute Fedorov's nomenclature of systems and classes by that at one time suggested in Germany, such as gyroidal, tetragyroidal, axial and planar had no success. It is difficult to understand why the Russian word has to be replaced either by gyroid or axis.

The practical mastery of the laws of symmetry by the aid of wooden models must be preserved. As before, faces are of major importance in these models. In accordance with the basic role played in microcrystallography by symmetrically connected points is the concept of point-polyvertex models. One should touch upon them lightly, for their role is very insignificant, inasmuch as in microcrystallography the basic connecting symmetry elements are screw axes and glide planes which contain translational components and therefore finite sets of points are rare exceptions.

As a concession to the new currents in pedagogy, it is necessary to add to the usual models first of all the twisted cubes, i. e., the tetragonal trapezohedra, which, in spite of the rules of classical crystallography, are truncated by pinacoids exactly at the intersection points of equatorial edges with polar ones (Fig. 3). This is, as is

known, the most "economical" form of the coordination polyhedron with eight vertices. The twisting of the upper face of the pinacoid with respect to the lower one must be by 30°, either clockwise or counterclockwise.

The two other models are the twisted (right and left) hexagonal prisms, i. e., hexagonal trapezohedra, truncated by pinacoid planes at the intersection points of the equatorial edges. It must be noted that the ordinary octahedron is the twisted trigonal prism and can be left- or right-handed if it is insufficiently turned to either side.

The cubo-octahedral model (Fig. 4, a) (archimedes) which also violates the rules of classical crystallography, is essential. This is the 12-vertex coordination figure for cubic closest packing. "The hexagonal cubo-octahedron" (Fig. 4, b) is the corresponding figure for hexagonal closest packing; it is obtained from the archimedes one by slitting the latter along the equator, normal to the three-fold axis and thenturning the upper half with respect to the lower by 180°. Its symmetry – rare in classical crystallography – is D_{3h} = 3/mm2 = $\bar{6}$m2.

The author is of the opinion that Fedorov's method of deriving all kinds of forms on geometric bodies by using a 5th order axis is good pedagogy; the different correlations of one pyramid above and one below are: bipyramid, trapezohedron and deltohedron (Fig. 5). It is the latter that is the normal form of combination of two n-gonal pyramids and a center of symmetry when n is odd; in crystallographic bodies, however, the deltohedron degenerates into a rhombohedron (= trigonal deltohedron) and into a tetragonal tetrahedron (= digonal deltohedron). After examining the forms of the pentagonal system, we pass to the crystallographic one, where some forms will be omitted on account of "the basic law," but a part will be degenerate: the rhombohedron and the tetragonal tetrahedron indicated, then the forms of the "digonal" system: didigonal bipyramid (orthorhombic bipyramid), digonal trapezohedron (orthorhombic tetrahedron), and so forth.

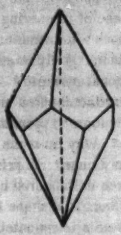

Fig. 5. Dipentagonal deltohedron.

It will probably be of interest to physicists (mathematicians) to stress some remarkable geometric peculiarities of crystallographic polyhedra; such as, that the rhombododecahedron, besides its mineralogical synonym garnetohedron, is sometimes called a zonohedron, due to the four clearly marked zones of the 4 three-fold axes. From this the rhombic angle is immediately determined in this characteristic polyhedron as the angle between two three-fold axes, or the tetrahedral angle (for example, between the valences of a C atom) as arc cos $(-\frac{1}{3})$ = 109°21'16".

The second polyhedron with all faces rhombic is a 30-hedron with six five-fold axes (not crystallographic, but sufficiently closely true of some pyrite crystals); it is also a zonohedron and the angle of its rhomb is equal to the angle between the five-fold axes of the icosahedron.

Unfortunately, several widely used notations for the symmetry classes, such as L_4, P, C; L_4, $4L_2$, 5P, C are untenable. They are too rich, inasmuch as they give more than the essential minimum of information; thus, in the first case C is a consequence of the other two; in the second case, the second and fourth groups are a consequence of the first and the third. On the other hand, such an important element of symmetry as the 4th order mirror axis does not appear. Doubtless the best notations are the "international" ones, which are really the fruit of international cooperation and are based on the crystallographically most important concept of "special directions." The international symbols derived for the 230 space (Fedorov's) symmetry groups [2] are particularly good. It is apparently necessary to give up correct, but ultraschematic notations, such as $\bar{6}/4$ or m·2:m. For the purpose of the most rational derivation of the space groups, for which various aspects are possible, it is convenient to give the classes and groups in two notations: that of Schoenfliess, which is independent of the aspect, and the international one which separates out the required aspect [2].

From the point of view of group theory the notations for mirror axes using indices above the line are undesirable. L_4^2 is a rotation of the second kind about the four-fold axis ($L_4^2 = 2$), but not at all a mirror axis of the fourth order, and $L_4^2 = C$ likewise.

Students absorb the concept of group theory well if they are trained to give, for each crystallographic class, the number of symmetry elements, equal to the order of the corresponding group, and then to write out Cayley's squares for some of them. Thus, for example, for the first of the classes indicated (the class of the tetragonal

bipyramid)* the complete collection of symmetry elements (operations) consists of 8 members: 1, 4, $4^2 = 2$, $4^3 = 4^{-1}$, $\dot{4}$, $\dot{4}^3 = \dot{4}^{-1}$; $\underline{m}$ and $\underline{i}$. The corresponding Cayley's square has 8 x 8 elements:

1	4	2	4^{-1}	$\dot{4}$	$\dot{4}^{-1}$	m	i
4	2	4^{-1}	1	i	m	$\dot{4}$	$\dot{4}^{-1}$
2	4^{-1}	i	4	$\dot{4}^{-1}$	$\dot{4}$	i	m
4^{-1}	1	4	2	m	i	$\dot{4}^{-1}$	$\dot{4}$
$\dot{4}$	i	$\dot{4}^{-1}$	m	2	1	4	4^{-1}
$\dot{4}^{-1}$	m	$\dot{4}$	i	1	2	4^{-1}	4
m	$\dot{4}$	i	$\dot{4}^{-1}$	4	4^{-1}	1	2
i	$\dot{4}^{-1}$	m	$\dot{4}$	4^{-1}	4	2	1

For the matrix to have nothing but 1's along its diagonal, the mutually inverse elements must be arranged symmetrically across the diagonal, for example, for the $C_{3h} = \dot{6}/m$ group:

1	$\dot{6}$	$\dot{6}^{-1}$	$\bar{6}$	$\bar{6}^{-1}$	$\bar{6}$	$\bar{6}^{-1}$	3	3^{-1}	2	m	i
$\dot{6}^{-1}$	1	3^{-1}	m	$\bar{6}$	i	$\bar{6}$	6	2	3	$\bar{6}^{-1}$	$\dot{6}^{-1}$
6	3	1	$\bar{6}^{-1}$	m	$\dot{6}^{-1}$	i	2	$\dot{6}^{-1}$	3^{-1}	$\bar{6}$	$\bar{6}$
$\bar{6}^{-1}$	m	$\bar{6}$	1	3^{-1}	2	6	$\bar{6}$	i	$\bar{6}^{-1}$	$\dot{6}^{-1}$	3
$\bar{6}$	$\bar{6}^{-1}$	m	3	1	$\dot{6}^{-1}$	2	i	$\bar{6}^{-1}$	$\bar{6}$	6	3^{-1}
$\dot{6}^{-1}$	i	$\bar{6}$	2	6	1	3	$\bar{6}$	m	$\bar{6}^{-1}$	3	$\dot{6}^{-1}$
$\bar{6}$	$\bar{6}^{-1}$	i	$\dot{6}^{-1}$	2	3	1	m	$\dot{6}^{-1}$	$\bar{6}$	3^{-1}	6
3^{-1}	$\dot{6}^{-1}$	2	$\bar{6}^{-1}$	i	$\dot{6}^{-1}$	m	1	3	6	$\bar{6}$	6°
3	2	6	i	6°	m	$\bar{6}$	3^{-1}	1	$\dot{6}^{-1}$	$\dot{6}^{-1}$	$\bar{6}^{-1}$
2	3^{-1}	3	$\bar{6}$	$\bar{6}^{-1}$	$\bar{6}$	$\bar{6}^{-1}$	$\dot{6}^{-1}$	6	1	i	m
m	$\bar{6}$	$\bar{6}^{-1}$	6	$\dot{6}^{-1}$	3^{-1}	3	$\bar{6}^{-1}$	$\bar{6}$	i	1	2
i	$\bar{6}$	$\bar{6}^{-1}$	3^{-1}	3	6	$\dot{6}^{-1}$	$\bar{6}$	$\bar{6}^{-1}$	m	2	1

The operations of right- and left-handed rotation about a mirror axis of the fourth order are denoted by $\dot{4}$, $\dot{4}^{-1}$, in contradistinction to $\bar{4}$ and $\bar{4}^{-1}$, which are used as symbols in the "international" system to denote the inversion axes. In the case of fourth-order axes there is no great difference between these two kinds ($\bar{4} = \dot{4}^{-1}$, $\bar{4}^{-1} = \dot{4}$), but the corresponding hexads ($\bar{6}$, $\dot{\bar{6}}$, $\bar{\bar{6}}$) differ considerably among themselves.

Although our crystallographers had resigned themselves to the notation system of the Fedorov Institute (but not proceeding from Fedorov) they were divided in their opinion concerning the introduction of inversion axes: some accepted them, and others (Shubnikov, Flint, and the author of this article) prefer mirror axes as more graphic. It is difficult, in ordinary thinking, to characterize a trigonal prism with its six vertices as characterized by the hexad inversion axis $-\bar{6}$. A physics student must know that all three kinds of hexad axes are equivalent, primarily from the point of view of abstract group theory. The introduction of the odd inversion axes $\dot{\bar{6}} = \bar{3}^{-1}$ ($\bar{\bar{6}} = \dot{\bar{3}}^{-1}$) is necessary only for the comprehension of the international tables. Both the axes $\dot{\bar{3}}$ and $\bar{3}$ are elements of 6th order symmetry, but their third powers are not equal to 1. $\dot{6}^3 = 2$, $\dot{\bar{6}}^3 = 1$, $\bar{\bar{6}}^3 = m$.

From the abstract point of view, the similarity of many classes must be indicated: the 32 classes are distributed among 18 abstract groups. Thus, classes $C_6 = 6$, $C_{3i} = \dot{\bar{6}}\,(\bar{3})$, $C_{3h} = \bar{\bar{6}}\,(3/m)$, merge into one abstract group; also classes $D_4 = 422$, $C_{4v} = 4\,mm$, $D_{2d} = \bar{4}\,2m$. The richest group contains four classes: $D_6 = 622$, $C_{6v} = 6\,mm$, $D_{3d} = \dot{\bar{6}}\,2/m\ (\bar{3}\,m)$, $D_{3h} = \bar{\bar{6}}\,m2$.

One must be completely exact in dividing the 32 classes into systems. The assembling of isolated classes into systems is carried out not according to the rather tenuous trace of similarity between some elements of symmetry (cf. 1), but rather according to the principle of similarity of corresponding coordinate systems. The latter

* Such nomenclature is superfluous. However, one must recommend calling the highest symmetry class of each system "holohedral."

are determined by the presence of specialized directions. Into one system enter all the classes with similar specialized directions, and corresponding to the existing 6 and only 6 crystal settings there are six and only six crystallographic systems. There is no trigonal and especially no rhombohedral system, inasmuch as there are no special rhombohedral directions. To a mineralogist the rhombohedral system must bring to mind the pseudocubism of crystals, and is therefore most appropriate for describing calcite with its pseudocubic cleavage rohombohedron. X-ray structure analysis showed that it is this particular pseudocube, and the choice of coordinate axes parallel to its edges, that leads to an improbably large cell containing 32 particles of $CaCO_3$, whereas a "correctly" chosen rhombohedron contains only $2CaCO_3$. Unfortunately there is no prescription for the correct choice of the required rhombohedron, and calcite belongs to the hexagonal system when its specialized directions are traced.

In the transition to infinite space, the same six possible crystallographic settings, based exclusively on specialized directions, create six and only six different shapes for the elementary parallelepiped of the crystal lattice. This lattice should be considered as the collection of nodal points without the connecting rods, which we then take parallel to the specialized directions, and in this way break up the lattice into cells. As has been thoroughly explained in this author's book [3] such a joining by rods does not always cover all the lattice nodes. Nodes not covered can remain either in the centers of right parallelepipeds, or right-angeled faces, or finally at two points of the hexagonal parallelepiped one on each of the three-fold axes. The selection of possible cases leads to 14 elementary parallelepipeds, either primitive (empty) or centered in various ways. The corresponding lattices are usually known as Bravais' 14 lattices.

The introduction into microcrystallography [3] of a "basic symmetry element"* – the lattice, makes it possible to prove the theorem that the axes of 5, 7, 8 and higher order cannot be found in crystals. In addition the case of the five-fold axis cannot be considered separately, but it must be shown that in systems with axes of odd order n all plane lattices, perpendicular to such axes, are themselves characterized by axes of order 2n, and since lattices with axes of order higher than 6 are not possible, then the highest axis of odd order is 3.

If the crystal has one specialized direction (monoclinic classes) or has no such directions at all (triclinic) then it is possible to pass the connecting rods through the lattice, which is considered as an infinite assemblage of nodes, in many ways, in particular in those that lead to primitive (empty) cells. It is easy to see that all primitive cells will have the same volume. New coordinates (indices) of all planes and points correspond to changes of coordinate axes, and, due to the obliqueness of the coordination systems, the difference, not very apparent in analytical geometry, between the covariance of the indices (coordinates) of the planes and the contravariance of the indices (coordinates) of the points becomes apparent. These indices condition the difference between the transition formulas for the first and the second cases.

Formerly, there was no difficulty in this matter in crystallography that considered mainly planes (faces), since the indices of the faces vary covariantly, i. e., if the transition formulas of the vectors that determine new axes (A, B, C) from the old ones (a, b, c) are

$$\begin{aligned} \mathrm{A} &= m_1\mathrm{a} + n_1\mathrm{b} + p_1\mathrm{c}, \\ \mathrm{B} &= m_2\mathrm{a} + n_2\mathrm{b} + p_2\mathrm{c}, \\ \mathrm{C} &= m_3\mathrm{a} + n_3\mathrm{b} + p_3\mathrm{c}, \end{aligned}$$

then the transition formulas for the indices of faces are

$$\begin{aligned} H &= m_1h + n_1k + p_1l, \\ K &= m_2h + n_2k + p_2l, \\ L &= m_3h + n_3k + p_3l, \end{aligned}$$

but the coordinates of points, which are the most interesting for modern (micro) crystallography, vary according to the contravariant law, and the coefficients of the corresponding transition are taken from the matrix of the inverse transition: from the new axes to the old ones

$$\begin{aligned} \mathrm{a} &= q_1\mathrm{A} + r_1\mathrm{B} + s_1\mathrm{C}, \\ \mathrm{b} &= q_2\mathrm{A} + r_2\mathrm{B} + s_2\mathrm{C}, \\ \mathrm{c} &= q_3\mathrm{A} + r_3\mathrm{B} + s_3\mathrm{C}, \end{aligned}$$

* Which distinguishes crystals without the usual symmetry elements from amorphous bodies.

but, however, not along the rows but in columns, i. e.,

$$X = q_1x + q_2y + q_3z.$$
$$Y = r_1x + r_2y + r_3z.$$
$$Z = s_1x + s_2y + s_3z.$$

LITERATURE CITED

[1] V. V. Dolivo-Dobrovol'skii, A Course in Crystallography [in Russian] (1937).

[2] N. V. Belov, "The class method for deriving the space groups of symmetry," Trudy Inst. Krist. 6, 25-62 (1951).

[3] N. V. Belov, Structural Crystallography [in Russian] (1951).

Received April 18, 1957

Institute of Crystallography, Academy of Sciences, USSR

BRIEF COMMUNICATIONS

ON THE STRUCTURE OF THE OXIDE Au_3O_2

N. A. Shishakov

Recently [1] it was reported that on heating pure gold in an atmosphere of oxygen at 500°C a thin film of oxide presumably of the formula AuO_2, where three monovalent O_2^- ions are attached to each trivalent gold ion, appears on the surface of the metal. However, under roughly the same conditions, another structure is found which is interesting in that the crystals appear to be oriented with one of their axes normal to the surface of the metal (Fig. 1). Direct measurement on the texture diagram gives the period along the indicated axis as 3.375 or 6.75 A. Careful measurement of all the radius vectors of the arcs, and of their azimuths, made it possible to index all the arcs, which led to the conclusion that the lattice was hexagonal with the following constants: a = 5.28 A and c = 6.75 A. It is very significant that Trillat and Oketani [2] had found this same constant a = 5.28 A also in a hexagonal structure which appeared on gold leaf on heating it to the same 500°C. It is true that these authors did not succeed in determining the second constant, but judging by the similar orientation of the hexagonal crystals in question, with the c axis normal to the metal surface, it may be concluded that in both cases the structures were one and the same.

Additional material for determining this structure is provided by the atomic radial distribution curve for our previous 500° structure, shown here in Fig. 2 as an unbroken curve. For purposes of comparison of the line profile at the first maximum r = 1.4 A. A second broken curve is given for d = 1.007 A, instead of the former 0.570 A. The good agreement of the two curves shows that this first maximum is real. Therefore, our previous conclusions on the existence of the molecular oxygen ion in the given structure are justified. Among the other special features of the radial distribution curves, the existence of maxima at 2.5, 3.7, 4.8 and 5.7 A should be noted. All of these, of course, have their origin in gold-gold separations, in addition to which the first of them is very close to half of the observed lattice constant a = 5.28 A.

From this we draw certain conclusions regarding the structure of the hexagonal (001) nets of gold (see Fig. 3 left). It follows from the second constant found, c = 6.75 A, that it will only be possible to pack two such hexagonal layers into the height of the cell (see Fig. 3 right).

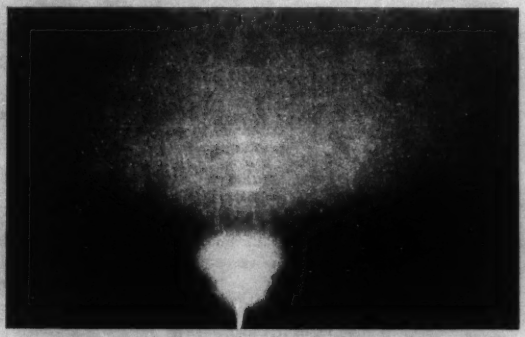

Fig. 1.

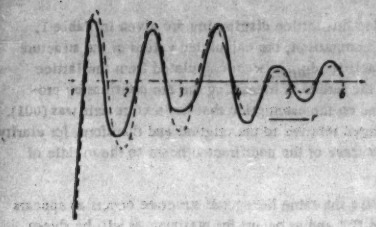

Fig. 2.

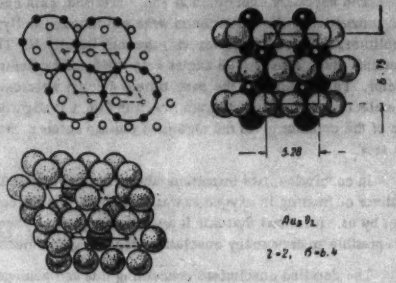

Fig. 3.

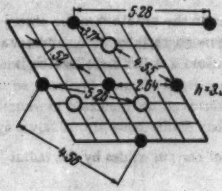

Fig. 4.

It is clear that with the diameter of the gold atoms (2.64 A) empty spaces must exist in the structure; the size of these, as is shown, is quite sufficient for the insertion in each of them of one molecular oxygen ion. Hence, it would also be possible to ascribe to this structure the chemical formula Au_2O_2 and the density $\sigma = 6.4$.

To explain the stability of such a structure it should be borne in mind that there is a partly ionic bond between the gold and the oxygen, resulting in the gold layers carrying a positive charge by virtue of which they repel each other.

In order to understand the presence of the other maxima on the radial distribution curve, it is necessary to refer to Fig. 4, which represents a projection of the structure on (001), and which contains information about the interatomic distances in the structure. The 3.7 A maximum appears to be a simple Au–Au maximum. The remaining maxima are probably composite.

TABLE 1

The 15 Observed Lattice Spacings for Au_2O_2 and the Corresponding Theoretical Data. $L\lambda = 13.5$

Experimental data from the electron diffraction diagram				Theoretical data					
I	s	r	d	hkl	d	structure amplitude A	structure amplitude B/√3	s	H
Weak	55°	3.6	3.73	101	3.79	−0.5	+0.5	56°	24
Strong	0°	4.0	3.38	002	3.375	+6.0	0	0°	2
»	40°	5.0	2.70	102	2.716	−1.5	−0.5	36°	24
Strong, broad	30°	6.5	2.08	112	2.079	−2.0	0	28°	12
Very strong	0°	8.0	1.69	103	2.020	−0.5	+0.5	27°	24
Medium	25°	8.6	1.57	004	1.687	+6.0	0	0°	2
»	40°	9.5	1.42	104	1.583	−1.5	−0.5	20°	24
Weak	15°	10.3	1.31	114	1.422	−2.0	0	20° & 32°	12
Medium	0°	12.0	1.125	105	1.295	−0.5	+0.5	16°	24
»	15°	12.3	1.098	006	1.125	+6.0	0	0°	2
Weak, broad	25°	13.2	1.023	106	1.092	+1.5	+0.5	14°	24
Very weak	unclear	14.1	0.957	116	1.035	−2.0	0	23°	12
Weak	0°	16.0	0.843	224	1.039	+6.0	0	28° & 49°	12
				107	0.951	−0.5	+0.5	52° & 65°	24
				008	0.843	+6	0	0°	2

Note. The remaining spacings in the range up to d = 0.843 A were not observed for the following reasons: 1) the spacings hhl with $l = 2n + 1$ and hkl with $h - k = 3n$ and $l = 2$ are systematically absent; 2) the reflections with small l in comparison with h and k have too large an angle δ and fall into the sphere of the shadow on the electron diffraction diagram; 3) the remaining spacings, as calculation shows, have too weak an intensity.

The necessary experimental and theoretical data concerning this lattice distribution are given in Table 1. The intensities in the first column were estimated visually. For comparison, the calculated values of the structure amplitudes are given, together with the multiplicity N. The quantities $d_{theor.}$ were calculated from the lattice constants given above. The angles δ in the second column are the results of measuring the arc positions by protractor. The angles δ in the penultimate column were calculated on the assumption that the texture axis was (001). The electron diffraction diagram shown in Fig. 1 is slightly enlarged relative to the original and therefore, for clarity, one of the columns gives the measured radius vectors $\underline{r}$ from the trace of the undiffracted beam to the middle of the arcs.

In conclusion, two important comparisons can be made. First the same hexagonal structure occurs as appears in silver on heating in oxygen as was seen in the work mentioned [2], and as occurs for platinum as will be shown later by us. It follows that this is a somewhat general phenomenon. Secondly, on examination of this structure, it is possible to draw many conclusions regarding the mechanism of the interaction of oxygen with the noble metals.

The detailed conclusions concerning this and analogous studies will be given in the article "On the absorption of oxygen by metals" in the Journal of Physical Chemistry (USSR), and in the monograph by V. V. Andreeva and N. A. Shishakov, "Optical and Electron Diffraction Studies of Oxide Films on Gold and Platinum," which is being prepared for publication.

LITERATURE CITED

[1] N. A. Shishakov, "An investigation of the atomic-molecular structure of certain oxides by the radial distribution method," J. Phys. Chem. (USSR) 31, 33-41 (1957).

[2] J. J. Trillat and S. Oketani, J. Phys. Radium 8, 59, 93 (1957).

Received April 24, 1957

Institute of Physical Chemistry Research, Academy of Sciences, USSR

ON THE STRUCTURE OF THE OXIDE PtO_2

N. A. Shishakov

Although the significance of the structure of the oxide PtO_2 is of great interest from the catalytic, electrochemical and other points of view, this structure remains unknown up to the present. Some information about it can be obtained from the early work of Finch, Murison, Stuart and Thomson [1] on the catalytic properties and structure of platinum films, obtained by cathode ray scattering. In this connection, the list of interplanar spacings given in this work, which undoubtedly belong to the oxide referred to, is of great value. It is shown that all the observed reflections can be indexed uniquely, as is done in Table 1.

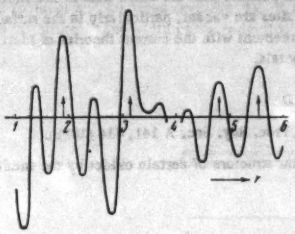

Fig. 1.

TABLE 1

The Results of the Interpretation of the English Authors' Electron Diffraction Diagram from Catalytically Active PtO_2

Intensities of reflections	Interplanar spacing	Indices of hexagonal lattice	Lattice constants
Strong	2.69	100	3.11
»	1.56	110	3.12
Weak	1.35	200	3.12
»	1.01	210	3.09
»	0.90	300	3.12
»	0.775	220	3.10
»	0.74	310	3.09
»	0.67	400	3.10
»	0.61	320	3.07
»	0.58	410	3.07
		Average	3.10A

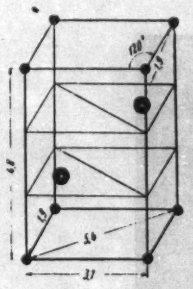

Fig. 2.

These data on the structure of PtO_2 can be supplemented by applying the radial distribution method to the interpretation of the electron diffraction diagram, as was mentioned in the previous work [2]. The data in Table 2, derived from the previous table, were used in calculating the interatomic distances.

The form found for the radial distribution function is shown in Fig. 1. It may be taken as certain that the four strongest maxima in the curve are real maxima, i. e., that there are in the structure interatomic distances 1.9, 3.1, 4.8 and 5.6. The correspondence of the strongest maximum with the hexagonal lattice constant found above supports the correctness of the indexing.

The second real maximum with r = 1.9 A may be attributed to the Pt—O separation, since this distance is roughly equal to the sum of the ionic radii of oxygen and quadrivalent platinum. The number of oxygen ions surrounding each platinum ion may also be deduced from this. In fact, if the coordination polyhedron edge be 3.1 A,

then the radii of the empty spaces between the anions must be 0.34 A for tetrahedral coordination, and 0.64 A for octahedral coordination. The first case is obviously not possible. However, from this we may also form a conclusion as to the reason for the lattice constant having this value, namely, 3.1 A.

In this way the arrangement in the structure is close-packed. This means, however, that the axial ratio c/a must be close to 1.63, i.e., that besides the two spacings indicated there must also exist in the lattice a spacing roughly 1.6 times larger, i.e., r = 5.0 A. Therefore, the spacing of 4.8 A, which occurs in the radial distribution curve, could be assigned to the c translation of the hexagonal lattice, whence c/a would equal 1.55 (Fig. 2). The last spacing, 5.6 A, may be assigned to the longer diagonal of the rhombus which must theoretically be 5.4 A.

TABLE 2

Intensity	Sin/λ	Intensity	Sin/λ
2	0.186	1	0.665
2	0.321	1	0.674
1	0.370	1	0.745
1	0.495	1	0.820
1	0.555	1	0.865

It is not possible to calculate in addition, in detail the best agreement between the distances in the assumed cell and the positions of the maxima on the radial distribution curve, since in the construction of the curve only the hk0 reflections were used, the remaining reflections being unobserved.

The reason for the absence of 00*l* and hk*l* reflections is probably the absence of periodicity along the c direction, which indicates the defect nature of the lattice. It is quite possible that the anion sites in the structure are completely filled, while, on the other hand, many of the cation sites are vacant, particularly in the surface layers of the oxide film. Such a representation would be in good agreement with the current theories of Mott and Wagner concerning the mechanism of formation of oxide films on metals.

LITERATURE CITED

[1] G. J. Finch, C. A. Murison, N. Stuart, and G. P. Thomson, Proc. Roy. Soc. A 141, 414 (1933).

[2] N. A. Shishakov, "An investigation of the atomic-molecular structure of certain oxides by the method of radial distribution," J. Phys. Chem. (USSR) 31, 33-41 (1957).

Received April 24, 1957

Institute of Physical Chemistry Research, Academy of Sciences, USSR

A SIMPLE METHOD FOR THE DETERMINATION OF CRYSTAL LATTICE CONSTANTS BY ELECTRON DIFFRACTION PATTERNS FROM THE SURFACE OF AN OBJECT

N. A. Shishakov

The existing opinion that it is impossible to measure with great accuracy electron diffraction patterns made by reflections from the surface of a flat object appears unjust. This can be ascertained by examining the path of the incident and scattered rays (Fig. 1). It is clear that reflection occurs from all points of the straight line which the ray strikes. The width of the reflection represents a projection of a part of this line on the photographic plate.

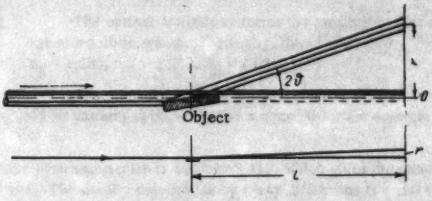

Fig. 1.

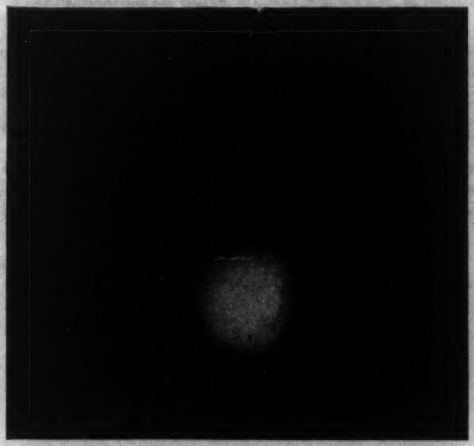

Fig. 2.

Therefore, a measurement of the position of the center of the reflection is exactly proportional to the distance L from the center of the object. To find the center of the picture, and also the wavelength of the electrons, on the exposed photographic plate, a second exposure is made from a standard substance deposited on a celluloid film on a wire loop, which is located next to the flat slide just near its center. To move aside the slide, place the film in the path of the incident beam, and perform the same operation with the standard object takes 1-2 sec. An example of such a combined electron diffraction is given in Fig. 2. Nickel oxide was on the surface of the object. A film of sodium chloride was used as a standard. The accuracy of the measurements in this case was just as good as for work using x-rays.

Received April 4, 1957

Institute of Physical Chemistry, Academy of Science, USSR

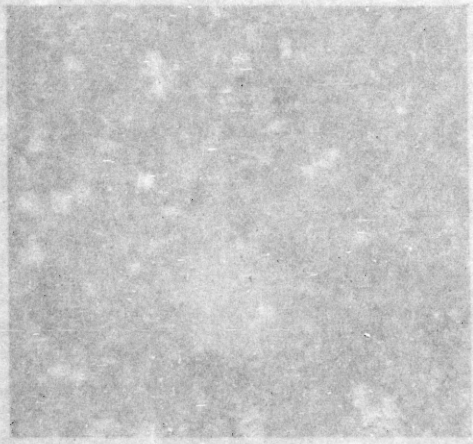

X-RAY STRUCTURAL ANALYSIS OF CRYSTALS OF $[Ru(NH_3)_4(NO)(OH)]Cl_2$

G. B. Bokii and N. A. Parpiev

The salt of the composition $[Ru(NH_3)_4(NO)(OH)]Cl_2$ was first synthesized by Klaus [1]. It appears as golden yellow crystals of the type shown in Fig. 1.

According to Dufet's data [2], these crystals belong to the prismatic symmetry class of the monoclinic system; however, our researches show that they belong to its dihedral axial symmetry class.

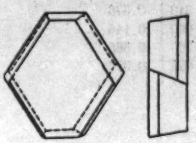

Fig. 1.

On the basis of the results of goniometric measurement the ratios $a:b:c = 1.535:1:0.722$, $\beta = 101°15'$, were obtained. Within the limits of experimental accuracy, the x-ray axial ratios coincide with the goniometric ones, if the parameter along the c axis is doubled.

The optical analysis confirms the assumption that these crystals belong to the monoclinic system. Optically, they are biaxial. The indices of refraction are $n_g = 1.830$, $n_m = 1.708$, $n_p = 1.661$.

The dimensions of the elementary cell were determined by x-ray oscillation patterns and were then refined by patterns obtained in the reciprocal lattice camera: $a = 11.48 \pm 0.02$ A, $b = 7.44 \pm 0.05$ A, $c = 10.75 \pm 0.02$ A.

The density as determined pycnometrically is equal to 2.112, which gives the number of formula units in the elementary cell $n = 3.97 \approx 4$. The density determined by x-ray diffraction is equal to 2.126.

The space group was determined as a result of indexing the x-ray diffraction patterns. The indices of the reflections that are present satisfy the following conditions: hkl only with $h + k = 2n$, $0k0$ only with $k = 2n$, $h0l$ only with $h = 2n$, which is characteristic of the space group $C_2^3 = C2$ [3].

The structural analysis was made from x-ray photos taken with the KFOR, with Mo K_α-radiation, and with the RGNS, with Cu K_α-radiation. The intensities were evaluated visually using a comparison scale. Only the polarization and kinematic factors were taken into account.

To determine the heavy-atom coordinates and to elucidate the general character of the structure, three projections of the interatomic vector function were constructed on the x0z, 0yz, and xy0 planes. For greater precision, in determining the coordinates of the ruthenium and chloride atoms, and to obtain those of the light atoms, projections of electron density were constructed on the x0y and 0yz planes. Since there was no center of symmetry in the structure, further refinement, especially in determining the coordinates of the "light" atoms, was not carried out.

The reliability coefficient, which was calculated according to the formula

$$R = \frac{\sum_{hkl} ||F_{exp}| - |F_{calc}||}{\sum_{hkl} |F_{exp}|},$$

turned out to be equal to 0.224 for the h0l reflections and to 0.207 for the 0kl. All the atoms without exception occupy four-fold general positions.

Analyses show that there exist $[Ru(NH_3)_4(NO)(OH)]^{++}$ complex ions in the crystal lattice, in which the ruthenium atom occupies the center of an octahedron, the vertices of which are occupied by the four NH_3 groups located in a square, and by (OH) and (NO) groups in the trans-position.

Ru, N and O atoms do not lie on a straight line, but form an angle Ru – N – O ≈ 150°. The Cl^- ions have the coordination number 12, with eight neighbors (NH_3) closer than the remaining four (NO and OH).

It is interesting that the two chloride ions have different environments: one ion is surrounded by eight NH_3 groups, by three NO groups and by one OH group; the other ion by eight NH_3 groups, by three (OH) groups and by one NO group. The atomic coordinates are given in the table.

Atoms	Coordinates (axial lengths)			Atoms	Coordinates (axial lengths)		
	x	y	z		x	y	z
Ru	0.250	0 000	0.250	$(NH_3)_{III}$	0.349	0.210	0 376
Cl_I	0.116	0.500	0 365	$(NH_3)_{IV}$	0.349	– 0.210	0.376
Cl_{II}	0.375	0.500	0.146	(OH)	0 375	0.000	0.146
$(NH_3)_I$	0.149	0.210	0.126	N (in NO)	0.125	0.000	0.365
$(NH_3)_{II}$	0 149	– 0 210	0.126	O (in NO)	0.058	– 0.093	0.397

Distances between atoms inside the complex:

$Ru - N(in\ NH_3) = 2.23\ A$
$Ru - N(in\ NO) = 2.07\ A$
$Ru - O(in\ OH) = 1.98\ A$
$(NH_3) - (NH_3) = 3.15\ A$
$(NH_3) - N(in\ NO) = 3.06\ A$
$(NH_3) - O(in\ OH) = 3.07\ A$
$N - O(in\ NO) = 1.14\ A$

Distances between atoms of neighboring complexes:

$(NH_3)_{III} - (NH_3)_{II} = 4.80\ A$
$(NH_3)_{III} - (NH_3)_{IV} = 3.88\ A$
$(NH_3) - O(in\ OH) = 3.85\ A$
$(NH_3) - O(in\ NO) = 2.78\ A$*
$O(in\ NO) - O(in\ NO) = 2,80\ A$

Distances between chloride ions and addends of complex ions:

$Cl^- - (NH_3) = 3.43\ A$
$Cl^- - N(in\ NO) = 3.72\ A$
$Cl^- - O(in\ OH) = 3.72\ A$
$Cl^- - O(in\ NO) = 3.20\ A$

The shortest distance between Cl^- ions of the outer shell is $Cl^- - Cl^- = 4,13$ A.

The authors consider it their pleasant duty to express their deep gratitude to M. A. Porai-Koshits for his constant advice concerning this work.

LITERATURE CITED

[1] K. Klaus, "Neue Beiträge zur Chemie der Platinmetalle," Bl. Acad. Petersb. 1, 97-122 (1860); 4, 453-455 (1862).

* Here, the shortening of the intermolecular distance relative to the normal intermolecular distance between N and O atoms (which is 3,1 A) apparently is explained by the formation of a hydrogen bond between the oxygen atom of the NO group and the nitrogen atom of the NH_3 group.

[2] H. Dufet, "Chlorure de reutendiammonium nitrate," Bl. Soc. Min. 12, 469 (1889).

[3] Internationale Tabellen zur Bestimmung von Kristallstrukturen (Berlin, 1935).

Received December 4, 1958

M. V. Lomonosov Moscow State University

ON THE STATE OF CARBON IN ANNEALED SILICON STEEL

E. L. Gal'perin and Iu. S. Terminasov

The experimental data obtained in recent years from x-ray, electron microscopic and magnetic analyses confirm the formation of interstitial carbide phases, different from cementite, during the tempering of chilled carbon steel. In analyzing the results of these studies, as well as his own experimental data, B. A. Apaev [1] came to the conclusion that the composition of the carbide phases of steels with different carbon content can differ sharply under the same tempering conditions, i. e., there is no universal scheme of carbide formation during the tempering of chilled carbon steels. The presence of an interstitial carbide phase, to which the authors ascribed the formula Fe_2C, was detected during the tempering of steel alloyed with Cr, Mo and V [2].

The present work gives the basic results of the x-ray analysis of the carbide phase in tempered silicon steel $55C_2$ (0.55% C, 1.84% Si).

The material for the analysis was the carbide precipitate isolated electrolytically [3] from samples subjected to chilling and to subsequent tempering for one hour at 300-700°C.

Rods 0.55 mm in diameter were prepared from carbide powder to be photographed by the RKD camera using iron radiation (Mn filter).

Figure 1 shows the patterns of carbide precipitates after tempering at 400 and 600°C.*

hkl	Tempering at 400°, 1 hour		Data of [5] for tempering at 120°C (5 days)	
	d A	intensity	d A	intensity
100	2.35	average	2.33	average
002	2.18	average	2.12	very weak
101	2.07	strong	—	—
102	1.59	weak	1.60	strong
110	1.37	weak	1.36	weak
103	1.24	weak	1.23	very weak

As is obvious from Fig. 1, a, the lines on the diffraction pattern of the carbide precipitate isolated from the sample tempered at 400°C do not correspond to those of cementite [4]. The results of the analysis of these lines are given in the table, where those taken from the work [5] on steel with 1.3% of carbon tempered at 120°C for five days are also given for comparison.

It is obvious from the table that there is relatively good agreement between the interplanar distances, which points to the similarity of the structures of the carbide phases of the steels mentioned at the given temperatures. Indexing of the lines showed that on the pattern of Fig. 1, a, they correspond to the carbide phase with a hexagonal lattice with a = 2.72 A and C = 4.35 A.

The structure of the carbide phase when tempered at 300°C is apparently the same as at 400°C. The absence of the last three lines and a decreased intensity of the first ones are conditioned by a greater dispersion of the carbide particles, and also perhaps by the fact that a part of the carbon still remains in solid solution after being tempered at 300°C.

After tempering at 500°C, the lines of the diffraction pattern of the carbide precipitate correspond basically to the cementite lattice. Because of considerable blurring of lines, the θ's corresponding to large angles do not appear, neither does the line (023) appear which is rather intense on patterns of the carbide precipitate from samples subjected to tempering at t = 600°C (Fig. 1, b) and higher.

* Satisfactory reproductions of these patterns were not obtained because of the great blurring of lines on the patterns of these carbide precipitates.

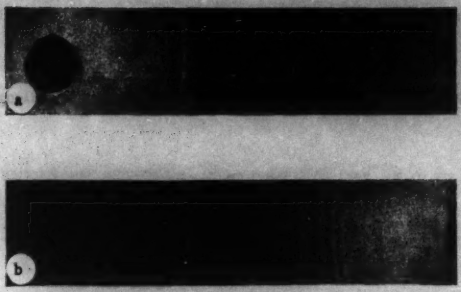

Fig. 1. X-ray diffraction patterns of carbide precipitates in $55C_2$ silicon steel: a) after tempering at 400°C; b) at 600°C.

This is explained by the small dimensions of the carbide blocks [4, 5] in the direction of the c axis, i. e., the blocks can be represented as thin sheets, the planes of which coincide with (001) planes of the cementite lattice. The lines of the metastable carbide are not observed, after tempering at 500°C.

The fact that the cementite lines are not observed after tempering at 400°C, shows that complete transformation of the metastable carbide into cementite takes place between 400-500°C. In ordinary carbon steels this transformation is always observed at lower tempering temperatures [6, 7]. The displacement of this process toward higher temperatures for $55C_2$ steel is probably connected with the presence of various additives, particularly of Si, which, as is known, retards the coagulation of carbide particles [8].

After tempering at 600°C the blurring of the cementite diffraction lines disappears; on further increase of the tempering temperature, the diffraction pattern remains unchanged.

Thus, from the data obtained, it was possible to establish (in the low-tempered $55C_2$ steel) the presence of interstitial metastable carbide with a hexagonal lattice having a = 2.72 A and c = 4.35 A, and which transforms into lamellar cementite at 400-500°C. At temperatures higher than 500°C an intense coagulation of the particles of the carbide phase occurs and a transformation of the lamellar cementite into three-dimensional crystals.

LITERATURE CITED

[1] B. A. Apaev, "The process of carbide formation during the tempering of carbon steel," Metalloved. i Obrabotka Metal. 1, 2 (1957).

[2] W. Craft and J. L. Lamont, "Secondary hardening of tempered martensite alloy steel," Trans. Am. Inst. Mining Met. Eng. 180, 471 (1949).

[3] V. M. Golubkov and V. K. Kritskaia, "X-ray diffraction analysis of the carbide phase of patented steel wire," Coll.: Problems of Metallography and the Physics of Metals 4 [in Russian] (1955), p. 461.

[4] M. P. Arbusov, "X-ray diffraction analysis of the carbide phase in steels," Coll.: Problems of Metallography and the Physics of Metals 3 [in Russian] (Akad. Nauk Ukr. SSR, 1952), p. 3.

[5] K. H. Jack, "Structural transformation in the temper of high-carbon martensite steel," J. Iron Steel Inst. 169, 26 (1951).

[6] M. P. Arbuzov and G. V. Kurdiumov, "The condition of carbon in tempered steel," J. Tech. Phys. (USSR) 10, 13, 1093 (1940).

[7] B. A. Apaev, "The phase composition of structures due to tempering, and the nature of the changes in magnetic properties in the zone of the third transformation," Coll.: Problems of Metallography and the Physics of Metals 1, 3 [in Russian] (Akad. Nauk Ukr. SSR, 1955), p. 467.

[8] S. Z. Bockshtein, "Coagulation and deterioration of carbides," Doklady Akad. Nauk SSSR 73, 2, 311 (1950).

Received January 3, 1957

A. I. Gertsen Leningrad Pedagogical State Institute

CONCERNING PROCEDURES OF STUDYING THE STRUCTURES AND PHASE COMPOSITION OF GRAIN BOUNDARIES

L. G. Sakvarelidze and L. M. Utevskii

The grain boundaries in metals and alloys have recently occupied increasingly the attention of researchers, particularly in connection with such important problems as heat stability, aspects of the brittleness of alloys, etc.

There is need to perfect the existing methods and to devise new ones for the study of the phase and chemical composition and structural condition of the surface layers of grains.

This is the goal of the work of the Institute of Metallography and of the Physics of Metals of the Central Scientific Research Institute of Ferrous Metallurgy.

1. In 1951 (first publication in June, 1952) the semidirect methodof electron microscopic and electron diffraction analysis of heterophase alloys [1] was proposed in the USSR and Fisher [2] subsequently took up this method.

Through this method, the presence of natural particles of the second phase in the specimen, and not solely their traces in the relief of the replica film, simplifies and, with the help of electron diffraction, makes more reliable the interpretation of the electron micrographs, and increases greatly (in comparison with the standard method of replicas) the possibility of identifying the highly dispersed particles.

These advantages of the semidirect analysis are of special significance in studying the grain boundaries and the surfaces of intergranular fracture , which leave the grain surface bare.

Fig. 1. Relief of grain boundaries, smoothed by etching, according to Popova's method. a) Electron micrograph of purest iron (grain boundaries are furrows). b) Electron micrograph of commercial iron (grain boundaries are ridges). × 5000.

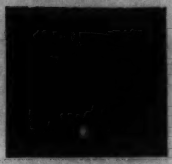

Fig. 2. Electron diffraction pattern of chrome-manganese steel containing 0.035% C. Chilled and tempered at 550°C. Ferrite and cementite.

Fig. 3. Electron diffraction pattern of fine-grained sample of alloyed iron. Diffraction from grain boundary ridges. Ferrite.

Fig. 4. Electron diffraction pattern of coarse-grained sample of alloyed iron. Grain boundary ridges do not shadow grain surfaces. Ferrite.

Fig. 5. Electron diffraction pattern of electrolytic iron remelted in vacuum. Spotty lines are ferrite, solid lines are GTsK phase (a_0 = = 3.62 Å).

The electron diffraction photography of the intergranular fracture specimen, together with the microdiffraction examination of the cross section of the specimen using the electron microscope, are the most reliable means of direct analysis of the crystalline nature of the precipitation of grain boundaries.

It must be stressed that the guarantee of obtaining a preparation containing completely preserved particles of the dispersed phase (this is all the harder, the smaller the particles) is provided by tested means and by those used for the isolation of this phase from the alloy when dissolving its base. For example, Popova's and Fitterer's [3] methods are widely used in the USSR to isolate the carbide phase from carbon and alloy steels.

2. By etching the grain boundaries of samples of various steels and iron alloys by Popova's method (1-5 min) more or less high (0.2-0.4 μ) almost unbroken "ridges" are formed, with a sharply defined "watershed" – essentially a geometric boundary of the coupled grains (Fig. 1, b). This effect was observed by several other authors. The etching retardation along the grain boundaries is definitely connected with the divergence of the chemical composition of the grain surface layers from the average composition of the alloy, since the same etching of the purest iron develops furrows (Fig. 1, a) along the grain boundaries, as ascertained by the "illumination" of the etching figures (always hollows): in commercial technical iron the boundary relief is "illuminated" in the opposite way, but in the purest iron in the same way as the etching figures.

Consequently, it is possible to obtain by an appropriate choice of the etchant a relief with "ridges" along the grain boundaries on the surface of cross section of iron or of technically pure steel.

By illuminating the sample with an electron beam at a glancing angle of less than 1°, these "ridges" leave the whole grain surface in the "shadow" if its diameter does not exceed 10-20 μ. This means that the cross section pattern is formed mainly by electrons diffracted as they pass through the sharp projections formed by the grain boundary layers which constitute only 10^{-3} to 10^{-2} of the volume of the sample. Further, this means that it is possible in principle to detect the presence of a specific precipitate of a phase in the grain boundaries (not found inside the grains) which constitutes ~ 10% of the volume irradiated by the electrons, i. e., 10^{-4} to 10^{-3} of the volume of the sample.

For example, it is possible to obtain from a steel sample containing 0.035% C a bright pattern from the cementite (Fig. 2) which occupies only 0.4% of the volume of the sample and which distributes itself, after chilling and tempering, mainly along the grain boundaries.

The shape of the diffraction spots makes it possible to estimate whether the "ridges" are sufficiently "high" along the grain boundaries, or whether the size of the grains is sufficiently small to consider the electron pattern as indicating in the main the phase composition of the intercrystalline material. The criteria used here may be the blurring of the spots on the electron pattern in the direction of the shadow of the sample – a blurring observed when the electron beam hits the curved grain surface. The corresponding examples are shown in Figs. 3 and 4.

Controlling the character of the relief of the etched surface in this way it is possible with the aid of the electron microscope to analyze the peculiarities

of the phase composition and the structures of the grain boundaries by using electron diffraction photography on the "ridges" along the grain boundaries.

By using a simple x-ray spectral attachment on the electron diffraction apparatus simultaneously with the photographing of the pattern it becomes possible also to make a local x-ray spectral analysis of the chemical composition of the grain boundary layers. (The results of the practical realization of this possibility will be conveyed in the near future.)

3. The presence of lines of a face-centered lattice (a = 3.62 ± 0.01 A) on the electron patterns of samples of various low-carbon steels (Fig. 5) annealed or tempered at a high temperature, prompted us* to undertake the systematic study of the chemical nature of this phase which many authors have taken for austenite [4]. The electron patterns of a series of alloy samples, prepared by vacuum melting of electrolytic iron and containing from 0.05 to 2% Mn, Ni, Cr, Mo to 0.01% P, C, or Sn, after annealing or high-temperature tempering (800°C) did not show any signs of the presence of "austenite." Neither did any "austenite" appear after carburizing, nor after nitriding of any of these alloys. But introducing only a small quantity (< 0.1%) of copper into pure iron or into any of its alloys brought about bright characteristic (solid, somewhat blurred) lines of "austenite."

Subsequent experiments with copper intentionally precipitated on the samples proved definitely that the "austenite" lines truly belong to the copper which is almost always present in technical iron and steel and which precipitates as a thin layer on the surface of the sample during etching.

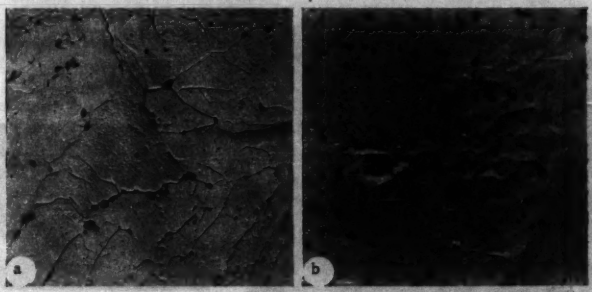

Fig. 6. Chrome-manganese steel (0.04% C). Chilled and tempered at 650-500°, 8 hr; a) the titanium preparation of the microsection, x 8000; b) the titanium preparation of the unetched surface of the brittle fractures (the separation of the compounds from the samples was electrolytic). x 8000.

It is interesting that the lattice constant of the crystalline copper precipitated on the anode is 3.65 A, and that on the cathode it is 3.62 A, which agrees with the data in [5].

Thus, there is no "austenite" along the grain boundaries of the low-alloyed steels and of iron, in particular, after high-temperature tempering or annealing.

4. A series** of chrome-manganese steels were investigated (~ 1% Cr and 2-3% Mn) and of chrome-nickel (2% Cr and 2% Ni); among them low-carbon ones (0.03-0.05% C) highly sensitive to reverse temper brittleness. The ductile conditions was obtained by chilling and tempering at 650°C and by cooling in water, and brittleness by additional tempering at 500°C.

---

* The experimental part of this work was done by L. G. Orlov and R. M. Koshelevskii.

** L. G. Orlov, N. I. Koltsova, and G. L. Ivanova participated in carrying out the experiments.

Fig. 7a

Fig. 7b

Fig. 7c

Fig. 7d

Fig. 7. Chrome-nickel steel (0.20% C) chilled and tempered at 650-500°C, 200 hr; a) electron diffraction pattern of sample (cementite and ferrite), b) electron micrograph of titanium preparation of sample; × 24,000; c) electron micrograph of titanium preparation of unetched fracture surface, × 20,000; d) electron diffraction pattern of plastic preparation of sample.

The idea generally accepted today is that brittle fracture of steel in a state of temper brittleness passes along the grain boundaries. It is easy to be convinced of this by comparing the electron microphotographs in Figs. 6a and 6b, with those in Figs. 7b and 7c. Only such (large, rounded) carbide particles as are visible only at grain boundaries in microsection preparations, appear on the unetched surface of the brittle fracture.

Unfortunately, the size and shape of these particles in high-tempered samples are such as to make it impossible to obtain electron patterns from the fracture preparations. However, in some cases, x-ray diffraction study of the carbide phase, isolated from a sample with a known structure, is helpful.

Thus, both the electron pattern of the preparation of the steel sample 0.2% C, 2% Cr and 2% Ni (Fig. 7d), and the reflection pattern of the same sample (Fig. 7a) showed the presence of only Fe_3C. The x-ray pattern of the carbide precipitate of the same sample gave sharp lines of the chromium carbide Cr_7C_3, and only weak, blurred cementite lines at small reflection angles. This leads to the conclusion that the large carbide particles, nontransparent to electrons and located along grain boundaries, are chromium carbides, and that the small particles inside the grains are cementite.

The brittle fractures of the "ductile" samples (broken at low temperature) also pass partially along grain boundaries, and in that case the brittle fractures of the "ductile" and embrittled samples are quite similar. No dispersed particles were observed on the surface of the grain-boundary fracture, the presence of which would distinguish the brittle sample from the nonbrittle one.

Consequently, the separation of any dispersed particles along the grain boundaries which might be considered as the cause of brittleness, is disproved by these results.

On the other hand, the electron diffraction photography by "reflection" from brittle and ductile samples of low-carbon steels sometimes shows a difference in the intensity of the diffraction pattern of cementite (it is brighter brittle samples). In other words, the connection between embrittlement and additional precipitation of Fe_3C is not excluded. But it is then necessary to assume a particular form of this precipitate as a very thin solid or almost solid film, enveloping the ferrite grains. But it is this form of carbide precipitate that could not be detected.

LITERATURE CITED

[1] L. M. Utevskii, "Concerning new possibilities of electron microscope study of disperse structures in two-phase alloys," Zavodskaia Lab. 6, 695 (1952).

[2] R. M. Fisher, "Electron microstructure of steel by 'extraction replica' technique," Symposium on Techniques for Electron Metallography (1953), Spec. Techn. Publ. No. 155 (Am. Soc. Testing Materials, Phil.), p. 49.

[3] Iu. A. Kliachko, I. A. Atlasov, and M. M. Shapiro, Analysis of Gases, Inclusions, and Carbides in Steel [in Russian] (Metallurgizdat, 1953).

[4] A. L. Tsou, J. Natting, and J. W. Menter, "The quench ageing of iron," J. Iron. Steel Inst. 172, Oct., 2, 163-171 (1952).

[5] Z. G. Pinsker, Electron Diffraction [in Russian] (Izd. AN SSSR, 1949), p. 211.

Received April 22, 1957

Central Scientific Research Institute for Ferrous Metallurgy

MONOCHROMATIZATION OF THE REFLECTED X-RAY BEAM

A. A. Katsnel'son

X-ray monochromatization in URS-50-I is accomplished by using a monochromator crystal, set between the anode of the x-ray tube and the specimen under study. This complicates and sometimes makes impossible the recording of the curve of x-ray intensity, diffracted by samples which contain components which fluoresce under the applied radiation. Thus, for example, it is practically impossible to obtain a clear Fe x-ray pattern from Cu K_α-radiation, and serious difficulties also arise during the photography of iron or copper-base alloys using MoK_α-radiation, and so forth.

We have set up a simple attachment for the URS-50-I (Fig. 1) which eliminates the above-mentioned defect by monochromatizing not the initial, but the reflected beam. A rail is fitted to the GUR stand instead of a counter support, on which the slide A is carried. The plate for the crystal holder B and the counter support C are independently fastened to the slide A by a common axle. The crystal holder D can be moved on special rails perpendicularly to the x-rays. Rotation of bearings B and C and the motion of A and D are necessary only in adjusting the mounting of the monochromator crystal for the radiation assigned. Later their positions are fixed by special stops. This arrangement makes it possible to convert quickly from monochromatic to nonmonochromatic recording without adjusting the GUR anew. To do this it is sufficient to remove the crystal holder and to turn the counter support so that its axis coincides with the direction of the axis of the rails.

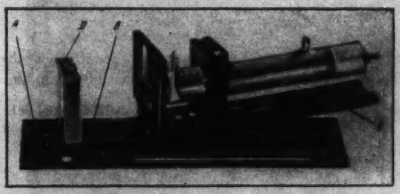

Fig. 1. General view of the apparatus. A) Slide, B) plate of the crystal holder, C) counter support, D) crystal holder.

An x-ray optical scheme with a curved monocrystal of NaCl has been applied for the monochromatization of the reflected beam [1]. We used a flat pentaerythrite crystal as a monochromator. Its merit is its very high degree of reflecting power compared to that of the majority of crystals (except graphite) used in the monochromatization of x-rays [2]. Pentaerythrite is easily obtainable in the laboratory [3], and the adjustment of a flat crystal is much simpler than that of a curved one.

The adjustment of our attachment is done in the following manner. First by moving the crystal holder, the surface of the monochromator crystal is set on the line which passes through the tube focus and the GUR axis. Then by rotating the plate, the monochromator is brought into reflecting position by using a fluorescent screen; then the counter is brought into working position by turning the counter support until maximum intensity of the reflected beam is observed. After this, a pentaerythrite crystal, put in place of the sample, and the monochromator crystal are arranged according to the scheme of a double-crystal-spectrometer. The angular position of the monochromator is made more accurate at this stage (also using the image on the screen) and the most favorable distance from the crystal to the sample is chosen.

To compare the standard method of monochromatization with the one suggested in this work, the intensities of Fe reflections were measured using CuK_α-radiation. Figure 2 depicts the intensities near the reflections 110, 200 and 211 of Fe using CuK_α-radiation by the use of monochromatization of the initial (Fig. 2, a) and of the reflected (Fig. 2, b) beam. The measurements were made when the tube was under the same conditions (34 kv, 9 ma), the width of all the slits was the same, 1 mm, and the area of the reflecting surface of the monochromator

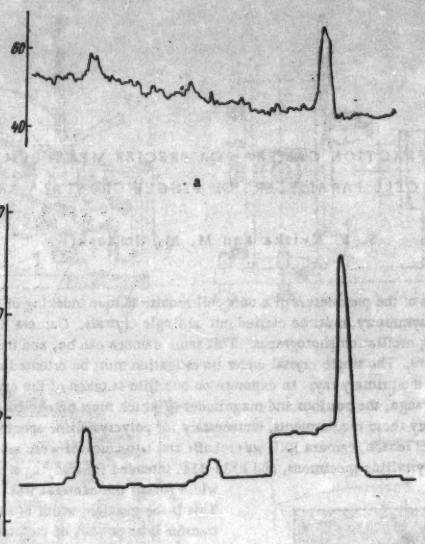

Fig. 2. Recordings of intensity curves of Fe using CuK_{α} radiation. a) Initial beam monochromated; b) reflected beam monochromated.

crystal was 7 x 4 mm^2. The integrated intensity of the reflection 211 increased from 400 to 600 counts on passing from monochromatization of the initial beam to that of the reflected one (subtracting the background). Moreover, the integrated intensity of the background fell from 6000 to 800 counts. The reflection 200 cannot be measured with monochromatization of the initial beam, but, by using the scheme suggested here, its intensity is measurable and equal to 200 counts. These results show that this scheme makes it possible to eliminate fluorescent radiation. The increase in the intensity of the reflections themselves is of interest. This apparently is connected with the decrease in the absorption of the x-rays in air, since the distance from the tube to the counter is decreased by 15% as compared with the standard scheme of monochromatization. Obviously, this effect becomes even more noticeable when using softer radiations.

In conclusion, I wish to express my deep gratitude to V. I. Iveronova for her interest in this work and her valuable discussions.

LITERATURE CITED

[1] R. Banerjee, "Reflected beam x-ray monochromator for Geiger counter diffractometry," Rev. Sci. Instr. 26, 6, 564-565 (1955).

[2] P. Renniger, "Absolut-Vergleich der Stärken Röntgenreflexe verschiedener Kristalle," Acta Cryst. 7, 677 (1954).

[3] Ia. I. Graevskaia, V. I. Iveronova, and V. P. Tarasova, "Specialized apparatus for the measurement of x-ray reflections with the aid of Geiger counters," Kristallografiia 1, 4, 442-445 (1956).

Received January 13, 1957

M. V. Lomonosov Moscow State University

X-RAY DIFFRACTION CAMERA FOR PRECISE MEASUREMENT OF THE UNIT CELL PARAMETERS OF SINGLE CRYSTALS RKM-114

S. S. Kvitka and M. M. Umanskii

Precise measurements of the parameters of a unit cell require unique indexing of the x-ray diffraction pattern and, for crystals of low symmetry, must be carried out on single crystals. Camera RKU [1] was built in 1948 for such measurements using oscillation photographs. This same camera can be, and frequently is, used for studying polycrystalline specimens. The single crystal under investigation must be oriented relative to the rotation axis and to the direction of the primary ray; an exposure on one film is taken of the crystal for several different positions of the oscillation range, the positions and magnitudes of which must be chosen to correspond with the given problem [2]. To satisfy these requirements, unnecessary for polycrystalline specimens, the construction becomes complicated. For this reason, camera RKU was rebuilt and two cameras were set up on its base: RKP-86, intended for studying polycrystalline specimens, and RKM-114, intended for studying single crystals. The film width for all the cameras was reduced from 38 to 35 mm. This is the standard width of cinefilm, so that one could transfer later to rolls of industrial x-ray film. On both this and the other camera, type SD-2 electric motors, switches, and plug sockets were installed, and the primary beam traps were changed, so that an exposure can be made without them, if desired; all this has made the cameras more convenient.

Fig. 1. RKM-114. Side view of the rotation and oscillation mechanism. The cam with motor is inside the casing. The T-shaped lever is lifted and rests on the lid of the casing.

A holder, allowing the specimen to be centered and moved along the axis of rotation, is in camera RKP-86 (of rated diameter 86 mm) instead of the goniometer head.

Camera RKM-114 (of rated diameter 114.59 mm) is shown in Fig. 1. A drawing of it is shown in Fig. 2. The camera is furnished with a type-2b goniometer head which gives micrometric inclination of the crystal to ± 15°, but also allows work with a type-2 head giving a possible crystal inclination of ± 60°. The goniometer head can be moved smoothly along its axis by rotating knob 1 (Fig. 1) disposed on the outside. The centering of the specimen is carried out in the camera itself by a socket wrench through hole 2. The specimen can be observed either through the collimator or by a special optical tube screwed on in place of the collimator. When the centering is completed, hole 2 is closed by a screw and the camera becomes lightproof.

The rotation and oscillation mechanism of camera RKM-114 is essentially different from the equivalent mechanism of RKU. In RKM-114, a type SD-2 motor is fixed on the base so that its axis of rotation is parallel to the axis of rotation of the goniometer head. On the axle of the motor are fixed a cylindrical disc, a gear and a cam having the form of two mirror-smooth Archimedes spirals. Two flat springs press on the cylindrical disc to take up the clearance to the motor axle.

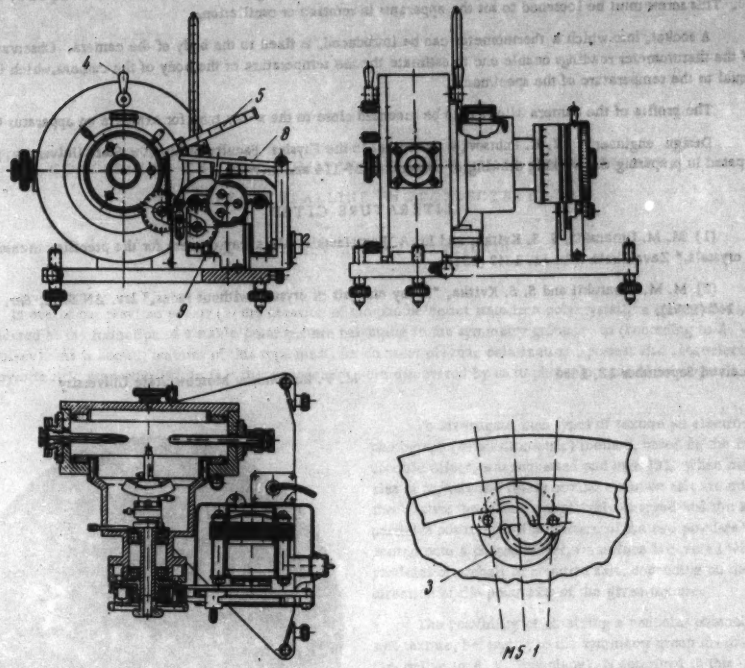

Fig. 2. RKM-114. Drawing, general view. On the bottom right is shown the helix which controls the circular spring pressing the film to the body of the camera.

The gear fixed to the motor axle can be connected to the gear on the rotation axis of the goniometer head by a pair of idlers with the result that the goniometer head, and the graduated circle rigidly joined to it, can turn at a speed of 1 rpm.

The oscillation mechanism is built in the following way. A straight lever (Figs. 1 and 2) is fitted to the axle of the goniometer head. This lever does not prevent the goniometer head from turning when setting the camera for rotation or changing the oscillation interval. Lever 5 is fixed to the axis by screw 6 only during an exposure by the oscillation method. Slider 7, the point of which slides along the upper edge of the T-shaped lever 8, can be moved and secured in any position by lever 5. The lower sharpened end of the T-shaped lever slides, in its turn, along the surface of cam 9. The result is that when the motor turns, the T-shaped lever oscillates with constant angular velocity and its oscillation interval does not change, while the straight lever together with the goniometer head oscillates with a velocity also almost constant, but the size of its oscillation interval, independent of the position of slider 7, can be arbitrarily chosen within limits from 1 to 10°. If the camera is set to rotate, it is advisable to raise that end of the T-shaped lever and rest it on the lid which closes the hole in the body of the motor, as shown in Fig. 1.

To take a Laue photograph on cylindrical film, the axis of the goniometer head can be clamped by screw 10. This screw must be loosened to set the apparatus in rotation or oscillation.

A socket, into which a thermometer can be introduced, is fixed to the body of the camera. Observations of the thermometer readings enable one to estimate the the temperature of the body of the camera, which is usually equal to the temperature of the specimen.

The profile of the camera allows it to be mounted close to the x-ray tube for exposure on apparatus URS-70.

Design engineer V. K. Rubtsov, a co-worker in the Physics Faculty of Moscow State University, participated in preparing the working drawing of cameras RKM-114 and RKP-86.

LITERATURE CITED

[1] M. M. Umanskii, S. S. Kvitka, and Iu. A. Bagariatskii, "An x-ray camera for the precision measurement of crystals," Zavodskaia Lab. 11, 1343 (1948).

[2] M. M. Umanskii and S. S. Kvitka, "X-ray analysis of crystals without faces," Izv. AN SSSR, Ser. Fiz. 15, 147 (1951).

Received September 13, 1956

M. V. Lomonosov Moscow State University

CONCERNING THE TWO LIMITING POINT GROUPS OF SYMMETRY OF POLYCRYSTALLINE PHOTOELECTRETS

I. S. Zheludev and V. M. Fridkin

In one of our previous papers [1] the creation of the photoelectret state in a polycrystalline specimen was considered as the formation of a stable polar texture belonging to the symmetry group $\infty \cdot m$ (according to A. V. Shubnikov). As is known, textures of this type must, for constant electric polarization, possess also piezoelectric and pyroelectric properties [2]. In fact these properties were discovered by us in photoelectrets of polycrystalline sulfur.

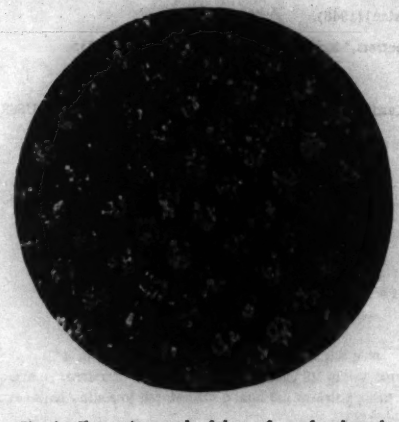

Fig. 1. Photomicrograph of the surface of a photoelectret with regions having mutually opposite electric polarization directions. x 10.

To investigate such types of texture an electrophotograph (or sensitometric) method, based on the triboelectric effect, was suggested and used [3]. When particles of asphalt and finely ground common salt are mixed, the latter becomes negatively charged and the asphalt particles positively. If a mixture of the two powders is poured onto a photoelectret, its surface is covered with particles of asphalt or common salt, depending on the direction of the polar axis of the given texture.

The possibility of obtaining a nonpolar photoelectret texture, belonging to the symmetry group $m \cdot \infty : m$ (according to A. V. Shubnikov), is described in this paper.

A layer of polycrystalline sulfur with a thickness of the order of 50 μ, dusted in a vacuum onto an aluminum plate, is polarized by an electric field of 5 kv/cm and by an illumination on the layer surface of $5 \cdot 10^{-5}$ w/cm^2 for 4 min. After cutting off the illumination and removing the potential, we obtained the polar texture mentioned above. A film with a dotted network, the diameter of the dots being 0.9 mm, was overlaid on the surface of the texture. After this the layer was polarized in the opposite direction across the grid, by the voltage of the polarizing field, with the illumination on the surface and the time of polarization having the previous values. As a result of this, the regions of the photoelectret covered with the dark dots of the network preserved the original direction of polarization since one can practically disregard the spotty depolarization of these regions. On the other hand, the parts of the photoelectret under the light dots of the network reversed the electrical polarization direction during this time. As a result, the polycrystalline photoelectret is broken up into a series of regions, neighboring regions having opposite polarization directions. If a mixture of asphalt and common salt is now poured into the photoelectret, one set of regions on its surface is covered with particles of asphalt and the other with crystals of common salt, corresponding to the opposite polarization directions in each neighboring pair of regions in the photoelectret. A photomicrograph of the surface of such a photoelectret is shown in Fig. 1, where the light regions covered with crystals of common salt and the dark regions covered with particles of asphalt are clearly seen.

It is easy to see that the photoelectret obtained shows a nonpolar texture with the symmetry m • ∞: m. In view of the presence of a center of symmetry such a photoelectret does not macroscopically possess piezoelectric and pyroelectric properties, which we verified experimentally (under the condition that the dimensions of the regions into which the photoelectret was broken up were small compared with the whole surface of the photoelectret being tested). The result obtained demonstrates that polycrystalline photoelectrets can be either of polar or nonpolar texture.

Both the textures we investigated belong therefore to two limiting point groups of symmetry, correspondingly designated ∞ • m and m • ∞: m. Particularly in the case of the photoelectret texture with symmetry m • ∞: m the electrophotographic method is shown to be the only one possible, since the over-all charge on the photoelectret surface is, in this case, zero.

The methods set forth above can be taken as a basis for two-color electrophotography on photoelectrets. In this case the regions of the photoelectret which are oppositely polarized can be shown as particles of another color.

The authors are sincerely thankful to Academician A. V. Shubnikov for his attention to this work.

LITERATURE CITED

[1] V. M. Fridkin, "Some results of research into the photoelectret condition of single sulfur crystals," Kristallografiia 1, 557-563 (1956).

[2] A. V. Shubnikov, Piezoelectric Textures[in Russian] (1946).

[3] V. M. Fridkin, "Electrophotography on photoelectrets," Kristallografiia 2, 1, 130-133 (1957).*

Received May 17, 1957

Institute of Crystallography, Academy of Sciences, USSR

* [Soviet Physics – Crystallography, pp. 125-27.]

THE DIELECTRIC, ELASTIC AND PIEZOELECTRIC PROPERTIES OF SINGLE CRYSTALS OF BENZOPHENONE

A. A. Chumakov, I. M. Sil'vestrova, and K. S. Aleksandrov

Benzophenone $(C_6H_5)_2CO$ belongs to the class of aromatic ketones and exists in 4 crystallographic forms which differ from one another in melting point and in other properties. In the present work a study was made of crystals of the stable orthorhombic form, belonging to the symmetry class 2:2 (see Fig. 1).

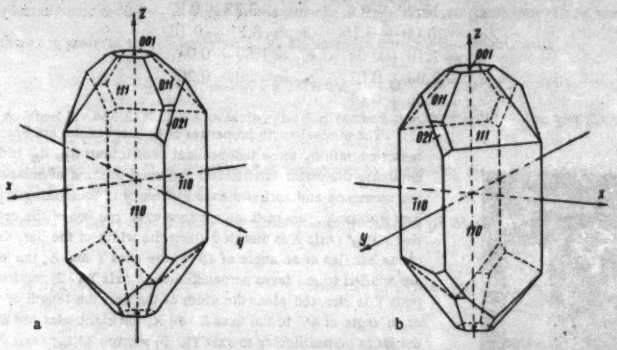

Fig. 1. Ideal growth forms of a right-hand(a)and left-hand(b)crystal of benzophenone.

The specimens for the measurement of the physical properties were prepared from large (200-300 cm^3), perfect, isometric single crystals (see Fig. 2), grown out of solutions in acetone and carbon tetrachloride. The measured values of the density ρ and the melting point T_m of these crystals are as follows:

$$\rho = 1.219 \text{ g/cm}^3 \text{ (for 20°C)}; \quad T_m = 47.0°C.$$

The values of the dielectric constants ε_{ii} and the tangent of the dielectric loss angle tan δ were measured with a Q-meter at a frequency of 10^6 cps and with a precision capacity bridge at a frequency of 10^3 cps with field strengths of $\sim$ 5-10 v/cm. The measurements were made on plates with a thickness of 0.5 to 2 mm and with an area of 0.5 to 10 cm^2, cut perpendicularly to the crystallographic axes X, Y and Z (see Fig. 1). As a result of the measurements the following mean values were obtained:

$$\varepsilon_{11} = 4.0 \pm 0.05, \qquad \varepsilon_{33} = 3.7 \pm 0.05,$$
$$\varepsilon_{22} = 4.1 \pm 0.05, \qquad \tan\delta = (6 \pm 0.5)\cdot 10^{-4}.$$

The dielectric strength E of the crystals of benzophenone in air was measured with dc voltage on flat specimens, perpendicular to the crystallographic axes X, Y and Z. Spherical depressions were ground in the samples [1]. The

minimum thicknesses of the plates in the depression were from 0.5 to 1 mm. The following values of E (in kv/mm) were obtained:

$$E_x = 28-30 \pm 3,$$
$$E_y = 22-25 \pm 3,$$
$$E_z = 40-50 \pm 4.$$

The elastic properties of benzophenone are described by a tensor containing 9 independent elastic moduli. The elastic moduli c_{ik} were measured by the pulsed ultrasonic method [2] on specimens having dimensions of 7 to 12 mm in the direction of propagation of the elastic waves.

The moduli c_{ii} were determined directly from measurements of the velocity of longitudinal and shear waves in the directions of the crystallographic axes. The moduli c_{ik} ($i \neq k$) were determined from the values of the velocities of the quasi-longitudinal and quasi-shear waves in the directions [110], [101], [011]. The accuracy of the measurements of these moduli is considerably lower than that of the measurements of the moduli c_{ii}, because the values of the moduli c_{ii}, each with its own error, enter into the formulas for the determination of the moduli c_{ik} ($i \neq k$). The following values of the elastic moduli (in 10^{10} dynes/cm^2) were obtained:

$$c_{11} = 10.70 \pm 0.15, \quad c_{66} = 3.53 \pm 0.03,$$
$$c_{22} = 10.00 \pm 0.15, \quad c_{23} = 3.21 \pm 0.13,$$
$$c_{33} = 7.10 \pm 0.04, \quad c_{31} = 1.69 \pm 0.08,$$
$$c_{44} = 2.03 \pm 0.01, \quad c_{12} = 5.50 \pm 0.20.$$
$$c_{55} = 1.55 \pm 0.01,$$

Fig. 2. Crystal of benzophenone grown from solution in acetone.

The piezoelectric properties of benzophenone are described by a tensor containing three independent coefficients d_{14}, d_{25} and d_{36}. For obtaining the piezo-coefficients the usual method of measurement of the resonance and antiresonance frequency of oscillating crystalline bars was used. Bars of three sections were cut out of the crystal: 1) section $XYt_{45°}$ (axis X is directed along the width of the bar, the length of the bar lies at an angle of 45° to the axes Y and Z, the electrodes are applied to the faces perpendicular to axis X); 2) section $YXt_{45°}$ (axis Y is directed along the width of the bar, the length of the bar lies at an angle of 45° to the axes Z and X, the electrodes are applied to the faces perpendicular to axis Y); 3) section $ZXt_{45°}$ (axis Z is directed along the width of the bar, the length of the bar lies at an angle of 45° to the axes X and Y, the electrodes are applied to the faces perpendicular to axis Z). All the specimens under study were excited with compression-extension oscillations longitudinally and had the dimensions 23 × 4 × 1.5 mm. The frequencies were measured by a heterodyne wave meter. The calculation of the piezo-coefficients d_{ik} was carried out with the formula

$$d_{ik} = \frac{\pi}{2} \frac{1}{f_R l} \sqrt{\frac{\epsilon_{ik} \Delta f}{4\pi\rho f_R}},$$

where f_R is the resonance frequency, $\Delta f = f_a - f_R$ (f_a is the antiresonance frequency), ϵ_{ik} is the dielectric constant, l is the length, ρ is the density.

As a result of the measurements the following values of the piezoelectric coefficients were obtained (in 10^{-7} cgs units):

$$d_{14} = 3.7 \pm 0.1,$$
$$d_{25} = 0.6 \pm 0.02,$$
$$d_{36} = 6.1 \pm 0.1.$$

The coefficient of electromechanical coupling is determined with the formula

$$k = \frac{\pi}{2}\sqrt{\frac{\Delta f}{f_R}}.$$

The following values of the coefficient of electromechanical coupling were obtained for the bars of sections indicated above:

$$k_{XYl\,45^\circ} = 7.2\%, \qquad k_{YXl\,45^\circ} = 3.8\%, \qquad k_{ZXl\,45^\circ} = 16.0\%.$$

From these data it is apparent that the $ZXt_{45}°$-section bar has the greatest coefficient of electromechanical coupling. These results contradict the data available in the literature [3], according to which benzophenone is related to a group of substances having a weak coefficient of electromechanical coupling. For the $ZXt_{45}°$-section, with longitudinal oscillations in length, the constant g_{36} has the magnitude $10.4 \cdot 10^{-3}$ cgs units/bar·cm, i. e., exceeds the magnitudes g_{1k} for all the rest of the crystals used in piezotechnology and operating in longitudinal oscillation. Since crystals of benzophenone are comparatively easily grown from solutions, have low dielectric loss and high piezoelectric modulus, they can be recommended for various technical uses at low temperatures.

The authors are grateful to Academician A. V. Shubnikov for supervision of this work.

LITERATURE CITED

[1] A. A. Vorob'ev and E. K. Zavadovskaia, The Dielectric Strength of Solid Dielectrics [in Russian] (State Tech. and Theoret. Lit. Press, 1956).

[2] K. S. Aleksandrov and O. V. Nosikov, "An instrument for measuring the elastic modulus of crystals," Acoustics J. (USSR) 2, 3, 244-247 (1956).*

[3] Iu. Mezon, Piezoelectric Crystals and Their Use in Ultrasonics [in Russian] (Foreign Lit. Press, 1952).

Received February 9, 1957

Institute of Crystallography, Academy of Sciences, USSR

* [Soviet Physics – Acoustics, p. 256.]

INVESTIGATION OF THE ANISOTROPY OF HARDNESS OF SINGLE CRYSTALS OF PbS BY SCRATCHING

Iu. S. Boiarskaia

In previous papers by the author the conclusion was drawn that the anisotropy of hardness of single crystals of NaCl and KCl under given conditions of scratching is connected with the disposition of the planes and of the directions of slip in these crystals [1, 2]. The correctness of this thesis is verified in the present paper on single crystals of PbS, the investigation of which was of special interest since they are analogous to single crystals of NaCl in type of lattice and in cleavage, but they differ from the latter in that they have two glide planes: (100), with the glide direction [110], and (110), with the glide direction [110] [3].

The measurements were carried out on the microhardness meter PMT-3, to which a simple adjustment was made for the investigation of the anisotropy of hardness by scratching. The scratching point was a four-sided diamond pyramid, with an angle of 136° at the tip. The load on the point equalled 5 g, the rate of scratching was of the order of 0.01 cm/sec.

The investigation of the anisotropy was carried out on three faces of single crystals of PbS: on faces (100), (110) and (111).

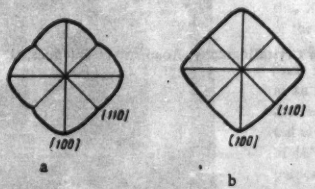

a b

Fig. 1. Rosettes of hardness on face (100) of PbS crystal: a) natural surface; b) polished surface.

The measurements were carried out in the following manner. On the face being examined, for each crystallographic direction being studied, 5-10 scratches were made, their width was measured, and from these data the average width $\bar{d}$ of the scratch was calculated, corresponding to the given direction. The hardness was then calculated according to the formula $H = P/\bar{d}^2$, where P is the load on the point. The error in the value of the hardness, ΔH, was also calculated.

As a result of the measurements the following data were obtained.

Cube face. Investigation of the anisotropy of hardness was carried out both on the natural (100) face, obtained by cleavage, and on the polished face. The results of the measurements are presented in Table 1.

TABLE 1

Direction of scratch	Natural face				Polished face			
	$\bar{d}$, μ	$\Delta\bar{d}$, μ	H, kg/m	ΔH, kg/m	$\bar{d}$, μ	$\Delta\bar{d}$, μ	H kg/mm²	ΔH, kg/mm²
[100]	11.4	0.15	38.3	1.0	11.9	0.25	35.7	1.5
15° [100]	12.4	0.20	32.4	1.1	12.3	0.20	32.1	1.1
30° [100]	13.0	0.3	28.6	1.3	12.7	0.25	31.0	1.0
[110]	13.0	0.25	28.6	1.2	13.0	0.15	29.0	0.7

Table 1 shows clearly that there is anisotropy of hardness both on the natural and on the polished face: in direction [100] the hardness is maximum, in direction [110] it is minimum.

For a graphic representation of the anisotropy of hardness on the cube face, rosettes of hardness were constructed, pictured in Fig. 1. The anisotropy of hardness is illustrated also by the photograph of the scratches made in the directions [100] and [110] (see Fig. 2), in which it is clearly shown that the scratch along direction [100] is narrower than the scratch along direction [110].

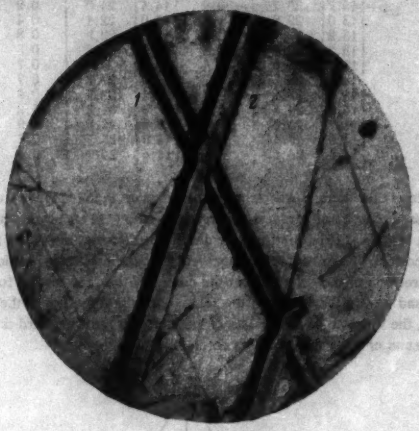

Fig. 2. Anisotropy of hardness on face (100) of PbS crystal. 1) Scratch along [100], 2) scratch along [110]. x 460.

Rhombododecahedral face. In the investigation of the anisotropy of hardness on the face (110), data were obtained which are given in Table 2.

TABLE 2

Direction of scratches	d, μ	$\Delta d, \mu$	H, kg/mm^2	ΔH, kg/mm^2
0° — [110]	13.3	0.15	28.1	0.7
15°	13.6	0.20	26.9	0.8
30°	14.4	0.3	24.1	1.0
45°	14.3	0.15	24.5	0.5
60°	13.4	0.15	27.8	0.6
75°	12.8	0.15	30.5	0.7
90° — [100]	12.1	0.1	34.2	0.6

Table 2 shows clearly that there is anisotropy of hardness on face (110) as well as on face (100).

For face (110), the rosette of hardness is four-leaved (see Fig. 3), as it is also for face (100), but in contrast to the latter is stretched out along the direction [100].

Octahedral face. In the investigation of the anisotropy on face (111) the question of polar anisotropy was considered, i. e., the dependence of the hardness on which direction the scratch is drawn along the given straight line. Therefore, the scratch along each straight line was made in both diretcions — from the center of the crystal and toward the center of the crystal. The results of the measurements are presented in Table 3.

TABLE 3

Direction of scratch	Scratch from center			Scratch toward center		
	d, μ	H, kg/mm	ΔH kg/m	d, μ	H kg/mm	ΔH, kg/mm^2
0°—[112]	14.4	24.0	0.4	14.1	25.1	0.5
15°	14.6	23.4	0.7	14.4	24.0	0.7
30°	14.7	23.2	0.6	14.4	24.0	0.9
45°	13.0	29.6	1.2	15.0	22.1	0.4
60°	13.2	28 7	0.7	14.8	22.9	0.8
75°	13.2	28 7	0.8	14.7	23.2	0.3
90°	13.0	29.6	0.6	14.1	25.1	0.7
105°	14.7	23.2	0.7	13.4	27.8	0.7
120°	15.0	22.1	0.8	12.4	32.7	0.9
135°	14.6	23.4	0.7	12.6	31.2	1.2
150°	14.7	23.2	0.7	13.0	29.6	0.9
165°	14.6	23.4	0.6	14.0	25.5	0.7
180°	14.1	25.1	0.5	14.4	24.0	0.4

From Table 3 it follows that there is anisotropy of hardness on face (111), as well as on the faces (100) and (110). In Fig. 4 are presented rosettes of hardness, wherein the face (111) is represented in the form of a regular triangle the sides of which are the [110] directions, for describing the relation of the form of the rosette with the given crystallographic directions. From Fig. 4 it is apparent that the rosettes of hardness on the (111) face are three-leaved. With the direction of the scratch from the center of the face toward its edges, the minima of the rosette of hardness are turned toward the angles of the face; with the direction of the scratch from the edges of the face toward its center, the maxima of the rosette of hardness are turned toward the angles of the face. Thus, on face (111) the phenomenon of polar anisotropy is observed.

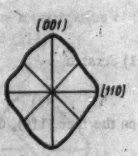

Fig. 3. Rosette of hardness on (110) face of PbS crystal.

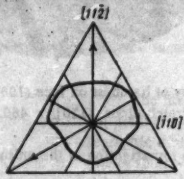

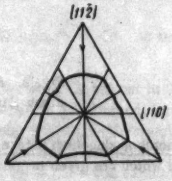

Fig. 4. Rosettes of hardness on (111) face of PbS crystal. The arrows indicate the direction of the motion of the point during scratching.

For crystals of NaCl, rosettes of a form similar to those for crystals of PbS were obtained; four-leaved for the faces (100) and (110) and three-leaved for the (111) face. However, the minima of hardness in NaCl occur in those directions which are characterized by maxima in PbS and vice versa – the maxima of hardness in NaCl occur in those directions which are characterized by minima in PbS [1, 2].

Since in crystals of PbS and NaCl the type of lattice and cleavage surface are identical, but the gliding elements are different, the conclusion may be drawn that the anisotropy of hardness under the given conditions of scratching is in fact connected with the position of the planes and the glide directions in these crystals.

In conclusion the author expresses sincere gratitude to M. V. Klassen-Neklindova and A. A. Urusovskaia for the valuable advice received in the execution of the present work, and also to G. P. Barsanov for submitting the single crystals of PbS for investigation.

LITERATURE CITED

[1] Iu. S. Bolarskaia, Investigation of the Microhardness of Crystals by the Impression Method and of the Anisotropy of Crystals by Scratching (Dissertation) [in Russian].

[2] Iu. S. Bolarskaia, "Investigation of the anisotropy of hardness of crystals of NaCl and KCl by scratching," Uchenye Zapiski Kishinevskogo Universiteta 17, 159-169 (1956).

[3] M. V. Klassen-Nekliudova and A. A. Urusovskaia, "Continuous diagrams of impact and pressure in cubic crystals," Trudy Inst. Krist. Akad. Nauk SSSR 11, 146-151 (1955).

Received September 1, 1956

Kishinevskii State University

ORIENTED CRYSTALLIZATION OF $KMnO_4$ AND $KClO_4$ ON BARYTES

V. A. Frank-Kamenetskii

It is known that $KMnO_4$ and $KClO_4$ belong to the isostructural type of barytes and are characterized by the space group Pnma orthorhombic crystal system. In Tables 1 and 2 are presented data which indicate the degree of similarity of the metric data of these compounds.

TABLE 1

Substance	Lattice row		
	[100]	[010]	[001]
$BaSO_4$	8.85 kX	5.44 kX	7.13 kX
$KMnO_4$	9.10 kX	5.60 kX	7.40 kX
$KClO_4$	8.85 kX	5.66 kX	7.24 kX

TABLE 2

Difference of the Parameters of $KMnO_4$ and $KClO_4$ and the Corresponding Parameters of $BaSO_4$, Expressed in % of the Smaller Value

Substance	Δ [100]	Δ [010]	Δ [001]
$KMnO_4$	2.82	2.94	3.79
$KClO_4$	0.00	4.05	1.54

The laws of the growth, with one another, of the substances in question were obtained long ago [1]. In this note are presented the results of a quantitative study of the regularities which arise during the crystallization of potassium permanganate and perchlorate on barytes,* which are probably connected with the character of the structural conformity [2].

The crystallizations of $KMnO_4$ and $KClO_4$ were carried out on the plane (001) of barytes from a drop of evaporating solution.** The growths obtained were studied under the polarizing microscope and the binocular microscope. It was thereby possible to establish that both the potassium permanganate and the perchlorate produce on the (001) face of the barytes (a fresh cleavage) crystals of different shape; the more or less isometric crystals of these substances are not oriented regularly on the (001) face of the barytes, while the thickened and usually elongated crystallites are oriented on it. A possible explanation of this is that the isometric crystals

TABLE 3

Substance	Total number of crystals	Number which were unoriented	Number which were oriented parallel [100]	[110]	[110]	% of oriented crystals
$KMnO_4$	390	72	243	33	42	81.5%
$KClO_4$	334	11	123	99	101	96.7%

were formed apparently on the surface of the drop and descended to the surface of the (001) face of the barytes during its drying, but the thickened crystallites were formed on the surface of the (001) face of the barytes. Such a conjecture is favored by the preferential disposition of the isometric crystals in the center of the preparation,

* It is interesting to note that in the crystallization under these same conditions on a freshly cleaved face (001) of barytes, of such substances as $NaNO_3$, KCl, KH_2PO_4, $CuCl_2 \cdot 2H_2O$, $PbCl_2$, $CuSO_4 \cdot 5H_2O$, $BaCl_2$, $Na_2SO_4 \cdot 10H_2O$, $KClO_3$, we were unable to observe any regularities in orientation.

** The best results were obtained with crystallization from a solution close to saturation at room temperature.

Fig. 1. Crystallization of $KMnO_4$ on the (001) face of barytes. × 30. The oriented crystals in the left portion of the photograph are arranged parallel to the [010] axis of the barytes.

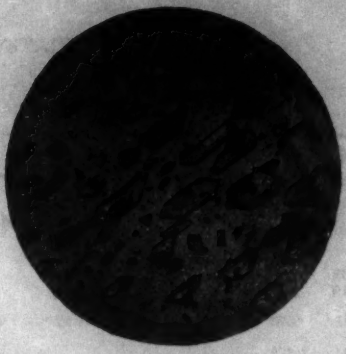

Fig. 2. Crystallization of $KClO_4$ on the (001) face of barytes. The oriented crystals are arranged essentially parallel to the [010] axis of the barytes.

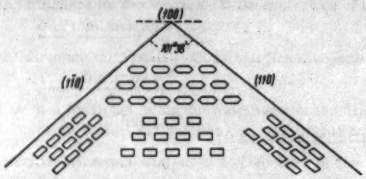

Fig. 3. Schematic representation of the three orientations of $KClO_4$ on the (001) face of barytes.

where the drop has a greater depth and where, consequently, the orienting role of the surface of the face of the barytes is less. There is further confirmation in the close arrangement of the isometric crystals of $KMnO_4$ and $KClO_4$ upon the oriented, elongated and thickened crystals of these substances.

On the (001) cleavage face of the barytes are clearly shown traces of prismatic cleavage which are inclined at an angle of 101°38'. The oriented crystals of $KMnO_4$ and $KClO_4$ are disposed mostly with their own elongation normal to the bisector of the obtuse angle of the barytes prism, i. e., parallel with the [100] edge (Figs. 1, 2). Considerably less clearly shown for $KMnO_4$ are two more directions of orientation, namely directions parallel to [110] and $[1\bar{1}0]$, which are probably connected only with another form of boundary. During the crystallization of $KClO_4$ all three directions of orientation parallel with [100], [110] and $[1\bar{1}0]$ have the same importance. In the schematic drawing of the oriented crystals of $KClO_4$ on barytes (Fig. 3) is graphically shown how the connection of the direction of the orientation with the boundary develops. The results of the calculation of the number of elongated crystals of $KMnO_4$ and $KClO_4$ in the three above-mentioned orientations are presented in Table 3.

The relatively greater precentage of oriented crystals of $KClO_4$ in comparison with $KMnO_4$ is probably connected with the greater structural conformity between barytes and potassium perchlorate than between barytes and potassium permanganate, as is seen from Tables 1 and 2 especially in a comparison of the distances along the [100] edge. With one structural type, the probability of oriented growth is proportional to the extent of agreement of the parameters, analogous to that which we have shown for oriented growth of barytes with chalcopyrite [2].

Student B. V. Motkina took part in the experimental work, previous to her untimely death.

LITERATURE CITED

[1] T. V. Barker, "Untersuchungen über regelmässige Verwachsungen," Z. Krist. 45, 1, 1-59 (1908).

[2] V. A. Frank-Kamenetskii, "The oriented intergrowths of crystals of chalcopyrite and cuprite in barytes from the Indishskaia lode (Northern Caucasus)," Uchenye Zapiski Leningrad Univ., Ser. Geol. 45, 91-117 (1940).

Received February 17, 1957

The A. A. Zhdanov Leningrad State University

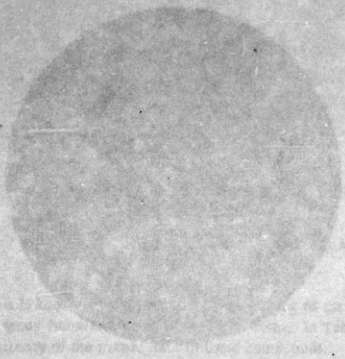

SOVIET PHYSICS – CRYSTALLOGRAPHY

(Translation of the Journal "Crystallography" of the USSR, Vol. 2, No. 5 published by the American Institute of Physics, April 1959.)

Volume 2, Number 5 September-October 1957

CONTENTS

	PAGE	RUSS. PAGE
The Development of Crystallography in the USSR in the Last Forty Years	573	577
On the Initial Forms of Spherulites. A. V. Shubnikov	578	584
On the Equilibrium Form of Crystals in a Gravitational Field. B. V. Beliustin	583	590
The Macroscopic Theory of the Formation of Dislocations in Crystal Growth. V. L. Indenbom	587	594
An Instrument for the Mechanical Determination of the Separation Between Lattice Planes. Dr. Frantishek Kgol'	597	604
The Structure of Crystals of Cobaltous Hexafluogermanate Hexahydrate $[Co(H_2O)_6][GeF_6]$. T. S. Khodashova	602	609
A Method for Determining the Amplitudes of the Thermal Vibrations of the Various Kinds of Atoms in Solid Solution. A. P. Zviagina and V. I. Iveronova	606	613
Electron Diffraction Analysis of the Processes of Decomposition of Supersaturated Solid Solutions in Systems Al–Cu and Ag–Cu. Z. G. Pinsker and N. A. Skobel'styna	610	618
Electron-Diffraction Investigation of Polymers. IV. A Study of the Structural Changes in Polychlorotrifluoroethylene in the Crystalline Melting Point Range. A. V. Ermolina, G. S. Markova, and V. A. Kargin	615	623
Electron-Diffraction Study of the Oxidation of Aluminum Alloys. Iu. D. Chistiakov and M. V. Mal'tsev	620	628
A Double-Crystal Neutron Spectrometer. V. N. Bykov, S. I. Vinogradov, V. A. Levdik, and V. S. Golovkin	626	634
Structural Coefficients of the Internal Field in Ferroelectrics with the Perovskite-Type Structure. G. S. Zhdanov, S. P. Solov'ev, and Iu. N. Venevtsev	630	639
The Packing of Chain Molecules. II. The Layers of Paraffin Molecules. A. I. Kitaigorodskii	637	646
Apparatus for Measuring Very Small Displacements of Oscillating Crystals. A. A. Fotchenkov	643	653
The Influence of Deformation Conditions on the Mechanism of the Formation of Slip Bands. E. V. Kolontsova and I. V. Telegina	648	658
On the Morphology of Spherulitic Graphite in High-Strength Cast Iron. Dr. I. Ezhek, I. Koritta, and K. Lebl'	653	663
An Investigation of Phase Equilibria in a Part of the System $H_2O–SiO_2–Na_2CO_3$ at High Temperatures and Pressures. V. P. Butuzov and L. V. Briatov	659	670

CONTENTS (continued)

	PAGE	RUSS. PAGE
Illarion Illarionovich Shafranovskii (On the Occasion of His 50th Birthday)	665	676
Letter to the Editor		
Concerning the Course in Geometric Crystallography for Physicists. N. V. Belov	667	678
Brief Communications		
On the Structure of the Oxide Au_2O_3. N. A. Shishakov	674	686
On the Structure of the Oxide PtO_3. N. A. Shishakov	677	689
A Simple Method for the Determination of Crystal Lattice Constants by Electron Diffraction Patterns from the Surface of an Object. N. A. Shishakov	679	690
X-ray Structural Analysis of Crystals of $[Ru(NH_3)_4(NO)(OH)]Cl_2$. G. B. Bokii and N. A. Parpiev	681	691
On the State of Carbon in Annealed Silicon Steel. E. L. Gal'perin and Iu. S. Terminasov .	684	693
Concerning Procedures of Studying the Structures and Phase Composition of Grain Boundaries. L. G. Sakvarelidze and L. M. Utevskii	687	695
Monochromatization of the Reflected X-ray Beam. A. A. Katsnel'son	692	700
X-ray Diffraction Camera for Precise Measurement of the Unit Cell Parameters of Single Crystals RKM-114. S. S. Kvitka and M. M. Umanskii	694	702
Concerning the Two Limiting Point Groups of Symmetry of Polycrystalline Photoelectrets. I. S. Zheludev and V. M. Fridkin	697	705
The Dielectric, Elastic and Piezoelectric Properties of Single Crystals of Benzophenone. A. A. Chumakov, I. M. Sil'vestrova, and K. S. Aleksandrov	699	707
Investigation of the Anisotropy of Hardness of Single Crystals of PbS by Scratching. Iu. S. Bolarskaia	702	709
Oriented Crystallization of $KMnO_4$ and $KClO_4$ on Barytes. V. A. Frank-Kamenetskii	706	713

SIGNIFICANCE OF ABBREVIATIONS MOST FREQUENTLY ENCOUNTERED IN SOVIET CRYSTALLOGRAPHY LITERATURE

AN SSSR	*Academy of Sciences, USSR*
FIAN	*Physics Institute, Academy of Sciences USSR*
GITI	*State Scientific and Technical Press*
GITTL	*State Press for Technical and Theoretical Literature*
GOI	*State Optical Institute*
GONTI	*State United Scientific and Technical Press*
Gosfizkhimizdat	*State Physical Chemistry Press*
Gozkhimizdat	*State Chemistry Press*
GOST	*All-Union State Standard*
Goztekhizdat	*State Technical Press*
GTTI	*State Technical and Theoretical Press*
GUPIAE	*State Office for Utilization of Atomic Energy*
IF KhI	*Institute of Physical Chemistry Research*
IFP	*Institute of Physical Problems*
IK	*Institute of Crystallography*
IL	*Foreign Literature Press*
IPF	*Institute of Applied Physics*
IPM	*Institute of Applied Mathematics*
IREA	*Institute of Chemical Reagents*
ISN (Izd. Sov. Nauk)	*Soviet Science Press*
IIaP	*Institute of Nuclear Studies*
Izd	*Press (publishing house)*
KISO	*Solar Research Commission*
LETI	*Leningrad Electrotechnical Institute*
LFTI	*Leningrad Institute of Physics and Technology*
LIM	*Leningrad Institute of Metals*
LITMiO	*Leningrad Institute of Precision Instruments and Optics*
MATI	*Moscow Aviation Technology Institute*
MGU	*Moscow State University*
Metallurgizdat	*Metallurgy Press*
MOPI	*Moscow Regional Pedagogical Institute*
NIAFIZ	*Scientific Research Association for Physics*
NIFI	*Scientific Research Institute of Physics*
NIIMM	*Scientific Research Institute of Mathematics and Mechanics*
NII ZVUKSZAPIOI	*Scientific Research Institute of Sound Recording*
NIKFI	*Scientific Institute of Motion Picture Photography*
OIIaI	*Joint Institute of Nuclear Studies*
ONTI	*United Scientific and Technical Press*
OTI	*Division of Technical Information*
OTN	*Division of Technical Science*
RIAN	*Radium Institute, Academy of Sciences of the USSR*
SPB	*All-Union Special Planning Office*
Stroiizdat	*Construction Press*
TsNIIChERMET	*Central Scientific Research Institute for Ferrous Metallurgy*
URALFTI	*Ural Institute of Physics and Technology*

NOTE: Abbreviations not on this list and not explained in the translation have been transliterated, no further information about their significance being available to us.—*Publisher*

The expanded program of the American Institute of Physics comprises translation of six leading Soviet physics journals, as listed below. These translations, by competent, qualified scientists, provide all research laboratories and libraries with accurate and up-to-date information of the results of research in the U.S.S.R.

Soviet Physics—Technical Physics

A translation of the "Journal of Technical Physics" of the Academy of Sciences of the U.S.S.R. The translation began with the 1956 issues. Twelve issues per year, approximately 3,000 Russian pages. Annually $75.00 domestic, $79.00 foreign. Libraries* $35.00 domestic, $39.00 foreign. Back numbers, all issues $8.00.

Soviet Physics—Acoustics

A translation of the "Journal of Acoustics" of the Academy of Sciences of the U.S.S.R. The translation began with the 1955 issues. Four issues per year, approximately 400 Russian pages. Annually $12.00 domestic, $14.00 foreign. (No library discounts.) Back numbers, all issues $4.00.

Soviet Physics—Doklady

A translation of all of the "Physics Sections" of the Proceedings of the Academy of Sciences of the U.S.S.R. The translation began with the 1956 issues. Six issues per year, approximately 1,500 Russian pages. Annually $35.00 domestic, $38.00 foreign. Libraries* $15.00 domestic, $18.00 foreign. Back numbers for Volumes 1 and 2, $5.00 per issue; Volume 3 and subsequent, $7.00 per issue.

Soviet Physics—JETP

A translation of the "Journal of Experimental and Theoretical Physics" of the Academy of Sciences of the U.S.S.R. The translation began with the 1955 issues. Twelve issues per year, approximately 4,000 Russian pages. Annually $75.00 domestic, $79.00 foreign. Libraries* $35.00 domestic, $39.00 foreign. Back numbers, all issues $8.00.

Soviet Physics—Crystallography

A translation of the journal "Crystallography" of the Academy of Sciences of the U.S.S.R. The translation began with the 1957 issues. Six issues per year, approximately 1,000 Russian pages. Annually $25.00 domestic, $27.00 foreign. Libraries* $10.00 domestic, $12.00 foreign. Back numbers, all issues $5.00.

Soviet Astronomy—AJ

A translation of the "Astronomical Journal" of the Academy of Sciences of the U.S.S.R. The translation began with the 1957 issues. Six issues per year, approximately 1,100 Russian pages. Annually $25.00 domestic, $27.00 foreign. Libraries* $10.00 domestic, $12.00 foreign. Back numbers, all issues $5.00.

Subscriptions should be addressed to the American Institute of Physics, 335 East 45th Street, New York 17, N. Y.

* For libraries of non-profit academic institutions.